

Cost-effective aperture arrays for SKA Phase 1: single or dual-band?

Tim Colegate¹, Peter Hall¹, Andre Gunst^{2,3}

27/02/12

Abstract

An important design decision for the first phase of the Square Kilometre Array is whether the low frequency component (SKA₁-low) should be implemented as a single or dual-band aperture array; that is, using one or two antenna element designs to observe the 70–450 MHz frequency band. This memo uses an elementary parametric analysis to make a quantitative, first-order cost comparison of representative implementations of a single and dual-band system, chosen for comparable performance characteristics. A direct comparison of the SKA₁-low station costs reveals that those costs are similar, although the uncertainties are high. The cost impact on the broader telescope system varies: the deployment and site preparation costs are higher for the dual-band array, but the digital signal processing costs are higher for the single-band array. This parametric analysis also shows that a first stage of analogue tile beamforming, as opposed to only station-level, all-digital beamforming, has the potential to significantly reduce the cost of the SKA₁-low stations. However, tile beamforming can limit flexibility and performance, principally in terms of reducing accessible field of view. We examine the cost impacts in the context of scientific performance, for which the spacing and intra-station layout of the antenna elements are important derived parameters. We discuss the implications of the many possible intra-station signal transport and processing architectures and consider areas where future work could improve the accuracy of SKA₁-low costing.

Contents

1	Introduction	2
2	Document structure	3
3	Parametric cost modelling	4
3.1	Parametric analysis	4
3.2	Scalable parametric cost models	5
3.3	Cost data sources	7
4	Single and dual-band representative implementations	11
4.1	SKA ₁ -low station design details	11
4.2	Comparison of the station sub-systems	13
4.3	Cost reduction from analogue (RF) tile beamforming	14
5	System implications of variable costs	15
5.1	Antenna element deployment and site preparation costs	15
5.2	Central processing facility sub-systems	16
5.3	Overall SKA ₁ -low costs	17
5.4	Power costs	17
6	Discussion of principal analysis	20
6.1	Cost trends	20
6.2	Performance trends	21
6.3	Risk and uncertainty	21
6.4	Relevance to SKA Phase 2	24
7	Supplementary analyses	25
7.1	Varying station diameter	25
7.2	Reducing the FoV requirement: defining a fixed beam–bandwidth product	26
7.3	Intra-station signal transport and processing architecture considerations	26
8	Further work	30
9	Conclusions	30
	Appendices	32

¹International Centre for Radio Astronomy Research, Curtin University, Perth, Australia (tim.colegate@icrar.org)

²ASTRON, Dwingeloo, the Netherlands

³SKA Program Development Office

1 Introduction

The release of a high-level concept design (Garrett et al., 2010) for the first phase of the Square Kilometre Array (SKA₁) represented an important milestone for the telescope. It describes a baseline telescope implementation with aperture array (AA) and dish receptors, to observe the 70–450 MHz and 0.45–3 GHz frequency ranges respectively. Further design details have been added through the subsequent development of a preliminary system description (Dewdney et al., 2010) and a high level system description (Dewdney et al., 2011b, hereafter HLSD). However, an outstanding question in the SKA community is whether the 70–450 MHz frequency range (SKA₁-low) should be observed with an array composed of a single wideband antenna element design (single-band implementation), or with two arrays, each observing approximately half the fractional bandwidth (dual-band implementation).

The choice of a single or dual-band implementation is a key design decision for SKA₁-low. The system descriptions present an overview of the telescope as a complex set of inter-connected parts (sub-systems). Although the design of the system and its sub-systems have been refined through Concept Design Reviews (CoDRs), most of the recent system-level studies (including the CoDRs) for the SKA have assumed a single-band implementation for SKA₁-low (e.g. Bij de Vaate et al., 2011 and references therein). Unfortunately, this means that the effects of a dual-band implementation on the system design are not currently well documented. However, the dual-band approach used in the LOFAR telescope gives many insights into a putative SKA₁-low instrument.

Furthermore, the *SKA AA CoDR panel report* (Dewdney et al., 2011a) recommends that the impact of the dual-band option on system design should be considered. Indeed, not meeting the SKA₁-low requirements with a single-band implementation is identified as a risk in van Es et al. (2011). While the *AA Concept Descriptions* document (Bij de Vaate et al., 2011) makes a quantitative technical analysis of the single and dual-band approaches, to date there has been no comparison of the cost-effectiveness of each approach. Such a comparison is important, because the chosen approach has consequences for antenna element design, manufacture and deployment costs, and influences the downstream signal processing costs.

This memo uses an elementary parametric analysis to determine if a dual-band implementation, with twice as many antenna elements, is significantly more expensive than the single-band implementation described in the HLSD. We use simple algebraic equations to model the cost and performance of each implementation, and consider the cost drivers of the single and dual-band SKA₁-low at two levels. The first level is simply the cost of the hardware required specifically for the low-frequency aperture array sub-systems (‘stations’). But because these stations are inter-linked with other sub-systems to realise SKA₁-low as a telescope, the effect of design choices within the stations is considered throughout the system. Thus our second, higher level, analysis incorporates costs which differ between the two implementations, such as those of the correlator, imaging processor and non-imaging processor sub-systems, as well as site-related costs specific to SKA₁-low.

The representative single and dual-band implementations are chosen for comparable sensitivity, field of view (FoV) and survey speed performance. The single-band implementation is that which is described in the SKA₁ HLSD, but there is no similar guidance to the design of the dual-band implementation. The illustrative comparison in this memo uses a canonical form of the dual-band implementation, composed of two single-band arrays, each of which simultaneously observes approximately equal bandwidth ratios of 2.5:1. This produces a low-band array (70–180 MHz) with the same physical layout as the HLSD, and an additional high-band array (180–450 MHz) with a 0.75 m spacing between antenna elements. Alternative implementations could, for example, have overlapping bands or a 50 MHz minimum frequency. However, consideration of the system implications of such comparisons is beyond the scope of the present document.

Our parametric modelling shows that the smaller inter-element spacing for the high-band array is a key driver in reducing the cost of the dual-band implementation, via reduced digital data transport and processing loads throughout the system. Although 0.75 m inter-element spacing is arbitrarily chosen as being half that used for the low-band and single-band arrays, such a spacing maintains similar sensitivity

performance to the single-band array, at least for the antenna elements described in the HLSD.

The goal of the trade-off and decision making processes for the SKA is to refine the design options by linking performance, cost and risk to science returns (Stevenson, 2011; Dewdney, 2010). This work is not an analysis of expected telescope performance and total cost, nor are the examined systems optimised for performance and cost. However, by drawing upon the existing documented studies of aperture arrays and the SKA, our analysis is intended to assist these trade-off and decision making processes.

2 Document structure

Section 3 outlines the parametric cost modelling approach, along with the models and cost data sources used. Section 4 details representative single and dual-band SKA₁-low implementations and compares the station sub-system costs. Other selected SKA₁-low sub-system costs, which vary between implementations, are considered in Section 5. Section 6 discusses the performance and cost trends, uncertainties and the relevance to SKA₂. Section 7 investigates some topical additional trade-offs: smaller station diameter, reduced beam-bandwidth product and changed intra-station architecture. Recommendations for further work are made in Section 8 and conclusions set out in Section 9. A list of symbols is given in Appendix A and a summary of major assumptions listed in Appendix B.

Although the comparisons and trade-offs are progressively developed in each section, there may be aspects of the system which are of interest to particular readers. These are cross-referenced as follows:

- station hardware sub-systems
 - cost data sources: Section 3.3
 - derived unit costs and models: Appendix D
 - station design details: Section 4.1
 - representative implementation costs: Section 4.2
 - RF tile beamforming vs. all-digital beamforming: Section 4.3
 - uncertainty in representative implementation costs: Section 6.3
 - alternative intra-station architectures: Section 7.3.3
 - station diameter variation: Appendix H.1
 - reduced processed FoV through a fixed beam-bandwidth product: Appendix I.2
- variable system costs
 - site-related costs and models: Appendix F.1
 - central processing facility sub-system costs and models: Appendix F.2
 - representative implementation costs: Section 5
 - station diameter variation: Appendix H.2
 - reduced processed FoV through a fixed beam-bandwidth product: Appendix I.3
- station power demand
 - power demand models: Appendix F.3
 - representative single and dual-band implementations: Section 5.4
 - alternative intra-station architectures: Section 7.3.3
 - station diameter variation: Appendix H.2
- general cost trends
 - single vs. dual-band comparison: Section 6.1
 - station diameter variation: Section 7.1
 - reduced processed FoV through a fixed beam-bandwidth product: Section 7.2
- station performance
 - single vs. dual-band comparison: Section 6.2 and Appendix G
 - hierarchical beamforming Section 7.3.2

Table 1: Recommended use of cost estimation methodologies at various stages in a project. SKA is currently in the design definition stage. Adapted from NASA (2008).

	Early concept definition	Design definition	Detailed design	Construction and deployment	Operations, support and disposal
Parametric	●	●	◐	◐	○
Reference class (analogous)	●	◐	◐	◐	○
Bottom-up (engineering)	◐	◐	●	●	●
● Primary ◐ Applicable ○ Not applicable					

3 Parametric cost modelling

The key to successful parametric analysis is to have a scalable model which is sufficiently general, but still describes the system with enough completeness and accuracy. To describe the actual cost of the system, the model should provide a cost estimate and associated uncertainty. Early in the project, the uncertainties are large, and as the project progresses and the cost models are refined, the uncertainties reduce. This is known as the ‘cone of uncertainty’, wherein the cost estimate eventually converges on the actual cost (GAO, 2009).

Defining a scalable model for the SKA is challenging because the project is currently in the design definition phase, where many design options and architectures are available, and a complete set of requirements is still being developed. For these reasons, the model for the parametric analysis is necessarily simple; in this case it is captured in a dozen scalable blocks. Although such a model has high uncertainties, it provides useful insight at this point and also indicates prime areas for further study.

3.1 Parametric analysis

Parametric analysis is a useful systems engineering tool, enabling understanding and exploration of performance and cost trends, and of key trade-offs. It involves defining the system with a set of variable parameters, and then modifying one or more of these parameters to model the effect on the performance and cost of the system. In a complex system such as the SKA, many parameters are closely inter-linked.

In terms of parametric cost estimation, the *2008 NASA cost estimating handbook* (NASA, 2008) lists parametric cost models as one of three cost estimation methodologies. The second methodology is analogous (or reference class) costing, where cost data from similar sub-systems (or projects) is used. The cost data is adjusted, depending on the relative complexity of the projects, technological improvements, inflation and other factors. The third is an engineering (bottom-up) cost estimate, which builds up a cost estimate from all the individual cost elements in the system. The bottom-up approach requires a good understanding of all the costs involved (‘cost coverage’), as outlined in the *Draft SKA costing strategy* (McCool et al., 2010). Table 1 compares the project stages where these methodologies are most useful; the SKA is currently in the design definition stage. Parametric costing is the primary method in the earlier stages of the project, facilitating high-level trade-offs when there is insufficient data for a detailed approach. A bottom-up costing is more useful later in the project, as greater design detail and actual cost data are accumulated (NASA, 2007).

A complete parametric analysis would allow for the design to be optimised for cost while still meeting the system requirements (scientific, environmental and operational requirements). These requirements are being developed in the current design definition phase and will be documented in the requirements specifications (Stevenson, 2011). Importantly, the design will be optimised for the life-cycle cost, which is the total cost of ownership over the lifetime of the system (NASA, 2007). However, all costs in the life-cycle need to be considered to make the like-for-like trade-off. For the SKA, costs such as construction,

site operations, power infrastructure and software development must be considered in life-cycle costing (McCool et al., 2010). These are additional to the hardware and operations costs of the sub-systems, on which most of the SKA costing focus has been placed thus far. There are also some SKA project overhead costs, such as contingency, taxes and system integration costs, which do not contribute to current cost estimates (McCool et al., 2010). Not all these life-cycle costs are currently available or sufficiently understood, nor are the requirements specifications complete. For these reasons, this work does not give a final cost, but instead makes a comparative cost analysis of the single and dual-band SKA₁-low implementations.

3.2 Scalable parametric cost models

The parametric cost model encodes the telescope system design using a small number of blocks, where each block describes the quantity and cost scaling relationships of one or more sub-systems. Relatively simple algebraic equations are used to describe the cost of these blocks as a function of one or more variables (parameters). The scalable models enable performance and cost exploration and trade-offs; these are much more difficult to make with, for example, a bottom-up cost estimate that assumes a specific design. However, the parametric equations themselves are derived from one or more cost estimates, and reference class and bottom-up cost estimates can be suitable sources of data.

The cost data sources usually have itemised costs; each cost item is assigned to a particular block, producing an aggregate cost for each block. Because this aggregate cost is for a given set of parameters (as per the HLSD in this case), solving the parametric equation determines the value of the cost coefficients. The cost of the block can then be expressed as a function of its variable parameters, and the total cost of the model calculated from the summation of the quantity and cost product of each block.

For example, the parametric equation of a particular block is given by

$$C_{\text{block}} = C_{\text{fix}} + C_{\text{var}} x, \quad (1)$$

where C_{block} is the cost of a single ‘instance’ (occurrence) of the block, C_{fix} and C_{var} are the cost coefficients (unit costs) and x is a scaling parameter. Say an aggregate cost estimate of the block gives $C_{\text{block}} = \text{€}200$, for $x = 8$. Using a reasonable estimate of what proportion of cost is fixed (say 20%), the unit costs for the block can be determined: $C_{\text{fix}} = \text{€}40$ and $C_{\text{var}} = \text{€}20$. The cost of the block can then be determined for other values of x (within reasonable design limitations). The total cost C_{total} is simply the summation of the product of the quantity (N) and cost (C) of each block:

$$C_{\text{total}} = N_{\text{blockA}} C_{\text{blockA}} + N_{\text{blockB}} C_{\text{blockB}} + \dots \quad (2)$$

Although these algebraic equations do not capture all the nuances of a design, they do provide a scalable, first-order cost estimate. Also, as is done in the present analysis, a direct comparison of different cost data sources can be made by running the model with the different unit costs derivations, but using the same parametrisation. This highlights areas of the design where costs differ, thus are most uncertain and require further investigation.

The SKA₁ high level system description (HLSD, Dewdney et al., 2011b) is a useful starting point to create a parametric cost model for SKA₁-low, because it defines a system hierarchy which describes how the sub-systems relate to each other. For example, the low-frequency aperture arrays, signal transport and networks, signal processing, computing and software, and infrastructure are all immediate sub-systems of the telescope system. Although the HLSD will evolve as the system requirements are refined, it forms a ‘representative system’ as a common basis for the analysis of sub-system performance and cost.

To model the differences between the single and dual-band SKA₁-low, we decompose the low-frequency aperture array sub-system into another level of sub-systems. As mentioned in Section 1, the term ‘SKA₁-low’ encompasses hardware specifically related to the low-frequency aperture array sub-system as well as

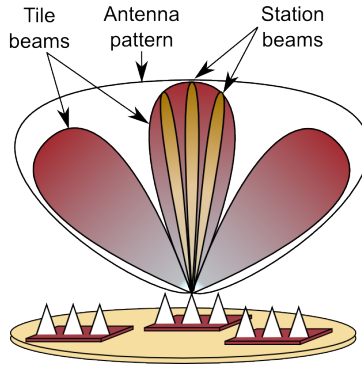


Figure 1: Aperture array schematic, showing the antenna elements (triangles), tiles (squares) and the station (disc), and their corresponding beam pattern.

other SKA sub-systems. Although not explicitly defined in the HLSD, the low-frequency aperture array sub-system approximately describes the hardware for the SKA₁-low stations.

The SKA₁-low antenna elements are grouped into ‘tiles’ and ‘stations’, as shown in Figure 1, to reduce the data transport and processing loads. This grouping of antenna elements may affect the physical layout or may only change the signal processing architecture; the partitioning of the processing is termed hierarchical beamforming. The ‘processed FoV’ is synthesised from the formation of multiple station beams, which are cross-correlated in the telescope’s signal processing system.

The HLSD also describes the geographical layout (configuration) of the stations. Approximately half the AA stations are located in a closely packed ‘core’ region, and the others placed with exponentially increasing density away from the core. A similar layout applies to the dishes. Because the AA and dish cores are densely packed, these are located nearby to each other but separate. At larger radii from the core, the stations and dishes are co-located, so that the data transport, timing signals and power distribution infrastructure can be shared.

Although the SKA₁-low sub-systems are captured in a small number of blocks to maintain clarity, it is important that the quantity of each of these blocks still scales correctly when the parameters are varied. This approach is similar to some of the previous SKA costing efforts (Chippendale et al., 2007; Bolton et al., 2009b), except the blocks in this analysis describe the system at a higher level. Because only a small number of blocks are used, most of the results in this analysis have been calculated using a spreadsheet. However, the parametric models have been developed with a view to transferring them to SKACost, an SKA performance and cost modelling tool. (See Ford et al., 2010 for a description of the tool.) SKACost will allow further exploration of trade-offs in the SKA₁-low design space, and enable statistical treatment of uncertainties. SKACost is used to make the preliminary uncertainty analysis in Section 6.3.3.

The blocks (sub-systems) follow the elemental signal path, in an approach similar to Hall (2004) and Horiuchi et al. (2004). The blocks used in this analysis to describe the elemental signal path are:

active antenna element: reception and amplification at the antenna element

RF tile beamformer: analogue beamforming of the elements in a tile. Digital tile beamforming is also possible, see Section 7.3.1

RF link: analogue signal transport from the active antenna element or the tile beamformer

digitiser: digitisation

station beamformer: coarse channelisation (filterbank) and digital beamforming of elements or tiles in the station

station ‘bunker’: controlled environment and infrastructure at the station processing node to house the beamformer hardware

digitiser–bunker link: digital signal transport from the digitiser to the bunker

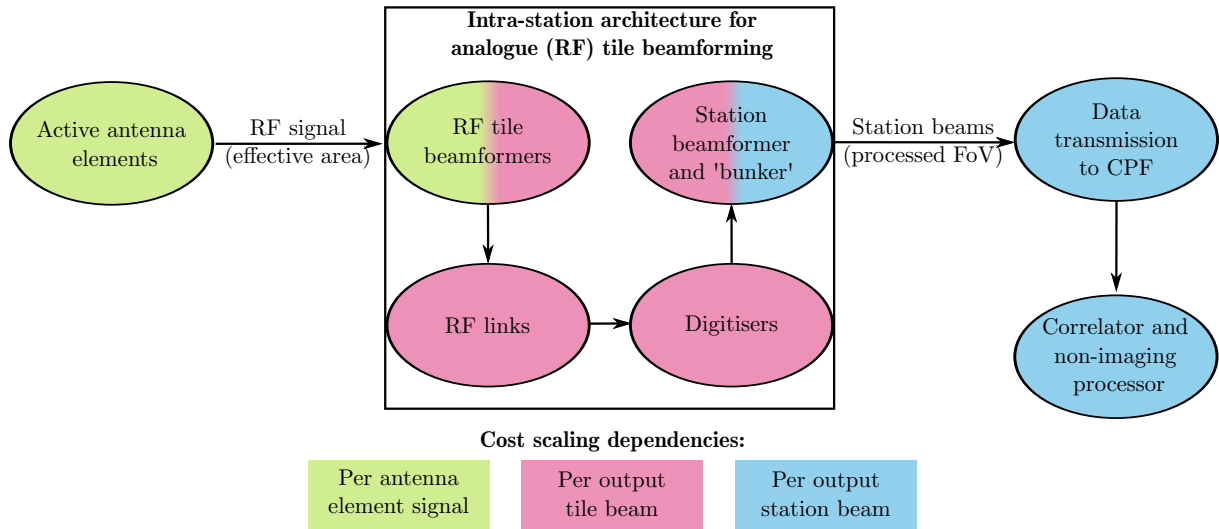


Figure 2: Conceptual diagram showing the general cost scaling dependencies of key blocks (ovals), for the RF tile beamforming intra-station architecture. The gradient indicates that both scaling dependencies apply.

central processing facility (CPF): central signal processing and science computing sub-systems (specifically, the correlator, imaging and non-imaging processing). The CPF serves both the AA and dish arrays. Some parts of the CPF may be located off-site

data transmission to CPF (station–CPF link): digital signal transmission from the station processing node to the central processing facility (excludes network infrastructure).

These blocks assume a time to frequency domain transformation and cross-correlation ‘FX’ correlator architecture, being the most cost-effective architecture for the SKA (see Appendix C).

The blocks are combined to form a specific signal transport and processing architecture within a station, shown conceptually in Figure 2. A station will have some number of antenna elements (to realise effective area, hence sensitivity) and produce some number of station beams (to form the processed FoV). The rectangular box in Figure 2 encompasses the intra-station signal transport and processing architecture. The exact path of the signal from one block to the next depends on the architecture chosen; this is discussed in Section 7.3.

Figure 2 also shows the general cost scaling dependencies of each block, as relevant to the single versus dual-band comparison. The dependencies are linear parametric equations, with the key variable parameters being the number of antenna element signals, output beams formed by the tile beamformer and output beams formed by the station beamformer. For the digital signal transport links, the number of signals or beams transmitted is a proxy for the data rate transmitted. The scaling relationships and unit costs of each block are detailed in Appendix D. The two intra-station signal transport and processing architectures analysed in this work are discussed in the next section.

3.3 Cost data sources

The cost data sources for this analysis are shown in Table 2. Two cost estimates were developed in the AA CoDR (Faulkner et al., 2011) for the SKA₁-low stations; one based on the SKA Design Studies (SKADS) work (e.g. Faulkner et al., 2010), the other extrapolated from the existing Low Frequency Array (LOFAR) telescope⁴. Although these estimates describe stations which achieve similar sensitivity and FoV performance, they present two alternative intra-station signal transport and processing architectures, and also use different cost estimation methodologies and assumptions, as summarised in Table 3.

The principal architectural differences between the two estimates are how and where the digitisation and hierarchical beamforming is performed. The SKADS architecture uses all-digital beamforming, where

⁴www.lofar.org

Table 2: Sub-system cost data sources

Sub-system	Cost data source			
	SKADS ^a	LOFAR ^a	Signal Processing CoDR ^b	Professional opinion
Active antenna element	×	×		
RF tile beamformer		×		
RF links	×	×		
Digitiser	×	×		
Digitiser–bunker links	×			
Station beamformer	×	×		
Station bunker	×	×		
Data transmission to CPF	× ^c			
Correlator			×	
Non-imaging processor			×	
Correlator–computing data transport				×
Computing (imaging processor)				×
Deployment				×
Site preparation				×

^a Faulkner et al. (2011)
^b Turner (2011)
^c Bolton et al. (2009b)

Table 3: Costing methodologies and data sources

Costing methodology		Cost data source	
		SKADS	LOFAR
Bottom-up	Reference class	×	
	Tile beamforming	digital	RF
Intra-station architecture	Tile–station signal transport	digital	RF
	Station beamforming	digital	digital

both the tile and station beamforming are done digitally, while the LOFAR architecture uses analogue tile beamforming. These are the architectures considered in our study; the cost and performance implications of some other intra-station architectures on the SKA₁-low sub-system costs are discussed in Section 7.3.

The parametric models for the stations are based on these two cost estimates and their architectures. The all-digital beamforming architecture, as broken down into the sub-system blocks for this analysis, is shown in Figure 3. In this architecture, the signals are digitised close to the antenna elements, but no beamforming occurs at the tiles. Instead, two or more stages of hierarchical beamforming are assumed to occur within the station beamformer block. This differs slightly from Faulkner et al. (2011), where a first stage of beamforming is done at the tile. Figure 4 shows the sub-system blocks for the second architecture, which uses a first stage of analogue (RF) beamforming at the tile. In this architecture, the analogue signals are transported to the station processing node and digitisation occurs at that node.

Alongside the all-digital and RF tile beamforming architectures, we consider the different cost estimation methodologies and assumptions used for the two estimates in Faulkner et al. (2011). The cost estimate for the all-digital beamforming architecture primarily uses the bottom-up cost method described earlier; we

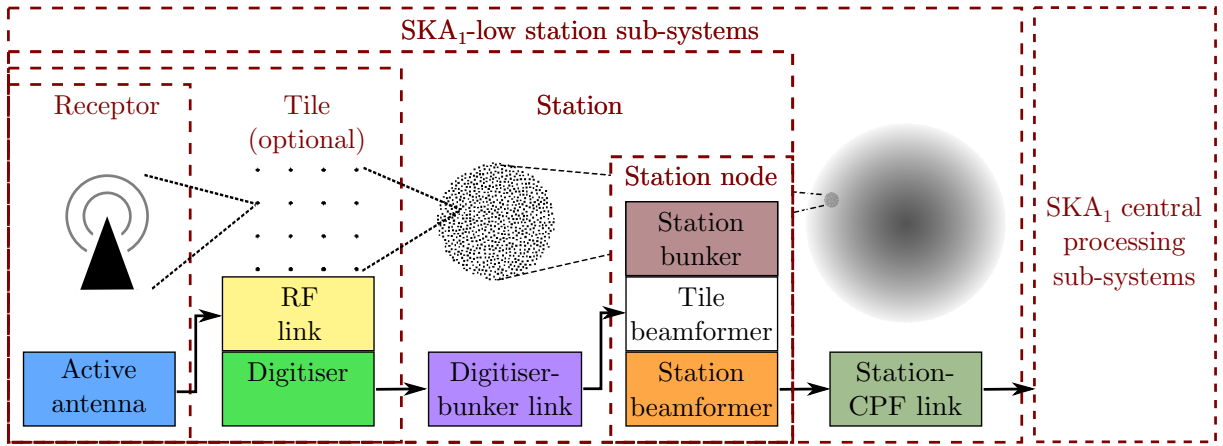


Figure 3: Schematic of the all-digital beamforming architecture, showing the signal path through the SKA₁-low sub-systems to the central processing facility. Two or more stages of hierarchical beamforming are assumed to occur within the station beamformer block.

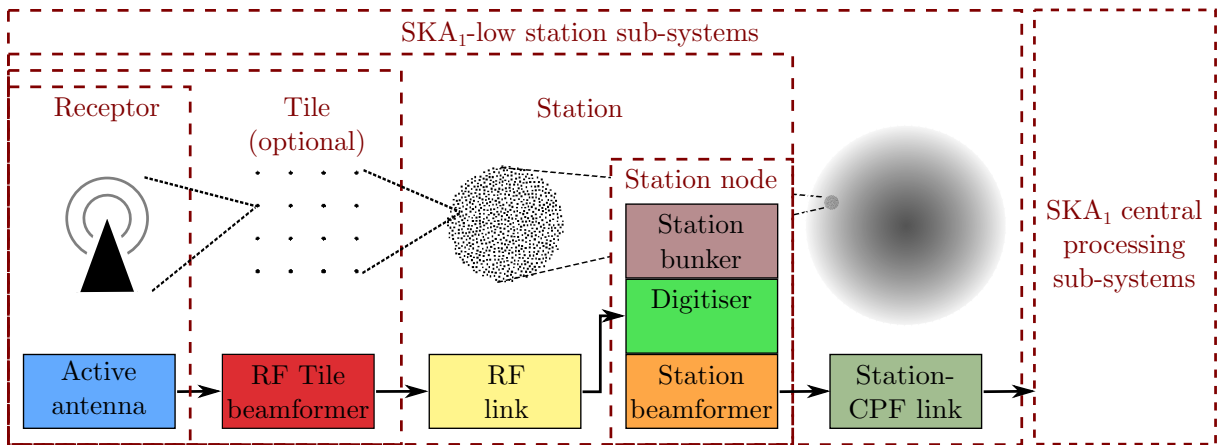


Figure 4: Schematic of the RF tile beamforming architecture, showing the signal path through the SKA₁-low sub-systems to the central processing facility.

term this the ‘bottom-up SKADS’ estimate. The cost estimate for the RF tile beamforming architecture uses LOFAR station costs to make an analogous cost estimate of the SKA₁-low station, hence we term it the ‘reference class LOFAR’ estimate. Although it is an example of a reference class cost estimate, it is implemented at a more detailed sub-system level, instead of at the system level where the reference class estimation methodology is often applied.

Understanding the epoch of the source cost estimate is also important, especially in regards to the digital hardware. Digital technology advancements can often be generalised by exponential laws; the most common being Moore’s law, where the cost of an equivalent digital product halves every 1.5–2 years. Thus the year for which the cost data applies, and the technical capability of the hardware to which it applies, are relevant factors. The bottom-up SKADS estimate makes the assumption that technology advances reduce costs and that SKA₁-low construction commences in 2016. In contrast, the reference class LOFAR estimate is based on 2007 technology and is only for an output bandwidth of approximately 50 MHz. We make the assumption that by 2016, newer technology will allow for the processing of the full 380 MHz bandwidth for the same cost.

The unit costs for the station sub-systems are derived from the cost data in Faulkner et al. (2011), as described in Appendix D. The derivation method is that described earlier, where the cost data is aggregated for each block, and the unit costs are derived from these block aggregates and the parameters in the HLSD (see Table 4). The costs, especially some of the digital costs, are necessarily simplistic in order to transcend the design details and multitude of options for each sub-system; however, the simplifications do introduce another level of uncertainty into the analysis. The costing of the dual-band

array uses a similar parametrisation process, but applies multipliers (discounts) to the unit costs to account for the design differences between sub-systems of the single-band and low and high-band arrays, as discussed further in Section 4.1.

The bottom-up SKADS unit costs are consistently lower than the reference class LOFAR unit costs. From Table 12 of Appendix D, the relative difference in cost is a factor of 2–3 for the active antenna element and fixed cost portion of the station bunker, 4.5 for the digitiser, 26 for the station beamformer and 43 for the variable cost portion of the station bunker. While useful for this first-order analysis, these cost differences show that more work is required to confirm the accuracy and precision of the unit cost derivation and the cost estimates themselves, as discussed in Sections 6.3 and 8. Note that the bottom-up methodology does not necessarily produce a lower cost estimate than the reference class methodology. Adjustments such as technology improvements and learning curves for mass production can be used to change the cost estimate (NASA, 2008). Thus the relative costs also depend on what cost adjustments are applied to each cost estimate, as well as the method of arriving at the cost data.

Many of the station sub-systems have a cost data source from both the bottom-up SKADS and reference class LOFAR estimates (Table 2). Not all aspects of each cost estimate are comparable because of the different architectures used. However, the active antenna element, digitiser, station beamformer and station infrastructure sub-systems are comparable and these costs comprise most of the SKA₁-low station costs. These comparable sub-systems mean that the unit costs derived from the bottom-up SKADS and reference class LOFAR estimates can be applied to either the all-digital or RF tile beamforming architectures, allowing four different cost scenarios to be modelled:

- reference class LOFAR, RF tile beamforming
- bottom-up SKADS, RF tile beamforming
- bottom-up SKADS, all-digital beamforming
- reference class LOFAR, all-digital beamforming

Because the bottom-up SKADS, RF tile beamforming and reference class LOFAR, all-digital beamforming architectures are extrapolated, they are less optimised for technical performance and cost than the other two scenarios; this is an extra source of uncertainty for those scenarios. Uncertainties are analysed in Section 6.3.

The costs discussed thus far are for the station sub-system hardware. Section 5 considers hardware cost for the central processing facility sub-systems. But even with these costs included, this does not represent the total telescope cost. The *Draft SKA costing strategy* (McCool et al., 2010) discusses some of the other costs to be considered for the SKA. The sub-system hardware cost is included in the present analysis, although with some caveats discussed in Appendix D. The costs excluded in the analysis are:

- sub-system hardware operations[†]
- temporary construction and integration facilities
- site operations infrastructure
- construction[†] (including network trenching)
- annual fibre costs
- antenna siting costs (inclusive of foundations)
- land acquisition
- power infrastructure[†]
- software development

[†]these costs can depend on the intra-station architecture, see Section 7.3.

Also listed in the McCool et al. (2010) are project overheads, which are outside the scope of this analysis.

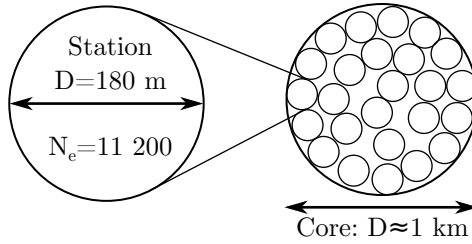


Figure 5: Representation of a single-band station within the densely packed core region.

Table 4: Single-band SKA₁-low system details, as per the HLSD except where noted.

Frequency range	70–450 MHz
Number of stations N_{st}	50
Average spacing between elements d_{avg}	1.5 m ($\lambda/2$ at 100 MHz)
Number of elements per tile ^a $N_{\text{e}/\text{tile}}$	16
Station beam taper ^b \mathcal{K}_{st}	1.02 ^c
Number dual-polarisation beams per station (averaged over the band) $\overline{N_{\text{b-st}}}$	210 ^d
Dense-sparse transition ^e	115 MHz
Gain of an isolated element	6.2 dBi

^a For the RF first-stage beamforming architecture.

^b Where station beam FoV $\Omega_{\text{st}} = \pi/4(\mathcal{K}_{\text{st}}\lambda/D_{\text{st}})^2$.

^c A uniform aperture distribution is assumed (Rohlfis & Wilson, 2004), whereas the HLSD specifies $\mathcal{K}_{\text{st}} = 1.3$.

^d This differs from the 160 beams specified in the HLSD.

^e See Appendix G.1.

However, many of the excluded costs remain approximately constant between the single and dual-band implementations. Hence Section 5 makes some zeroth-order estimates of those excluded costs that will vary between implementations, namely site preparation and antenna element deployment costs. This allows for a comparison to be made in the absence of all the cost information.

4 Single and dual-band representative implementations

This analysis is based on a single and dual-band representative system, rather than an optimised system. Most of the recent SKA₁ design work, as presented in the sub-system concept design reviews, has been developed with the SKA₁ high level system description in mind. For this reason, the single-band SKA₁-low in the HLSD is used as the starting point for a comparison of the single and dual-band implementations. No dual-band implementation is described in detail in the *AA Concept Descriptions* document; in our study, the canonical (not optimised) dual-band design has been chosen so that its scientific performance will be similar to the single-band system.

4.1 SKA₁-low station design details

Using a dual-band implementation with similar performance characteristics to the single-band implementation ensures the like-for-like comparison. In particular, the low-band array (70–180 MHz) has the same physical layout as the single-band array to achieve the same sensitivity at the lower frequencies. The high-band array (180–450 MHz) has the same number of antenna elements as the low and single-band arrays, so despite the smaller inter-element spacing, sensitivity is maintained as equivalent to the single-band at most frequencies (see Appendix G.1), while reducing the geometrical area occupied by the station. The required processed field of view (FoV) is a minimum of $\Omega_{\text{req}} = 20 \text{ deg}^2$, observed concurrently across the frequency band. Dual-polarisation ($N_{\text{pol}} = 2$), or full-Stokes signals, are assumed throughout this analysis.

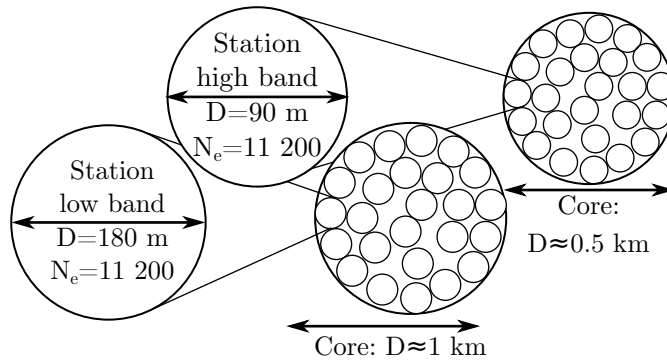


Figure 6: Representation of a low and high-band station within two densely packed core regions.

Table 5: Dual-band SKA₁-low system details.

	Low band	High band
Frequency range	70–180 MHz	180–450 MHz
Number of stations N_{st}	50	50
Average spacing between elements d_{avg}	1.5 m ($\lambda/2$ at 100 MHz)	0.75 m ($\lambda/2$ at 200 MHz)
Number of elements per tile $N_{e/tile}$	16	16
Station beam taper \mathcal{K}_{st}	1.02	1.02
Number dual-polarisation beams per station (averaged over the respective band)	44	70
Dense-sparse transition	115 MHz	230 MHz
Gain of an isolated element ^a	6.2 dBi	6.2 dBi
Observing mode	Simultaneous (i.e. 70–450 MHz)	

^a Gain is assumed to be the same for each band, to ensure that the first-order station A/T estimates are comparable. Actual gain values will depend on the antenna element designs.

The representative single-band implementation is that which is described in the HLSD. The pertinent features of the system are shown in Figure 5 (station diameter D_{st} and number of elements per station $N_{e/st}$) and Table 4. As shown in Appendix E, the required FoV Ω_{req} is synthesised from an average number of station beams over the band $\overline{N_{b-st}}$; enough processing is costed to form these beams. An irregular intra-station element layout of approximately uniform element distribution is assumed.

The key differences in the dual-band implementation are the separate low and high-band stations, and the average inter-element spacing of 0.75 m in the high band. Figure 6 and Table 5 show the details of this system. The stations and the two cores are assumed to be separate, as portrayed in Figure 6. Rather than the two cores shown in the HLSD (the second core being composed of dishes), an SKA₁ with a dual-band SKA₁-low implementation would have three cores. The separated cores means each core can be densely packed, resulting in a higher filling factor. Such densely packed cores allow for more efficient searches of pulsars and other high time resolution events (see Appendix F.2.5). However, other science applications for the high-band (180–450 MHz) would require evaluation to ensure that the array configuration composed of the smaller, 0.5 km diameter high-band core remains suitable. Consideration of other configurations, such as interspersed or interleaved stations, is beyond the scope of the present analysis.

The cost of the dual-band implementation is estimated by costing the low and high-band stations separately. This means determining C_{total} in Equation 2 for each band, and then summing the costs. To determine C_{total} for each band, the unit cost of every block is given as some fraction of the single-band cost, as detailed in Appendix D.9. These costs are considered to be reasonable estimates but are not based on detailed investigation.

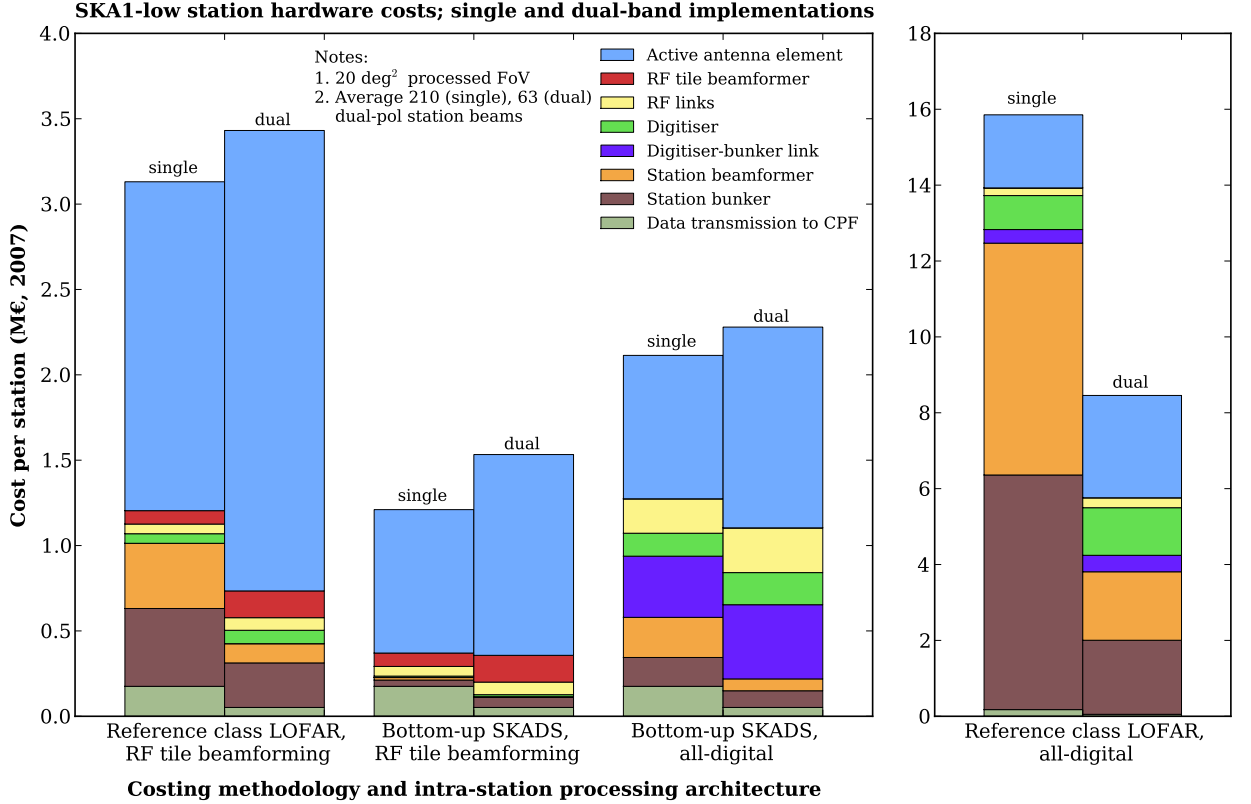


Figure 7: SKA₁-low station hardware cost, for permutations of single or dual-band implementations, costing methodologies and intra-station processing architectures. (Reference class LOFAR, all-digital beamforming, right, has a different y-axis scale.) The reference class LOFAR, RF tile beamforming and bottom-up SKADS, all-digital beamforming scenarios are derived from the cost estimates and architectures in Faulkner et al. (2011); the other two scenarios are the extrapolations from those derivations. Station bunker refers to the station beamformer housing and infrastructure (racks, power supply etc.). Sub-systems are colour-coded to match Figures 3 and 4.

For this analysis, infrastructure such as housing for the station processing node is not shared. However, it is assumed that stations are co-located beyond the core, hence the trenching and cables for the data transmission and power to these stations can be shared. Costing the systems separately ensures clarity for comparison purposes; an actual implementation could share some infrastructure and possibly signal processing units, while still being capable of observing the full 70–450 MHz frequency range. Some of the implications of station co-location are discussed in Bij de Vaate et al. (2011) and Faulkner et al. (2010).

4.2 Comparison of the station sub-systems

Figure 7 plots the SKA₁-low station hardware costs for the four different cost scenarios (Section 3.3), each scenario being a combination of:

- reference class LOFAR or bottom-up SKADS cost estimate, and
- RF tile beamforming with subsequent digital station beamforming or all-digital beamforming.

These cost scenarios are plotted for both the single and dual-band implementations. The costs shown here are for the SKA₁-low station sub-systems, from the active antenna element up to and including the data transmission to the central processing facility (see Figures 3 and 4).

The sub-system costs which dominate the station hardware cost in the single-band implementation differ between the RF tile beamforming and all-digital architectures. For the all-digital architecture, the active antenna element cost is less than half the total station cost. With RF tile beamforming, the majority of the cost is active antenna element costs. All the other blocks have a decreased cost, due to the factor of 16 decrease in the number of signal chains after the RF tile beamformer (with the exception of the

station–CPF link, which remains constant). This implies that understanding the active antenna element costs is more important for the RF tile beamforming architecture. The dual-band array displays the similar broad trend as the single-band array, where the active antenna element cost is more dominant in the RF tile beamforming architecture than the all-digital architecture.

Comparing the single and dual-band implementations shows the driving costs for each. Because the dual-band implementation has twice the number of stations, hence twice as many antenna elements and therefore signal chains, the active antenna element costs are significantly higher. However, the increase is less than double, because of the cost discounts applied in Table 14 (Appendix D.9). These discounts reflect the less onerous requirements on the components in the dual-band implementation, due to the smaller fractional bandwidth and the 180 MHz frequency split between the low and high bands.

The opposing trend is that the smaller average number of beams across the band puts downward pressure on the dual-band cost. This is reflected in the lower cost of the station beamformer, station bunker and station–CPF data transmission sub-systems. The cost reduction is significant for the all-digital architecture, but is less pronounced for the RF tile beamforming architecture, where the reduced number of digital signal paths already decreases the digital processing and data transport costs somewhat.

A conspicuous feature of Figure 7 is that the station beamforming and related bunker cost in the reference class LOFAR estimate is significantly larger than the bottom-up SKADS estimate. This is due to the large difference in unit cost estimates (see Appendix D.6.1). The most likely reasons for this cost discrepancy are related to the type of beamforming processing technology and architecture, and the technology advancements which have been assumed. For example:

- The LOFAR beamformer is not optimised for processing the larger number of inputs, hence the unit cost derivation may over-estimate the processing cost.
- The unit cost derived from the bottom-up SKADS estimate already includes a cost discount for hierarchical beamforming (see Appendix D.6.2).
- The LOFAR station beamformer uses field-programmable gate array (FPGA) processors, while the SKADS design (Faulkner et al., 2010) uses more customised processing chips.
- The technology advancements may be more optimistic for the SKADS estimate than those assumed for the LOFAR estimate (p 9), and production would be for larger quantities than for LOFAR.

The station beamformer cost is an example of the potential for further investigation to determine: the accuracy and uncertainties of each of the cost data sources and their subsequent derivation into unit costs, the accuracy of the first-order station beamformer model, the requirements that contribute to the beamformer cost and design solutions or trade-offs to reduce this cost.

4.3 Cost reduction from analogue (RF) tile beamforming

While not the main focus of this work, the parametric analysis allows a preliminary cost comparison to be made between the two intra-station architectures: RF tile beamforming and all-digital beamforming. The results show that for tiles composed of 16 elements, a first stage of analogue tile beamforming significantly reduces the station hardware cost. The cost reduction is irrespective of whether a single or dual-band system is implemented, or the bottom-up SKADS or reference class LOFAR cost estimate is used.

The station costs for RF tile and all-digital beamforming architecture can be compared in Figure 7, for the single and dual-band implementations and reference class LOFAR and bottom-up SKADS cost estimates. Table 6 makes a direct comparison for each implementation and cost estimate combination. The cost of the SKA₁-low sub-systems with analogue tile beamforming is 20–67% of the all-digital beamforming; a factor of approximately 1.5–5 reduction in cost. The cost reduction, both in relative and absolute (euro) terms, is most significant when the cost of the digital sub-systems is high (e.g. the single-band implementation of the reference class LOFAR cost estimate). However, no cost reduction applies to the sub-systems in the central processing facility; because those sub-systems act on station beams, their costs are independent of the intra-station architecture.

Table 6: SKA₁-low station cost for RF tile beamforming, as a percentage of all-digital beamforming cost.^a

Cost estimate	Implementation	
	Single-band	Dual-band
Reference class LOFAR	20 %	41 %
Bottom-up SKADS	57 %	67 %

^a Percentage shown applies to that cost estimate and implementation combination.

The cost reduction is due to the FoV accessible at the station beamformer (and inherent observational flexibility) being restricted early on in the signal path; the number of digital signal chains is reduced by a factor equal to the number of elements per tile, in this case 16. The cost of the digitiser and station beamformer blocks is thus reduced, as can be seen in Figure 7. This is because fewer digitiser and digitiser–bunker links are required, and fewer inputs into the station beamformer reduces the processing load. The performance reduction due to tile beamforming is further discussed in Section 7.3.2.

Faulkner et al. (2010) present a qualitative comparison of the all-digital and RF tile beamforming approaches. The all-digital beamforming is more flexible, in terms of generating multiple beams, RFI excision and calibration of the antenna elements, if needed. With upgraded digital signal transport and processing, the correlation of every antenna element is also possible; whereas only the RF beamformed tiles can be correlated, not the individual elements. The main disadvantage for the all-digital beamforming approach is cost, as outlined, as well as the increased power demand of the digital components, and the distribution (or local generation) of this extra power throughout the array. This is further discussed in Section 7.3, in the context of the intra-station architecture.

5 System implications of variable costs

The results thus far present the costs of the SKA₁-low station hardware for each scenario and representative implementation. However, there are other cost implications on the telescope system, some of which are considered in this section. To put the costs analysed here in the context of the whole SKA budget, the simplest comparison between the single and dual-band implementations is to say that some costs remain approximately constant, such as project overheads, and some costs vary between the two implementations, such as the SKA₁-low stations costed in Section 4.

The variable costs considered in this analysis to most significantly impact on the total system cost are:

- station sub-systems
- antenna element deployment
- site preparation
- central processing sub-systems
- power provision and distribution.

There is no published work on the relative cost between these, hence the full effect of each implementation on the total cost is difficult to determine. However, the different attributes of the two implementations, as shown in Table 7, gives some insight into the cost trends. Appendix F makes a more detailed analysis of these variable costs and estimates some zeroth-order costs.

5.1 Antenna element deployment and site preparation costs

The cost of deploying the antenna elements (i.e. building the array on-site) will be higher for the representative dual-band array, because twice the number of antenna elements need to be deployed. Because the element size is defined by being sufficiently electrically large at the lowest observing frequency, it is reasonable to expect that the size of the low-band element will be similar to the single-band element,

Table 7: Attributes of the dual-band implementation compared to the single-band.

Attribute	Percent of single-band
Number of antenna elements	200 % ^a
Physical area	125 %
Average number of station beams ^b	30 %

^a Half these elements are physically smaller than the single-band elements.

^b Formed over the full 70–450 MHz band to achieve 20 deg².

such that comparable antenna gain is obtained. However, the high-band element will be significantly smaller, and cheaper manufacturing and deployment options may be available. This means that the increased deployment cost for the dual-band array would be less than 200 %. Deployment is further discussed in Faulkner et al. (2011).

On a related topic, it is reasonable to expect that some fraction of the site preparation cost will increase with the physical area occupied by SKA₁-low. However, whether this cost is significant relative to the total site preparation costs is not known. Site-related data is being collected as a part of the site selection process (Schilizzi et al., 2011) and is not currently available. We have used the initial deployment and site preparations cost estimates outlined in Section 5.3 to illustrate their potential significance.

5.2 Central processing facility sub-systems

The central processing facility is a broad term to encompass the signal processing and science computing sub-systems in the HLSD. The processing is centralised, because it acts on signals from all the antennas (AAs and dishes) in the array. However, it does not necessarily imply that all these sub-systems will be on-site; the on-site processing is required to sufficiently reduce the rate of data sent to the off-site processing. The principal sub-systems are the correlator and imaging processor, and the non-imaging processor. The correlator and non-imaging processor costs are derived the Signal Processing Concept Design Review, as collated in Turner (2011). These costs focus on the processing units required (the sub-system hardware), rather than total cost of the sub-systems. The parametric cost equations of the major sub-systems within the central processing facility are derived in Appendix F.2; the assumption being that these sub-systems operate on a ‘per beam’ basis.

Table 8 summarises the relative costs between the representative single and dual-band implementations. The difference in cost between the two implementations is due to the larger beam size of the smaller (90 m) diameter high-band station. This reduces the number of station beams required to fill 20 deg² FoV, resulting in lower central processing facility costs. To ensure comparable performance between the single and dual-band implementations, 20 deg² FoV over the full 380 MHz bandwidth is correlated and imaged. Following Alexander et al. (2009), the cost of the imaging processor is assumed to be dominated by the cost of the data buffer rather than the imaging operations; these imaging processing costs are discussed further in Appendix F.2.4. The non-imaging processor acts on phased or ‘tied’ array beams formed from the densely packed core stations, and is further described in Appendix F.2.5. Only array beams formed with the high-band core of the dual-band implementation are considered, because the current required frequency range for pulsar surveys with the non-imaging processor is 0.3–3 GHz (SSWG, 2011).

A key aspect of the correlator–imaging data transport and imaging processor cost is that for SKA₁-low, the correlator frequency resolution requirement is derived from the more stringent science requirements, rather than from the requirement to keep radial (u, v) smearing below an acceptable threshold (see Appendix F.2.1). If instead the latter dominates, then the correlator output data rate becomes independent of station diameter, for a fixed processed FoV. In that case, the imaging processor is therefore the same for the single and dual-band implementations.

Table 8: Dual-band implementation central processing sub-system costs, compared to the single-band.

Central processing sub-system	Percent of single-band
Correlator	30 %
Correlator–imaging data transport ^a	53 %
Imaging processor ^{a, b}	53 %
Non-imaging processor (NIP) ^c	25 %

^a Required correlator frequency resolution is derived from the science requirements (Appendix F.2.1).

^b Cost dominated by data buffer (Appendix F.2.4).

^c Only the high-band core is used in the NIP, and the processing for the AAs, not the dishes, dominates the cost (Appendix F.2.5).

Table 8 only applies to items such as processing components (and associated hardware and cooling), the cost of which, as a first-order approximation, scales linearly with the processing load. Correlator and non-imaging processing costs are summarised in Turner (2011), representing a range of processor technologies and architectures. Those costs are highly dependent on the processing technologies and the trade-off between efficient processing devices with larger development (non-recurring engineering) costs, and less efficient but more flexible processing devices.

5.3 Overall SKA₁-low costs

Although obtaining accurate total costs of the single and dual-band implementations is not yet possible, some zeroth-order estimates can be used to illustrate the system-level costs outlined in this section. Figure 8 plots these significant variable system costs (excluding power) for single and dual-band implementations. The plot includes the four different station cost scenarios, reflecting the different cost estimates, and intra-station signal transport and processing architectures. The variable and ‘other’ costs remain unchanged for each scenario; they are independent of the intra-station architecture and station cost estimates. The correlator–imaging data transport cost is not significant (<1%) and is not plotted. To indicate the sensitivity of the comparison to changes in the deployment and site preparation costs, Figure 9 is a similar plot, but the deployment cost is doubled to €100 per antenna element, and the site preparation cost increased by an order of magnitude to €100 m⁻².

5.4 Power costs

Investigations for the provision and distribution of power for the SKA are on-going (e.g. Hall, 2011), alongside analyses of the power demand of the telescope sub-systems. Although the details of supplying and distributing power are beyond the scope of this document, simplified power demand estimates are possible with the parametric models. To make a zeroth-order estimate of the power costs for the SKA₁-low stations, it is reasonable to expect that the power demand of each sub-system is linearly proportional to one or more of the following:

- number of antenna elements
- digital processing load
- number of station beams formed, hence data rate transmitted from the stations to the CPF.

Figure 10 shows power demand, estimated from the bottom-up SKADS power budget in Faulkner et al. (2011). The ‘unit power demand’ is parametrised, as was done for the cost data, and listed in Appendix F.3. The power budget is for the all-digital station architecture, but is extrapolated to the RF tile beamforming architecture by including an estimate for the RF beamformer power demand.

The station power demand depends on both the implementation and intra-station architecture. The dual-band implementation reduces the station beamformer power demand, but the demand of the other

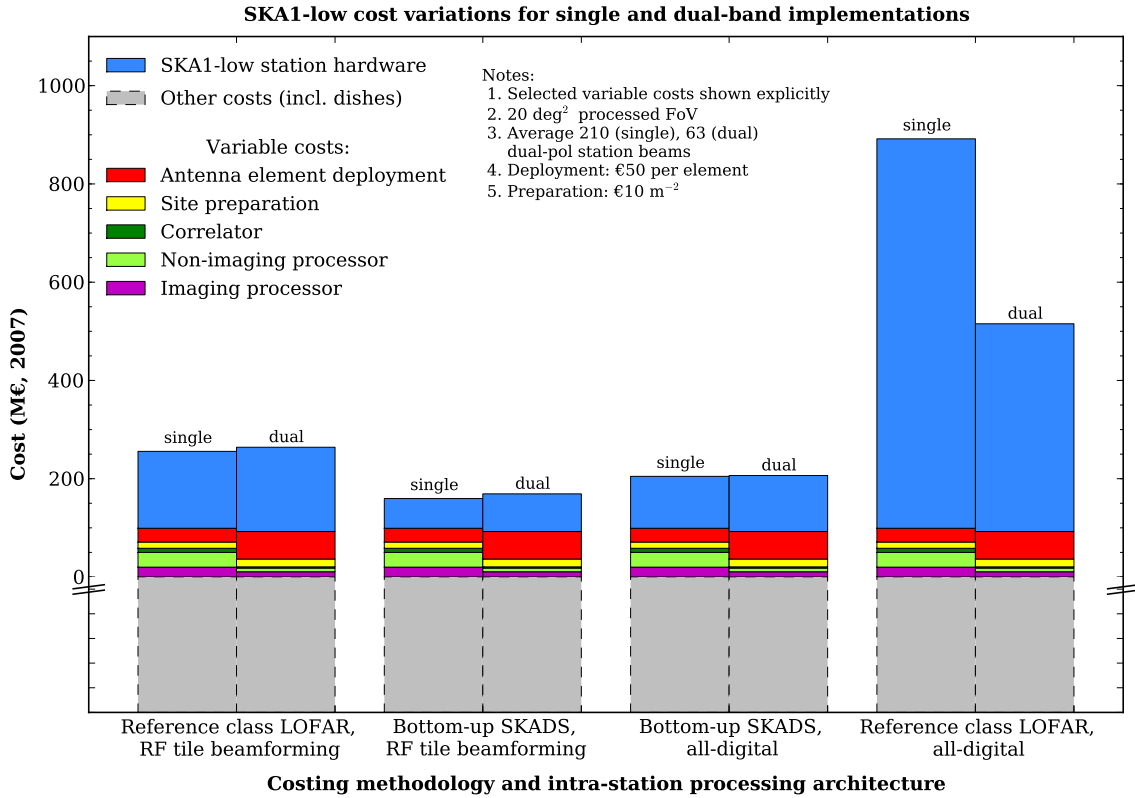


Figure 8: Significant variable costs (excluding power) for the representative single and dual-band implementations of SKA₁-low, for the different cost estimates and intra-station architectures. A deployment cost of €50 per element and site preparation cost of €10 m⁻² is assumed. ‘Other costs’ is a placeholder for the costs which do not differ between implementations.

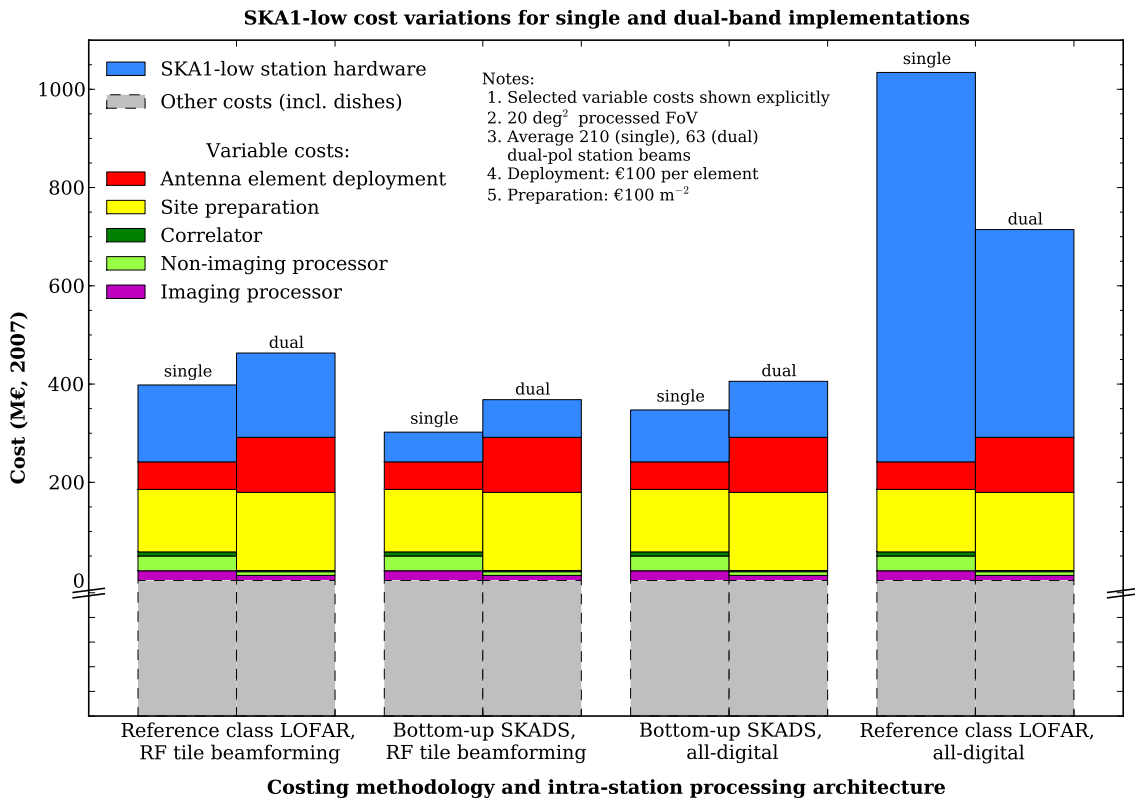


Figure 9: As per Figure 8, except a deployment cost of €100 per element and site preparation cost of €100 m⁻² is assumed.

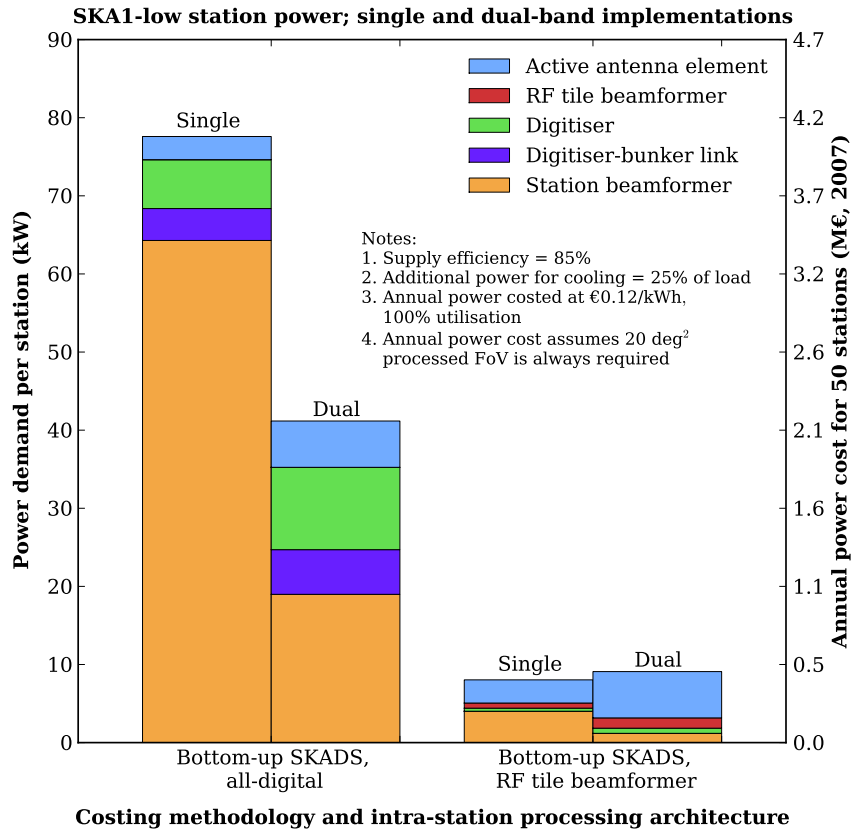


Figure 10: Single SKA₁-low station power demand estimate and annual power cost for single and dual-band implementations, and RF tile beamforming and all-digital intra-station processing. As per Faulkner et al. (2011): i) the power supply efficiency is assumed to be 85% (a 1/0.85 increase in power demand); and ii) an additional 25% power demand is applied to account for cooling the hardware. Power consumption is costed at €0.12 per kWh (Hall, 2011) and assumes 100% (continuous) utilisation of the hardware.

station sub-systems is increased. For the all-digital architecture, this results in a significantly lower power demand for the dual-band implementation. But for the RF tile beamformer architecture, there is little difference between implementations. Rather, the demand reduction from RF tile beamforming is the dominant effect.

The method, hence cost, for supplying the power demand of sub-systems within the station will depend on the intra-station architecture, as discussed in Section 7.3.3. The intra-station power distribution cost and power supply inefficiencies depend on load and distance, making the cost specific to each intra-station architecture. For example, in the RF tile beamforming architecture, power at the antenna elements is supplied via the RF link to the station. In contrast, the all-digital architecture transmits data via optic fibre, hence requires additional power distribution cabling (which is not costed here). Some architectures do not even have intra-station distribution costs, because the active antenna elements are self-powered. Bearing these caveats in mind, Figure 10 assumes an 85% supply efficiency, and includes a power consumption cost of €0.12 per kWh for illustrative purposes.

For the central processing facility, the absolute power demand depends on the technologies used; in general, there is an inverse relationship between the flexibility and power efficiency of the processing (Hall, 2011). But given that both cost and power demand increase with the amount of processing required, the values in Table 8 can be taken as an indication of the relative power demand between the single and dual-band implementation: the central processing facility power demand is lower for the dual-band implementation.

6 Discussion of principal analysis

The merits of single and dual-band implementations of SKA₁-low can be considered in terms of performance, cost and design flexibility. This section summarises the cost and performance trends, and the cost estimation uncertainties. We also discuss the challenge of designing a single-band implementation which meets the sensitivity requirements at the lower frequencies and achieves a sufficiently high filling factor (a measure of array sparsity), which may assist in calibration at the higher frequencies.

6.1 Cost trends

The cost difference between the single and dual-band implementations is fundamentally a comparison between costs that scale with the number of signal paths prior to station beamforming and costs that scale with the number of station beams. The single-band station is very sparse at high frequencies, requiring many more beams than the dual-band station to meet a given FoV requirement. This not only increases the station beamformer and bunker cost, but also the station-central processing facility (CPF) data transmission and central processing facility sub-system costs. The dual-band implementation has twice as many signal paths prior to station beamforming, which increases cost. However, this cost is less than double that of the single-band, primarily because the smaller fractional bandwidth entails less demanding design specifications for the active antenna elements.

The dual-band array decreases the total number of station beams to be formed, thereby reducing the corresponding signal processing costs. The decrease in the number of beams comes about from the smaller high-band station diameter. However, this is predicated on the system having sufficient processing capacity to concurrently form and process the number of beams corresponding to 20 deg² FoV across whole 70–450 MHz band. If less processing capacity is required for the high-band array, the cost advantage when implementing the dual-band array is lessened. This is further investigated in Section 7.2.

A related effect is the inter-element spacing chosen for the high-band array. A smaller inter-element spacing further reduces diameter, and therefore cost. However, this ultimately begins to reduce the high-band array sensitivity, as discussed in Appendix G.1. The frequency split of the dual-band array is another factor. The key metric of the average number of beams per station ($\overline{N_{b-st}}$) not only depends on inter-element spacing, but also the frequency split between the low and high-band arrays, as shown in Appendix E.2. The frequency split also affects the cost of the active antenna elements and digitiser (Appendix D.9), as they depend on minimum and maximum frequencies of each band, and the fractional bandwidth.

For the representative single and dual-band implementations, there are not significant differences in station hardware costs, except for the reference class LOFAR, all-digital beamforming scenario. But the variable costs which impact the system (Section 5) may be a discriminating factor between implementations. As discussed, the dual-band implementation lowers the cost of the CPF sub-systems. However, the increased number of active antenna elements and the extra area required for these elements increases the deployment and site preparation costs.

Power costs also bear careful consideration; capital cost may be significant and power is a major operations cost. Our study shows the station power demand of the dual-band implementation equals that of the single-band when RF tile beamforming is used, and is less than the single-band with the use of all-digital beamforming. The RF tile beamforming itself significantly reduces power demand for both implementations. For the CPF, the dual-band implementation reduces the power demand.

There are also some cost trends which depend on the intra-station architecture, but which do not affect the other variable costs which impact the system. The noteworthy trend is the significantly lower station cost for RF tile beamforming compared to all-digital beamforming. In fact, the differences in station cost between these architectures is more significant than the differences between the single and dual-band implementations. Also, Bij de Vaate et al. (2011) discusses a dual-band implementation which shares a common processing system to reduce processing requirements, although exactly how this sharing occurs

is not specified. While not specifically costed in this analysis, alternative intra-station architectures (including shared processing) are discussed in Section 7.3.

6.2 Performance trends

The performance characteristics of the canonical dual-band implementation used in this analysis is comparable to the single-band implementation described in the SKA₁ high level system description. This is achieved by using separate low and high-band arrays, observing simultaneously, to create a 20 deg² processed FoV over the 70–450 MHz band, while maintaining a sensitivity curve across the band which is similar to the single-band implementation. However, these representative implementations are not optimised for performance.

The performance and design flexibility of the implementations is compared in Bij de Vaate et al. (2011) and potential performance issues for the single-band system are identified. In particular, an antenna element design suitable for the wide fractional bandwidth of about 6.5:1 is required. The antenna must then be matched to the low noise amplifiers (LNAs) across the frequency band, which is more difficult for the wide fractional bandwidth. These steps are less challenging for the dual-band implementation, with the 2.5:1 fractional bandwidth in each band.

Another key performance issue is the frequency-dependent sensitivity (A/T) curve; the frequency range for which the sensitivity is optimised is a high-level design issue (Alexander & Hall, 2010). Figure 23 of the HLSD makes a simple estimation of sensitivity for SKA₁-low; this curve is replicated in Appendix G.1 (Figures 17 and 18). A key feature of the curve is that the sensitivity is lowest at the minimum (70 MHz) and maximum (450 MHz) frequencies of the band, with a peak between 100 and 200 MHz; there is also a factor of 3 difference between the highest and lowest sensitivity values.

Appendix G.1 shows the effect of inter-element spacing on sensitivity. In the single-band implementation, the inter-element spacing must be chosen to best satisfy requirements across a larger band, resulting in sub-optimal spacing at the lowest and highest frequencies in the band. At 70 MHz, the sensitivity is limited by the 1.5 m inter-element spacing. At 450 MHz, the 1.5 m spacing means that more beams are required to form the 20 deg² processed FoV, increasing the processing costs, as discussed in Section 6.1.

The dual-band implementation uses a smaller inter-element spacing in the high band, thus it can achieve beamformer cost savings in the high-band, while maintaining similar sensitivity to the single-band implementation. The only exception is the reduced sensitivity between 180 and 230 MHz. Another aspect of the dual-band flexibility is that a different number of antenna elements could potentially be used in the low and high band arrays, to better suit sensitivity requirements.

A single-band implementation may also present a greater calibration challenge than a dual-band array. As detailed in Appendix G.2, station calibration requires a sufficiently high filling factor so that enough calibration sources are detectable within a station beam FoV. At 400 MHz, the filling factor of the single-band station is too low to detect the required number of calibration sources. The representative dual-band implementation solves this problem because the filling factor for the high-band station is greater.

6.3 Risk and uncertainty

The modelling of uncertainties is an often overlooked aspect of the performance and cost analysis. However, these uncertainties can manifest themselves as project risks. As mentioned in Section 3, the parametric cost estimate should provide an associated uncertainty estimate, which is large in the early stages of the project. As the project progresses, the cone of uncertainty reduces and the cost estimate eventually converges on the actual cost. This section discusses the station hardware cost uncertainties and makes an initial uncertainty estimate for the reference class LOFAR, RF tile beamforming scenario.

6.3.1 SKA₁-low station uncertainties

The range of cost estimates for the SKA₁-low station hardware give some indication of how sensitive the single and dual-band implementations are to different cost projections. Table 9 provides a summary of

Table 9: Comparison of SKA₁-low station cost for the single and dual-band implementations.

Cost scenario		Implementation ^a		Dual to single-band ratio
		Single-band	Dual-band	
RF tile	Reference class LOFAR	100 %	110 %	108 %
beamforming	Bottom-up SKADS	39 %	49 %	127 %
All-digital	Bottom-up SKADS	68 %	73 %	110 %
beamforming	Reference class LOFAR	506 %	270 %	53 %

^a Percentage of the single-band, reference class LOFAR, RF tile beamforming scenario.

the single and dual-band station costs plotted in Figure 7. All costs are normalised to the cost of the reference class LOFAR, RF tile beamforming scenario of the single-band array. For each cost scenario, the table shows the normalised total for each implementation and the ratio of the dual-band station cost to the single-band. For three of the scenarios, the dual-band station is more expensive than the single band, while for the fourth, the opposite is true.

In Table 9, there is a factor of 7.5 difference between the reference class LOFAR and bottom-up SKADS cost estimates of the all-digital, single-band implementation, and a factor of 3.7 for the dual-band. For the scenarios with RF tile beamforming, the difference is a factor of 2.6 and 2.2 for the single and dual-band respectively. Some of the unit costs only have a single data source (estimate) and are used for both cost estimates; those costs do not contribute to the cost differences. Some potential reasons for the cost differences were discussed in Section 3.3, but this is an area for further investigation.

Importantly for the single and dual-band comparison, the range in the relative station hardware costs between the two representative implementations (as indicated by the final column of Table 9) is much lower than the range of absolute station hardware costs. This implies that the uncertainty of the single and dual-band station cost comparison is less than that of the individual station cost estimates.

6.3.2 Sensitivity analysis: cost drivers

The parametric model allows for sensitivity analysis of the inputs, to determine which blocks in the system significantly affect the total cost. By identifying these cost drivers, extra attention can be paid to them during the design phase, thereby reducing risk (NASA, 2008). Sensitivity analyses can also involve assessing the impact of changed requirements.

Within the context of the SKA₁-low stations, an inspection of Figure 7 gives an indication of the cost drivers. The dominant blocks are the active antenna element, digitiser–bunker links and the station beamformer and bunker. For both the single and dual-band implementations, the active antenna element is the largest cost block, except in the reference class LOFAR, all-digital beamforming scenario where the station beamformer and bunker costs dominate. For the bottom-up SKADS, all-digital beamforming scenario, the digitiser–bunker links are the second most costly block. However, the large variation of the cost of many of the blocks between the scenarios indicates that the cost estimates require further refinement before a conclusive set of cost drivers can be determined. The drivers also depend on the intra-station architecture, as discussed in Section 7.3.

Additionally, the other variable costs listed in Section 5 have the potential to be cost drivers in the comparison of single and dual-band implementations, and could exceed the most costly individual station sub-system. For example, Figures 8 and 9 in effect form a rudimentary analysis of the sensitivity of the SKA₁-low cost to changes in variable antenna element deployment and site preparation costs.

6.3.3 Statistical uncertainty analysis

Monte Carlo simulation provides a statistical approach for uncertainty analysis, using probability distribution functions (PDFs) for each ‘uncertain’ input in the parametric model. An input, for example, may

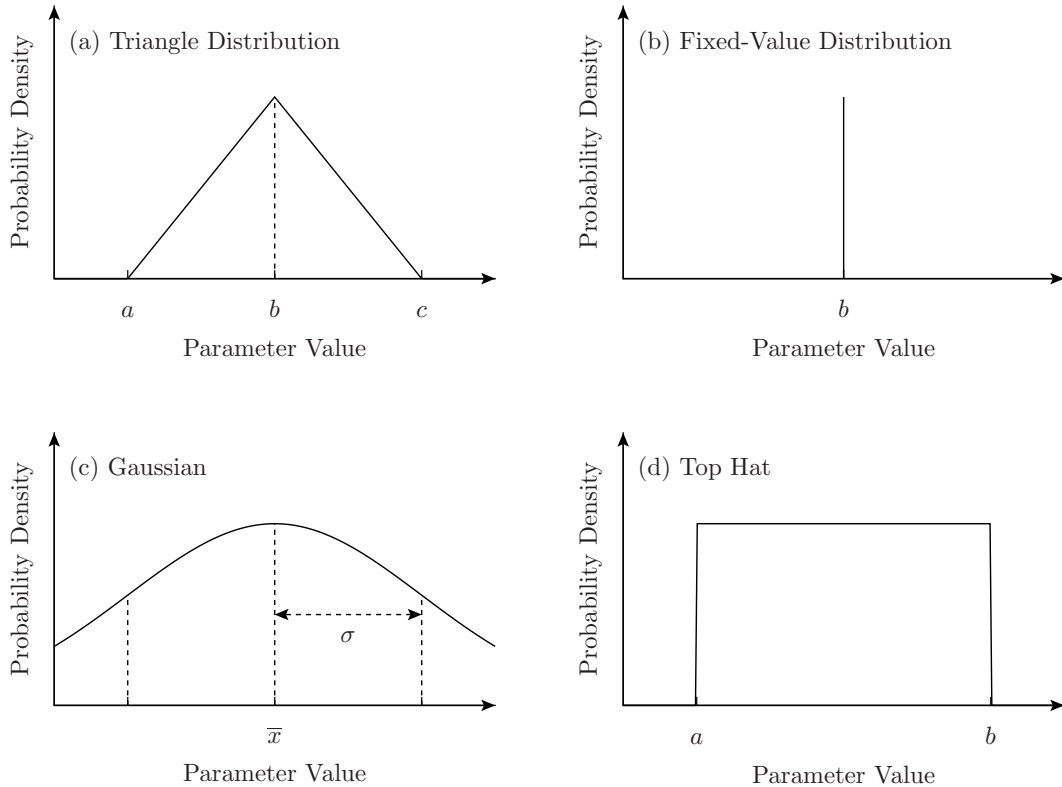


Figure 11: Input probability distribution functions (PDFs) available in SKACost. The PDF of a value may be described by (a) minimum a and maximum c possible values, with a peak-likelihood value of b ; (b) single-value at b ; (c) value with mean \bar{x} and standard deviation σ ; or (d) value ranging between minimum a and maximum b . Source: Ford et al. (2010)

be a variable parameter (such as number of elements per station) or a unit cost. The simulation then randomly picks values from these input PDFs and calculates a point cost estimate. Over thousands of iterations, this results in a new PDF which is the cost estimate with a statistical distribution (NASA, 2008). Monte Carlo uncertainty analysis has been implemented in SKACost (Chippendale et al., 2007; Ford et al., 2010); Figure 11 shows the input PDFs available in SKACost.

Although the input unit cost distributions require further expert attention, we make an initial estimate of the uncertainty of the reference class LOFAR, RF tile beamforming scenario. For this estimate, we only consider the uncertainties of the two largest costs; the active antenna elements and the station beamformer processing. For the active antenna element (which includes the ground plane), a triangular probability distribution function is applied, where the minimum unit cost is that derived from the bottom-up SKADS estimate (€75 per element), the most likely unit cost is that derived from the reference class LOFAR estimate (€172 per element) and the maximum cost is twice that (€344 per element). For the station beamformer processing and the portion of the bunker which scales with the amount of processing, a top-hat cost distribution is applied, because the most likely unit cost is unknown at present. The top-hat probability distribution function is used when only the minimum and maximum values are known, and the true cost could lie anywhere, with equal probability, between these limits. We use the unit processing cost derived from the bottom-up SKADS estimate (€0.1 per beamformer input per output beam) as the minimum value and the reference class LOFAR estimate (€2.6 per beamformer input per output beam) as the maximum value.

Figure 12 shows the resulting PDF of the Monte Carlo analysis of the reference class LOFAR, RF tile beamforming scenario with the above-mentioned input PDFs. The station cost is €3.1 (+0.8, -0.6) M (these percentiles are equivalent to the mean and 1 standard deviation of a Gaussian curve, 50% and 15.9%, 84.1% respectively). Figure 13 plots this mean and error onto the station hardware cost breakdown. For comparison, the single-value station cost plotted in Figure 7 is €3.1 M. With due consideration

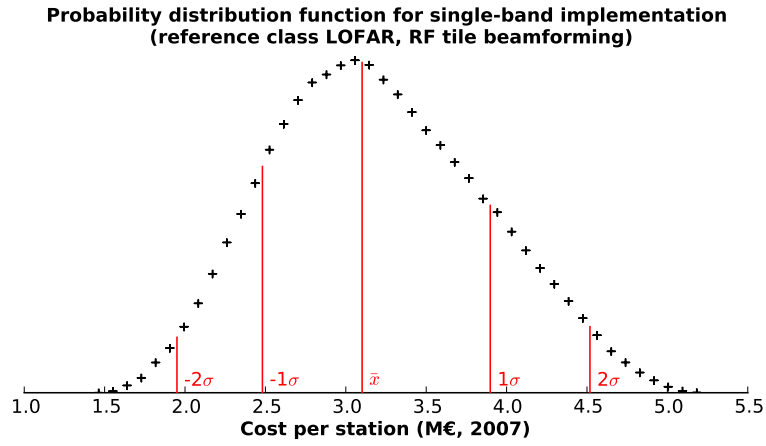


Figure 12: Probability distribution function for the single-band implementation of the reference class LOFAR, RF tile beamforming scenario, as calculated using SKACost. The crosses show the probability density for each sample bin and the red lines show the percentiles equivalent to the mean and 1 and 2 standard deviations of a Gaussian distribution. Refer to the text for the input probability distribution functions used.

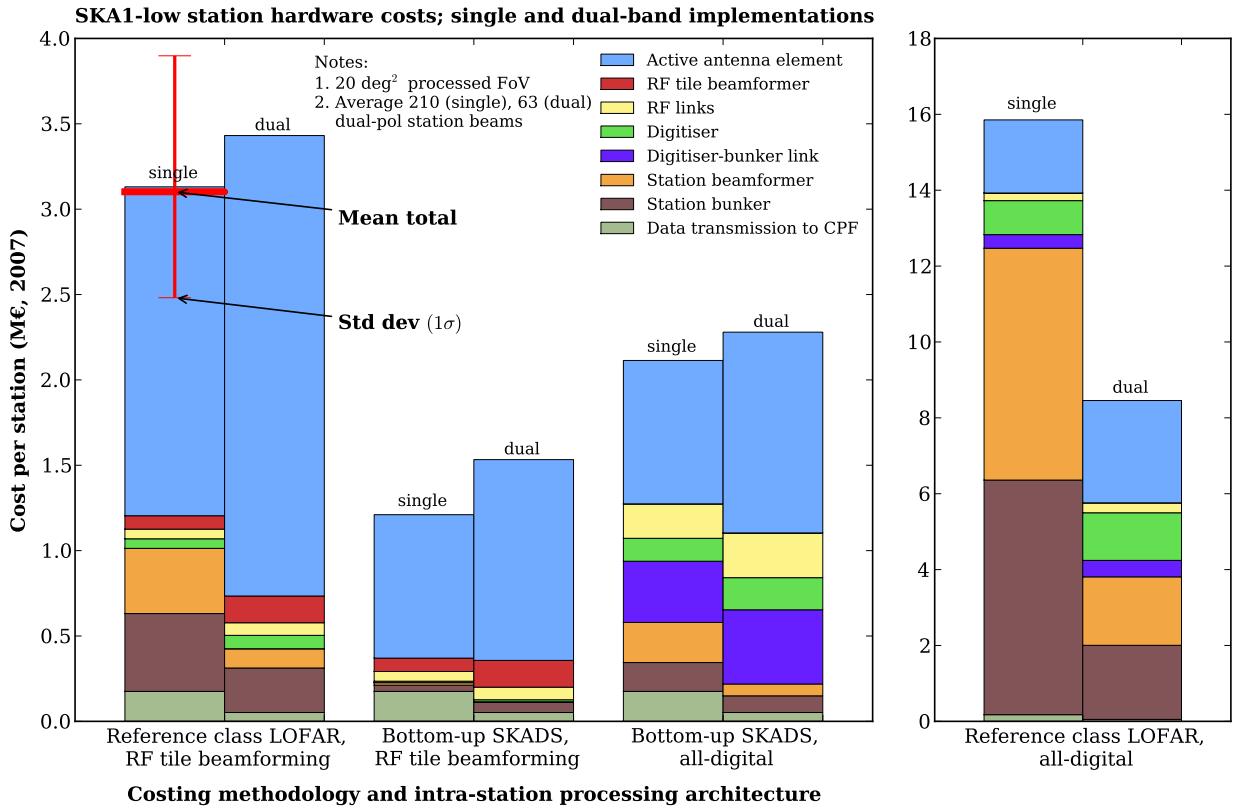


Figure 13: SKA₁-low station hardware cost as per Figure 7, but with the mean and 1σ error bars from Figure 12 shown for the reference class LOFAR, RF tile beamforming scenario.

of the PDFs of the major costs, similar uncertainty analyses can be made of the other station scenarios, and also the other variable costs (Section 5).

6.4 Relevance to SKA Phase 2

This parametric modelling analysis is applicable to SKA Phase 2 (SKA₂), although the unit costs and scientific requirements will differ. SKA₂ will most likely use the low-frequency receptors defined for SKA₁. If the intra-station signal transport and processing architecture is similar, then the parametric equations for the station hardware costs (Appendix D) will still apply. The main difference will be the cost for each

block. Although the cost of the digital blocks will reduce, the FoV requirements for SKA₂ will be much higher. Thus, it is possible that any digital cost reductions will be offset by the extra digital processing needed to form many more station beams to achieve the required FoV. For the other attributes shown in Table 7 (number of antenna elements, physical area and average number of station beams), the ratio between the two implementations still holds, regardless of required FoV. The same applies to the central processing facility costs (Table 8).

The SKA₂ science requirements must also be kept in mind when comparing the single and dual-band implementations. These requirements may place a difference emphasis on the frequency-dependent sensitivity and FoV performance, compared to SKA₁; this may affect the optimal inter-element spacing. While shorter term gains might be made by optimising the design for SKA₁, there may be implications for SKA₂ cost and performance which necessitate further investigation.

7 Supplementary analyses

In this section we extend our analysis to include some topical factors important to the design of the SKA₁-low system.

7.1 Varying station diameter

The HLSD discusses a potential change to the SKA₁-low system, where diameters smaller than 180 m are used, but the number of stations N_{st} is increased to maintain the SKA₁-low array effective area $A_{\text{e-arr}}$, thus sensitivity. The problem is posed as a trade-off between aperture array station diameter and the number of stations (where $N_{\text{st}} \propto 1/D_{\text{st}}^2$). But as Appendix G.3 shows, station diameter is not an independent parameter, because $D_{\text{st}} \propto \sqrt{N_{\text{e/st}}d_{\text{avg}}}$, where $N_{\text{e/st}}$ is the number of elements per station and d_{avg} is the average inter-element spacing. Assuming d_{avg} remains constant, a more exact description is that the number of elements per station is traded with the number of stations.

To illustrate the cost sensitivities of this N_{st} vs. $N_{\text{e/st}}$ trade-off, Appendix H considers a simple comparative example, where the diameter of every single-band, low-band or high-band station is halved (reducing $N_{\text{e/st}}$ by a factor of 4), which results in N_{st} increasing by a factor of 4 to maintain $A_{\text{e-arr}}$. The inter-element spacing for each band remains constant.

The hardware cost of the SKA₁-low stations shows no dominant trend between the smaller stations and their full-sized counterparts (Figure 19, p 56). For both the single and dual-band implementations, reducing the station diameter:

- decreases the total station beamformer cost and variable bunker cost
- decreases the total cost of links from the antenna element or tile to the processing bunker
- increases the total fixed bunker cost.

The effect of these trends on the total cost of the stations depends on the implementation, intra-station architecture and cost data source. However, given the cost uncertainty discussed in Section 6.3, there is no dominant trend for the station hardware cost of the smaller stations relative to their full-size counterparts; only the single-band implementation of the reference class LOFAR, all-digital beamforming scenario shows a significant change in total station hardware cost. (In this case a reduction in cost.)

Of the variable costs outlined in Section 5, only the correlator and imaging processing costs change with the N_{st} vs. $N_{\text{e/st}}$ trade-off; they increase by a factor of 4 and 8 respectively (Figure 20, p 57). The deployment and site preparation costs are unchanged, because the total number of antenna elements in the array remains constant. Although the correlator and the imaging processor become significant costs for the half-diameter station example, these are zeroth-order estimates. If smaller stations are being considered, more detailed investigation is required as to the accuracy of using the correlator output data rate as a proxy for the imaging processor cost scaling, and of the correlator and processor cost estimates themselves.

Cost is not the only factor to consider; there is also the effectiveness in meeting science requirements. For example, meeting (u, v) coverage requirements can depend on increasing N_{st} (e.g. Bolton et al., 2009a; Lal et al., 2009). But distributing the extra stations to improve (u, v) coverage will likely have additional infrastructure costs (Bolton et al., 2011). To not disadvantage the half-diameter example, we have chosen not to analyse a more widely distributed array configuration in this study. For stations within the core, Appendix H.3 discusses how N_{st} may be efficiently increased by creating a number ‘logical’ stations, each with fewer elements, which share a processing node and form a ‘physical’ station. However, any requirement to increase N_{st} needs to be traded with the signal processing costs; in such a trade-off, the hardware prior to the station beamformer is not a cost driver, but the imaging processor (and to some extent the correlator) has the potential to be a large cost driver.

7.2 Reducing the FoV requirement: defining a fixed beam–bandwidth product

Other trade-offs are emerging through analysis of the SKA₁ Design Reference Mission (DRM₁). DRM₁ captures the set of observations required to achieve the SKA₁ science goals and forms an ‘envelope’ of technical requirements for the telescope. One possible performance–cost trade-off is to reduce the SKA₁-low signal processing capacity, defined by the product of the bandwidth and the average number of station beams formed. In this approach, the processing capacity only meets the beam-bandwidth product required by the most demanding science application in DRM₁. In contrast, the SKA₁ high level system description (HLS) and the results presented thus far assume sufficient signal processing capacity to concurrently observe 20 deg^2 of processed FoV over the entire 70–450 MHz band.

To understand the cost advantages from such a trade-off, Appendix I considers the cost of a strawman design, where the representative single and dual-band implementations are modified such that the signal processing capacity is defined by the requirement to only observe 20 deg^2 across the 70–180 MHz band, resulting in a beam-bandwidth product of 4.8 GHz. By comparison, the beam-bandwidth capacity of our canonical single and dual-band implementations are 80 GHz and 24 GHz respectively, the latter being smaller because fewer beams are required in the 180–450 MHz frequency range to form the 20 deg^2 FoV.

Figures 22 and 23 in Appendix I show that for such a strawman, the cost of the sub-systems which scale with the number of station beams are no longer significant (those being the station beamformer and station–CPF transmission, as well as the correlator and imaging processor). The costs which dominate are those which scale with the number of antenna elements. Thus the dual-band implementation, with twice the number of elements, is more expensive in all scenarios, although the increase is less than the factor of two increase in cost which one might naively expect for twice the number of elements. However, this difference still makes the trade-off potentially significant.

7.3 Intra-station signal transport and processing architecture considerations

The scalable high-level view of the system, which follows the elemental signal path (Section 3), allows for the realisation of various signal transport and processing architectures. Section 3.3 describes the architectures used in this analysis, but a greater number of data transport and processing architectures are conceivable, through the combination of:

- using different technologies to perform the sub-system function
- rearranging the order of the sub-systems in the signal path
- changing physical location the sub-system.

Table 10 shows the most relevant options for intra-station signal transport and processing architectures. Although comparing the cost-effectiveness of the different architectures is beyond the scope of the present analysis, this section discusses the performance and cost implications of some of these architectures, focusing on the hierarchical beamforming and power supply aspects. Some architectures are also discussed in Faulkner et al. (2010), Bij de Vaate et al. (2011) and Faulkner et al. (2011).

Table 10: Principal options for intra-station architectures.^a

Sub-system	Physical location	Technology
Digitiser	receptor, tile or station	N/A
Tile BF (optional)	tile or station	RF or digital
Signal transport	receptor–tile and tile–station, or receptor–station	RF or digital
Station beamformer	station node, or node serving multiple stations	digital

^a The options listed illustrate the range of signal transport and processing architectures. This does not imply that every architecture would meet all the SKA₁-low requirements, nor is every option listed.

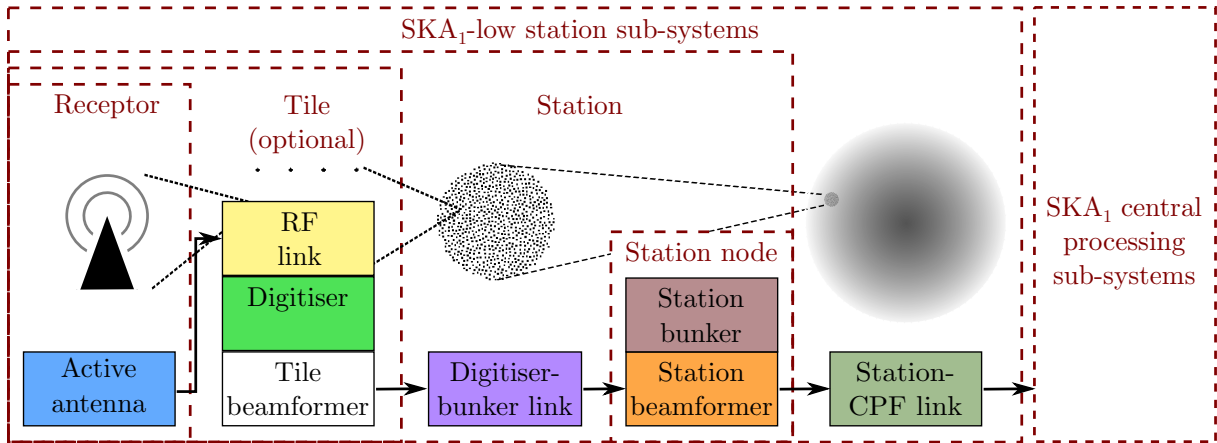


Figure 14: Schematic of the all-digital beamforming architecture, with a digital tile beamforming block located at the tile.

7.3.1 Digital hierarchical beamforming

Some caution needs to be applied to the comparison between the analogue tile and all-digital beamforming made in Section 4.3. This is because alternative intra-station architectures using hierarchical, or multi-stage, all-digital beamforming also have the potential to reduce cost. For the all-digital architecture in Figure 3, the digitised signal from every antenna element is transmitted to the station beamformer block and both the tile and station stages of beamforming are located in that block.

An alternative all-digital beamforming architecture is shown in Figure 14; this more closely represents the all-digital architecture in Faulkner et al. (2011). The architecture performs the first stage of digital beamforming at each tile to reduce the processed FoV earlier in the signal chain. Only $N_{b\text{-tile}}$ digital tile beams are transmitted to the station beamformer, reducing the total data rate transmitted, hence digitiser–bunker link cost, by a factor of $N_{b\text{-tile}}/N_{e\text{/tile}}$. Hierarchical beamforming also reduces the beamformer processing load as described in Appendix D.6.2, although this applies regardless of how the hierarchical beamforming processing is physically distributed. The bottom-up SKADS cost estimate for the station beamformer processing already includes a discount from hierarchical beamforming.

However, these savings may be offset or even exceeded by the extra costs introduced by performing digital tile beamforming at distributed locations in the station signal path, rather than just at the station node. For example, the processing for distributed tile beamforming could require extra power distribution infrastructure. The total cost of controlled environment housings (including cooling and RFI shielding) for each tile beamformer would probably be more expensive than implementing both stages of beamforming within a larger controlled environment housing at each station node. Also, upgrading the digital system is easier if the processing is concentrated at a single location.

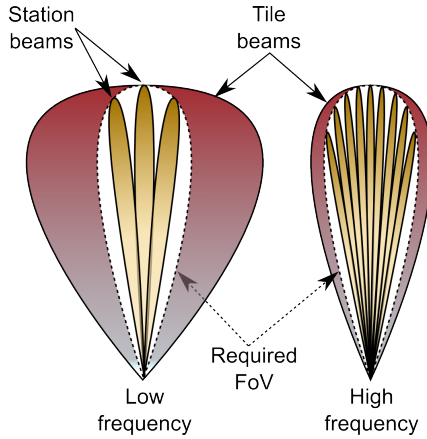


Figure 15: Schematic of the frequency-dependent relationship between the required FoV (dotted white) and the tile and station beams.

7.3.2 Hierarchical beamforming performance

Although hierarchical beamforming enables further design flexibility for the intra-station architecture, it also has the potential to decrease performance, regardless of whether the first-stage tile beamforming is analogue or digital. As mentioned in Section 4.3, tile beamforming reduces the accessible FoV and observational flexibility earlier in the signal path. If only a single tile beam is formed, it precludes the flexibility of pointing station beams at independent patches of the sky; the station beam pointing is restricted to within the single tile beam. Hierarchical beamforming also introduces errors in those station beams which are off-centre (i.e. not pointing in exactly the same direction as the tile beam), as discussed in Faulkner et al. (2010).

Tiles with more elements per tile further reduce the accessible FoV, because of the larger tile diameter (assuming the inter-element spacing is kept constant). If only one tile beam is formed, then the accessible FoV is defined by Ω_{tile} , the FoV of that tile beam. The required processed FoV, Ω_{req} , is limited by the accessible FoV, such that $\Omega_{\text{req}} < \Omega_{\text{tile}}$. As illustrated in Figure 15, Ω_{tile} is frequency-dependent, while Ω_{req} is not. Because Ω_{tile} is defined to be the FoV out to the half-power point of the beam, equal sized FoVs ($\Omega_{\text{tile}} = \Omega_{\text{req}}$) would result in sensitivity loss away from the centre of the tile beam.

For example, consider a 4×4 element tile, with regularly (uniformly) spaced elements. From Kraus (1986), the half-power beamwidth θ_{HP} at zenith for a linear array of n elements with inter-element spacing d is approximately

$$\theta_{\text{HP}} = 0.88 \sin^{-1} \left(\frac{\lambda}{nd} \right); \quad (3)$$

away from zenith, θ_{HP} is larger (Mailloux, 1995). For $d = 1.5$ m at 450 MHz, $\theta_{\text{HP}} \approx 5.6$ deg and $\Omega_{\text{tile}} \approx 31$ deg², while $\Omega_{\text{req}} = 20$ deg². Thus a single beam formed from a 16 element tile does provide sufficient FoV at the highest frequency, but there would be some sensitivity loss towards the edge of the tile beam. This loss reduces at lower frequencies, given $\Omega_{\text{tile}} \propto 1/\nu^2$.

Alternatively, more tile beams could be formed. However, this would result in more signal paths to the station beamformer, and the cost reduction would be less. Because this problem similarly applies to digital tile beamforming, the full benefit of a reduction in data transmission and signal processing cost is only realised if only one digital tile beam is formed. For example, the all-digital architecture in Faulkner et al. (2011) sends multiple tile beams from the 256 element tiles to the station beamformer, resulting in a total data rate at the station beamformer which is nearly as high as transmitting every digitised antenna element signal.

There is potential for both RF and digital tile beamforming approaches to be implemented in different phases of the telescope. If designed correctly, the analogue tile beamforming could be upgraded to all-

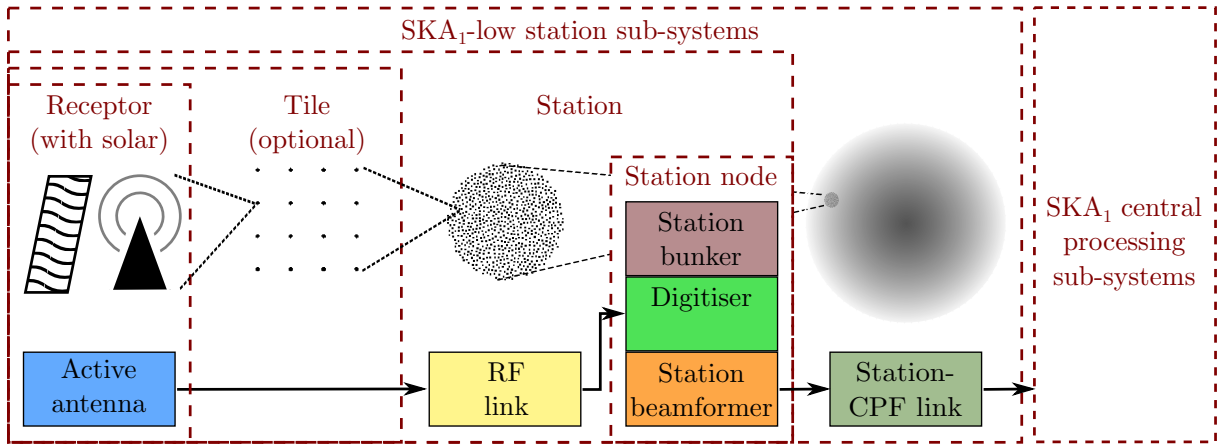


Figure 16: Schematic of a self-powered array, with the digital blocks located at the station node.

digital beamforming at a later date, once the cost and power consumption of the digital components reduce so that such an upgrade is cost-effective.

7.3.3 Example alternative architectures

Alternative intra-station architectures may prove to be more cost-effective than those considered in this analysis, with implications for the cost trade-offs. Technical factors also require consideration, such as dissimilar power losses at different locations in the architecture, and the deployability of different intra-station architectures.

In the all-digital architecture (Figure 3), digitisation occurs relatively close to the antenna element and the digitised signal is transmitted via optic fibre. Powering the active antenna electronics, digitiser and digital optical transmission components presents an extra cost, because they would require either an extensive power distribution network which is appropriately sized to the peak power load, or the installation of self-powered (solar power and energy storage) solutions (e.g. Hall, 2009; Faulkner et al., 2011). Self-powered antenna elements would remove the need to distribute power to the electronics at every antenna element. However, to cater for the 180 m station diameter, such an architecture would require an increase to the current maximum transmission distance of 50 m for short-range, high-speed digital optical transmission (Faulkner et al., 2011).

In contrast, the RF tile beamforming architecture (Figure 4) can deliver power to the active antenna element electronics and RF tile beamformer from the station node via a copper-based RF link, as is done for LOFAR (Gunst, 2007). Using the RF link for both signal transport and power delivery presents a cost saving, because the dedicated power distribution network only extends as far as the station nodes, rather than to every antenna element.

An alternative all-digital beamforming architecture, if technically feasible, could put the digitisation at station node and use similar RF links to power every antenna element and transport the signal to the station node. The obvious additional cost is the extra RF links required, but a separate power distribution network is not required.

A different architecture could have only the analogue components at the antenna element, and use radio over fibre (RoF) technology to transmit the analogue signals from each antenna element (Juswardy et al., 2011). These analogue signals would be transmitted to a node containing the digitisers, channelisation and beamforming equipment, as shown in Figure 16. The node could serve one or more stations; for transmission distances of 200–500 m, such an architecture would not be viable for analogue transmission over copper-based cable (Perini, 2011). The fibre cables are also physically smaller than copper-based cable, which may be important if there are tens of thousands of cables entering one node. The life-cycle cost benefits of these self-powered architectures with fibre links include simplified deployment from fewer connections (than the all-digital architecture with distributed power), potential for RFI reduction,

increased resilience against lightning strikes and increased upgrade flexibility because all the received data arrives at the node (Faulkner et al., 2011).

8 Further work

In the absence of all the necessary cost information to make a complete cost estimate, this first-order analysis provides a simple comparison of the cost differences between representative single and dual-band implementations. Along with obtaining new cost information, there is scope for continued expert attention to refine the existing cost estimates and better understand the uncertainties. Cost refinement means improving the accuracy and precision of the cost, using reference class costing from other projects or studies, or conducting new bottom-up cost studies. Prime candidates for cost refinement are:

- active antenna elements, for both the single-band (6.5:1) and dual-band (2.5:1) elements
- antenna deployment and site preparation
- central processing sub-systems.

There will always be a level of uncertainty in parametric studies because the models use fairly simple scaling relationships for the trade-off analysis. This uncertainty can be mitigated by solidifying the SKA₁-low performance requirements, and the specific trade-offs required.

The use of our parametric model need not be limited to comparing single and dual-band arrays. Section 7 illustrates just a few of the trade-offs which can be explored; other top-level parameters within our model which could be varied include:

- inter-element spacing
- antenna element gain
- the frequency split point of the dual-band array
- number of elements per station (to vary A/T while keeping the number of stations fixed).

The optimal number of stations and elements per station, for constant sensitivity, is an open question, but requirements other than cost must be considered. For example, the number and geographical placement of stations to achieve adequate (u, v) coverage and telescope calibration will also affect this optimisation. Such an optimisation requires a better understanding of the relative life-cycle costs between the SKA₁-low station digital sub-systems and the central processing sub-systems, in conjunction with refined performance requirements for station sensitivity and processed FoV (Appendix G.4).

We mention in Section 1 the close link between the telescope performance, cost and risk, and the science requirements. Our parametric model is sufficiently robust to consider differential cost trends between implementations, but is less suitable for determining absolute costs; calculating the monetary cost of changing a science requirement requires care.

9 Conclusions

We have developed a scalable parametric model to compare the cost of implementing SKA₁-low as a single or dual-band aperture array, considering the cost impact on both the station hardware costs and the broader telescope system costs. Perhaps somewhat surprisingly, despite the dual-band array having twice the number of antenna elements, neither the representative single or dual-band implementations are conclusively cheaper.

The cost difference between the single and dual-band implementations is, in essence, a comparison between the number and cost of the signal paths prior to station beamforming, and the downstream signal processing costs. The dual-band implementation has twice as many signal paths, but achieves a given field of view using fewer station beams, thereby reducing the downstream processing load. As a result, the dual-band implementation is more sensitive to changes in costs that scale with the number of signal paths, such as those of active antenna element hardware and deployment. Conversely, the single-band

implementation is more sensitive to changes in the cost of signal processing sub-systems such as the station beamformer, correlator, and imaging and non-imaging processors. The cost difference between the single and dual-band implementations depends on the fractional cost of each of these groupings.

A particularly important SKA-low parameter requiring further scientific consideration is the product of the processed FoV and bandwidth—the beam-bandwidth product, discussed in Section 7.2. If the beam-bandwidth capacity of the processing can be significantly reduced, the costs which then dominate are those that scale with the number of antenna elements. This increases the cost of the dual-band implementation relative to the single-band implementation, but the difference is much less than the factor of two increase which might naively be expected from an array with twice the number of elements.

We find that implementing a first stage of RF (analogue) tile beamforming prior to the digital station beamformer enables a potentially significant reduction in station hardware costs and power demand, the effect of which can outweigh any difference between single and dual-band implementations. Furthermore, if 90 m diameter stations are considered instead of 180 m, the correlator and imaging processor costs become cost drivers, dominating the station hardware costs.

To establish whether the single or dual-band array is the most cost-effective SKA₁-low implementation, improved cost information and further optimisation of the putative telescope designs are required. In terms of specific studies likely to assist in system design choices, we note that central processing, antenna deployment and site preparation costs are potentially significant cost drivers which have so far not had sufficient attention.

Acknowledgements

We thank Jan Geralt Bij de Vaate, Andrew Faulkner, Aziz Jiwani, and ICRAR, ASTRON, SPDO and University of Cambridge colleagues for the discussions surrounding this topic.

A List of symbols

Page where symbol is defined is listed.

A_{e-arr}	Array effective area (p 25)	$\overline{N_{b-st[L]}}$	Average N_{b-st} over the low-band (p 42)
A_{e-e}	Antenna element effective area (p 53)	$\overline{N_{b-st}}\Delta\nu$	Beam-bandwidth product (p 58)
A_{e-st}	Station effective area (p 52)	N_{b-tile}	Number of dual polarisation tile beams (p 27)
A_{g-st}	Station geometric area (p 52)	N_{ch}	Number of channels (p 45)
A/T	Sensitivity metric (p 50)	$N_{e/st}$	Number of elements per station (p 12)
C_{block}	Block cost (p 5)	$N_{e/tile}$	Number of elements per tile (p 11)
C_{fix}	Fixed cost (p 34)	N_{inputs}	Number of processing unit inputs (p 38)
C_{total}	Total cost (p 5)	N_{pol}	Number of polarisations (p 11)
C_{var}	Variable cost (p 34)	N_{st}	Number of stations in the array (p 11)
d_{avg}	Average inter-element spacing (p 11)	$N_{tile/st}$	Number of tiles per station (p 39)
d_{max}	Maximum inter-element spacing (p 51)	$R_{corr-out}$	Data rate out of the correlator (p 46)
d_{min}	Minumum inter-element spacing (p 51)	R_{dig}	Data rate from a digitiser (p 38)
D_{arr}	Array diameter (p 48)	R_{sample}	Digitiser sampling rate (p 37)
D_{st}	Station diameter (p 12)	R_{st}	Total data rate from a station (p 40)
FF_{st}	Station filling factor (p 52)	T_{sys}	System temperature (p 50)
G_e	Antenna element gain (p 53)	$\Delta\nu$	Processed bandwidth (p 33)
\mathcal{K}_{st}	Station beam taper (p 11)	Δt	Temporal resolution (integration time) (p 44)
$\overline{L_{e-st}}$	Average element-station link length (p 38)	$\Delta\nu_{ch}$	Spectral resolution (channel width) (p 44)
N_{b-arr}	Number of (phased or tied) array beams (p 48)	θ_{max}	Maximum scan angle (p 51)
$N_{bit-CFB}$	Number of bits out of coarse filterbank (p 40)	ν_{split}	Dual-band frequency split (p 42)
$N_{bit-dig}$	Number of bits out of digitiser (p 37)	$\nu_{transition}$	Dense-sparse transition frequency (p 50)
N_{b-st}	Number of dual polarisation beams per station (p 41)	Ω_{proc}	Station processed FoV (p 46)
$\overline{N_{b-st}}$	Average N_{b-st} over the band (p 12)	Ω_{req}	Required processed field of view (p 11)
$\overline{N_{b-st[H]}}$	Average N_{b-st} over the high-band (p 42)	Ω_{st}	Single station beam FoV (p 11)

B Summary of assumptions

For clarity, the key assumptions made for this analysis are summarised here and page references listed.

- Performance-related assumptions:
 - signals are dual-polarisation ($N_{pol} = 2$), or full-Stokes (p 11)
 - 20 deg² processed field of view is observed concurrently across the 70–450 MHz band (p 11)

- antenna element gain is the same for the single and dual-band (low and high) antenna elements to ensure that the first-order station A/T estimates are comparable (p 12)
 - the intra-station element layout is an irregular layout of uniform element distribution (p 12)
 - only one tile beam is formed for each tile (p 28).
- Cost-related assumptions:
 - the reference class LOFAR cost estimate is for 50 MHz output bandwidth with 2007 technology, so by 2016 newer technology will allow for the processing of the full 380 MHz bandwidth for the same cost (p 9)
 - the estimated costs do not represent the total cost of building the telescope, because costs are excluded when it can be shown that they remain constant between the single and dual-band implementations (p 10)
 - the low and high-band cores are separate (p 6)
 - low and high-band stations are co-located beyond the core, and the trenching and cables for the data transmission and power to these stations are shared (p 13)
 - infrastructure common to both stations, such as housing for the station processing node, is not shared (p 13).
 - Signal processing assumptions:
 - a time to frequency domain transformation and cross-correlation ‘FX’ correlator is used (p 7)
 - the number of coarse frequency channels and their channel width is constant (p 34)
 - the station beamformer cost scaling is the same for both frequency and time domain beamforming (i.e. the coarse filterbank does not dominate the beamformer cost) (p 39)
 - the SKA₁-low correlator frequency resolution is defined by the HLSD ($\Delta\nu_{\text{ch}} = 1 \text{ kHz}$) rather than D_{st} (p 45)
 - the central processing facility sub-systems operate on a ‘per beam’ basis (p 16)
 - the imaging cost is dominated by the data buffer, rather than the processing (p 47).
 - only the high-band core of the dual-band array is used in the non-imaging processor, and the processing for the AAs, not the dishes, dominate the cost (p 48).

C Filterbank and cross-correlation architecture

The models assume a time to frequency domain transformation and cross-correlation ‘FX’ correlator is used. This is the most cost-effective architecture for the SKA, as opposed to other correlator topologies such as ‘XF’. The FX correlator architecture is discussed in Bunton (2000); the architecture is more cost-effective with an increasing number of correlatable inputs (stations in this document). An FX architecture also allows signal processing actions, such as beamforming and RFI excision, to be efficiently performed (Hall et al., 2008).

In an FX correlator architecture, the signal from each element or tile input is filtered into frequency channels (‘F’) and for each channel, the input signals are cross-correlated (‘X’). Bunton (2003) shows that the filtering option can be efficiently implemented with a polyphase filterbank (PFB), such that the data rate of the output signal is equivalent to the input data rate. Although computationally more expensive, cascaded or multi-stage filterbanks allow for more efficient implementation on discrete processing units, such as ASICs and FPGAs, without the use of external RAM and the associated memory bandwidth costs. Oversampling is also required at all stages except the last to maintain performance where the channels overlap.

Cascaded filterbanks allow flexibility in the implementation architecture, where each filterbank stage is appropriately located to suit the architecture. The all-digital beamforming architecture in Bij de Vaate et al. (2011) integrates the first-stage coarse channel filterbank (CFB) between the digitisation

Table 11: Summary of blocks and scaling for SKA₁-low sub-systems.

Block name	Quantity in SKA ₁	Parametric equation	Block coverage
Active antenna element	$N_{\text{st}}N_{\text{e/st}}$	C_{fix}	mechanical element, LNA, gain and filter, housing and ground plane
Analogue (RF) tile beamformer ^a	$N_{\text{st}}N_{\text{tile/st}}$	$N_{\text{b-tile}}N_{\text{e/tile}}C_{\text{var}}$	hardware
Element/tile–digitiser RF link	RF: $N_{\text{st}}N_{\text{tile/st}}N_{\text{b-tile}}$ Dig: $N_{\text{st}}N_{\text{e/st}}$	RF: C_{fixRF} Dig: C_{fixDig}	RF cable
Digitiser	RF: $N_{\text{st}}N_{\text{tile/st}}N_{\text{b-tile}}$ Dig: $N_{\text{st}}N_{\text{e/st}}$	C_{fix}	digitiser
Digitiser–bunker link ^b	Dig: $N_{\text{st}}N_{\text{e/st}}$	$C_{\text{var1}}R_{\text{dig}} + C_{\text{var2}}\overline{L_{\text{e-st}}}$	C_{var1} : electronics, cable connectors C_{var2} : fibre cable
Station beamformer ^c	N_{st}	RF: $\overline{N_{\text{b-st}}}N_{\text{tile/st}}C_{\text{var}}$ Dig: $\overline{N_{\text{b-st}}}N_{\text{e/st}}C_{\text{var}}$	coarse filterbank, station beamformer
Station infrastructure (bunker)	N_{st}	RF: $C_{\text{fix}} + A_{\text{g-st}}C_{\text{var1}} + \overline{N_{\text{b-st}}}N_{\text{tile/st}}C_{\text{var2}}$ Dig: $C_{\text{fix}} + A_{\text{g-st}}C_{\text{var1}} + \overline{N_{\text{b-st}}}N_{\text{e/st}}C_{\text{var2}}$	C_{fix} : building etc. C_{var1} : preparation, trenching etc. C_{var2} : environmental conditioning, rack space etc.
Station–CPF link transmission	N_{st}	$R_{\text{st}}C_{\text{var}}$	fibre transmission

^aOptional block. If analogue tile beamforming is included, subsequent quantities and costs are denoted ‘RF’. If not, the system is all-digital beamforming, denoted by ‘Dig’.

^bOptional block. Assumes no digital beamforming at the tile. See Section 7.3 for alternative architectures.

^cApproximate cost scaling, see Appendix D.6.1.

and the tile beamforming blocks shown in Figure 14 (p 27). Channels outside processed bandwidth $\Delta\nu = \nu_{\text{max}} - \nu_{\text{min}}$ are discarded after the coarse filterbank, hence are not transported to the station beamformer. Although the data transport requirements are reduced, there are additional infrastructure and power supply implications in having the filterbank at the digitiser.

For simplicity, this analysis assumes that first-stage coarse channel filterbank (CFB) is implemented at the station bunker, prior to the beamforming; its cost is implicitly included in the station beamformer cost (Appendix D.6). The second-stage fine channel filterbank (FFB) is located at the correlator (Appendix F.2.2). Because any scalable digital signal processing description (e.g Bunton, 2010) requires a specific architecture with implicit assumptions, this first-order analysis keeps the number of coarse frequency channels and the channel width constant.

D Parametric models and costs for SKA₁-low stations

The parametric equations for the station sub-system blocks consist of fixed and variable units costs, C_{fix} and C_{var} respectively. The variable costs scale with one or more parameters. The total cost of a particular block in the system is the product of quantity and cost. Table 11 summarises the quantity and the cost scaling of the blocks in this analysis (see Section 3). The detailed block descriptions below provide further justification and references for the cost scaling. Table 12 lists the fixed and variable unit costs of each block.

These station cost estimates are for the sub-system hardware costs, where a sub-system is generally described by one of the scalable blocks. The station cost estimates include ‘sub-system infrastructure’, such as the housing for the signal processing units. But the sub-system hardware costs themselves are not just the procurable components (the physical hardware); they also include costs such as non-recurring

Table 12: SKA₁-low sub-system unit costs in € (2007).

Block name	Bottom-up SKADS cost estimate ^a	Reference class LOFAR cost estimate ^b	Block unit ^c
Active antenna element	C_{fix} : 75	C_{fix} : 172	per element
RF tile beamformer	C_{var} : 7.0 per output beam	C_{var} : same as low	per element
Element/tile-digitiser RF link	C_{fixRF} : 81 C_{fixDig} : 18	C_{fixRF} : same as low C_{fixDig} : same as low	per signal
Digitiser	C_{fix} : 12	C_{fix} : 80	per signal
Digitiser-bunker link	C_{var1} : 1 Gbps ⁻¹ C_{var2} : 0.01 Gbps ⁻¹ m ⁻¹	C_{var1} : same as low C_{var2} : same as low	per link
Station beamformer	C_{var} : 0.1 per input per output beam	C_{var} : 2.6 per input per output beam	per station
Station infrastructure	C_{fix} : 28 k C_{var1} : 0 C_{var2} : 0.06 per input per output beam	C_{fix} : 74 k C_{var1} : same as low C_{var2} : 2.6 per input per output beam	per station
Station-CPF link transmission	C_{var} : 100 Gbps ⁻¹	C_{var} : same as low	per link

^a All-digital beamforming, and technology advances. Most costs extrapolated from Table 3 of Faulkner et al. (2011).

^b LOFAR estimate for 50 MHz output bandwidth and analogue (RF) tile beamforming. Most costs extrapolated from Table 4 of Faulkner et al. (2011). The availability of only one cost estimate is indicated by ‘same as low’.

^c All elements, beams, inputs and signals are dual polarisation.

engineering, assembly and integration and testing for the sub-system. Faulkner et al. (2011) details the cost coverage for the AA CoDR estimates; in general, only the component costs are accounted for. Note that some components may implicitly include non-component hardware costs in the component purchase price. For example, the purchase price of a digitiser board would usually include assembly, integration and testing prior to delivery.

D.1 Active antenna element

The active antenna element describes an integrated system, which includes the mechanical element, LNA, gain and filter, housing and ground plane. We only consider a consolidated unit cost for the active antenna element, because its constituent components are specified and costed for a particular design. For example, the mechanical antenna element is matched to the LNA to minimise the receiver noise across the frequency band (van Ardenne et al., 2009), and the ground plane is designed for a given antenna element. Additionally, the active antenna element design should minimise manufacturing, transportation, deployment and operations costs, as discussed in Faulkner et al. (2011).

Consolidating the active antenna element cost does conceal potential trade-offs within that design space; a trade-off of topical interest is the cost of providing a ground plane for the element. However, a simple analysis in Appendix D.1.2 finds that there is not currently the justification for costing the ground plane separately to the rest of the active antenna element, because the cost of ground plane is more closely linked to the type of antenna element than the areal cost, and the ground plane cost is not significant in the broader SKA₁-low context, given the uncertainties of the present first-order analysis.

D.1.1 Active antenna element costs

The cost data sources in Faulkner et al. (2011) provide a consolidated cost for the active antenna element. The cost per dual polarisation active antenna element is €75 for the bottom-up SKADS estimate, the

cost being taken from existing arrays. The reference class LOFAR estimate for the same system is €179 and is a direct transfer from the cost of the LOFAR high band (120–240 MHz) antennas. For the purposes of our analysis, the antenna element’s RF beamformer cost of €7 per element is subtracted from this cost and listed separately in Table 12, resulting in a reference class LOFAR element cost of €172.

A comparison of the representative single and dual-band implementations clearly requires estimation of the low and high-band active antenna element costs. Factors to consider are:

- The fractional bandwidth of both the low and high-band elements is approximately 2.5:1, as opposed to 6.5:1 for the single-band element.
- The low-band elements, with a maximum frequency $\nu_{\max} = 180$ MHz, will require less exacting manufacturing standards than the single and high-band elements.
- The high-band elements, with a minimum frequency $\nu_{\min} = 180$ MHz, are physically smaller than the single and low-band elements.
- The average inter-element spacing for the high-band array is 0.75 m, compared with 1.5 m for the single and low-band arrays.

To provide a first-order estimate of the influence of these factors on the low and high-band active antenna element costs, multipliers (discounts) are applied to the single-band element costs (€75 and €172 for the bottom-up SKADS and reference class LOFAR estimates respectively). The cost of the active antenna element is assumed to be split 2:1 between the physical components and the electronics (LNAs, filters etc). The cost of the low-band physical components is estimated at 80 % of the single-band cost. The high-band ν_{\min} is about 2.5 times the single-band ν_{\min} , hence the cost of the physical components is estimated at 40 % of the single-band cost. The electronics for each band in the dual-band array are assumed to be only marginally cheaper, at 90 % of the single-band cost. The multipliers are thus calculated as

$$\text{Low-band} = \frac{2 \times 0.8 + 0.9}{3} \tag{4}$$

$$= 0.83 \tag{5}$$

and

$$\text{High-band} = \frac{2 \times 0.4 + 0.9}{3} \tag{6}$$

$$= 0.57. \tag{7}$$

These multipliers are first-order estimates; a detailed analysis, including the applicability to more directive antennas, is an important investigation for future SKA studies.

D.1.2 Ground plane costs

The bottom-up SKADS and reference class LOFAR active antenna element estimates include the cost of the ground plane. However, this section makes a simple analysis of ground plane costs to clarify its contribution to the consolidated active antenna element cost. The cost of a wire mesh ground plane will vary with the area of the mesh and the size of the openings in the mesh. One cost estimation method, applicable to both the single and dual-band implementations, is to calculate the total length of wire l_{wire} used to manufacture the mesh and assume that, for large quantities, the cost of the ground plane is linearly proportional to the cost of the wire. For a square mesh ground screen, $l_{\text{wire}} = 2/l_{\text{opening}}$ per m^2 of mesh, where l_{opening} is the opening width (distance between wires). To ensure a radio mirror surface, a rule-of-thumb is that $l_{\text{opening}} \leq 0.1\lambda_{\min}$, where λ_{\min} is the minimum wavelength to be observed. The ground plane area for an antenna element will depend on the inter-element spacing and the intra-station element layout. For an irregular layout of approximately uniform element distribution, the ground plane area for each element is approximately d_{avg}^2 , where d_{avg} is the average inter-element spacing. Thus, the total length of wire per antenna element is $l_{\text{wire}} = 2d_{\text{avg}}^2/l_{\text{opening}}$.

Table 13: Ground plane specifications and cost, for the single and dual-band implementations.

Band	d_{avg} (m)	Antenna element ν_{max} (MHz)	Suitable antenna types	Ground plane opening dimensions (mm) ^a	Ground plane usable ν_{max} (MHz) ^b	Example cost per m ² (€ 2007)	Example cost per antenna element (€ 2007) ^c
Single	1.5	450	all	50 × 50	600	6.0	13.5
			LPD	200 × 200 ^d	150	1.5	3.4
Low	1.5	180	all	150 × 150	200	2.0	4.5
			LPD	200 × 200 ^d	150	1.5	3.4
High	0.75	450	all	50 × 50	600	6.0	3.4
			LPD	100 × 100 ^d	300	3.0	1.7

^a Rounded to multiples of 25 mm.

^b Calculated assuming $l_{\text{opening}} \leq 0.1\lambda_{\text{min}}$.

^c For a ground plane of area d_{avg}^2 . Wire (€0.15 m⁻¹) costs assumed to represent the ground plane cost.

^d Sizes and usable ν_{max} are an example only and are not based on a particular antenna design.

Table 13 shows the ground plane specifications and cost for the representative single and dual-band implementations. A ground plane which reflects all frequencies in the band is shown, as is a ground plane suitable for antenna elements such as the more directional log-periodic dipole (LPD), where the higher frequency portion of the element uses the element structure as the ground plane (Braun & van Cappellen, 2006). In that case, the ground plane openings are sized only for the lower frequencies. Example ground plane costs (per m² and per antenna element) are given in Table 13, based on the total length and cost of the wire in galvanised steel mesh. For mesh with 50 × 50 mm openings, as used for the MWA, $l_{\text{wire}} = 40$ m per m² of mesh. Extrapolating actual MWA costs, this equates to a wire cost of €0.15 m⁻¹.

In Table 13, the type of antenna element is a dominant factor in determining the ground plane costs. This effect can be seen in the cost per m² column, where there is a factor of 4 variation. This means that rather than being costed as a distinct component, the ground plane should be considered in conjunction with the antenna element design and included in the consolidated active antenna element cost. Fortunately, the ground plane cost is not significant in the broader context of SKA₁-low station hardware and system variable costs. Even the largest cost difference, €10.1 per element between the two single-band ground planes, only equates to a €113k cost per station. In the context of station hardware costing at least €1.2M (see Figure 13), this is less than 10% of the hardware cost and is much smaller than the uncertainties described in Section 6.3.

An additional factor to consider is that the wire cost, which has been used as a proxy for ground plane cost, will depend on the wire diameter. The following practical requirements will influence the wire diameter:

- Rigidity: ensures a planar surface, within some level of tolerance.
- Deployability: is the ground plane to be deployed as sheets of mesh (larger diameter wire) or longer rolls of mesh (smaller diameter wire)?
- Durability: will the mesh entirely cover the station area, such that it needs to be durable enough to be walked on to enable hardware maintenance?

The wire diameter used for the MWA mesh sheets is approximately 3 mm, but if the requirements are less stringent and the wire diameter can be smaller, then the ground plane costs would further reduce.

D.2 Optional: RF tile beamformer

The RF tile beamformer is assumed to be a part of the active antenna element system. Only one tile beam is formed ($N_{\text{b-tile}} = 1$) for the comparisons made in this document. Multiple independent FoVs

require the formation of multiple tile beams.

D.3 Element/tile–digitiser RF links

The links listed in Faulkner et al. (2011) are CAT-7 for the all-digital system and co-axial cable for the RF tile beamformed system, although in principle, CAT-7 or co-axial cable could be used in either system. The co-axial cable for the RF tile beamformed system is more expensive because of the longer cable lengths required for that architecture.

D.4 Digitiser

The digitiser sample rate R_{sample} and number of bits $N_{\text{bit-dig}}$ are fixed at 1 GS/s and 8 bits respectively. The digitiser over-samples the data by having a sample rate larger than the maximum frequency.

D.5 Optional: digitiser–bunker links

The data from the digitiser is transmitted over fibre to the station processing. This link assumes digitisation occurs at or near the tile or element and the station processing is near the centre of the station. Table 3 of Faulkner et al. (2011) describes a unit cost of €152 for the short optical fibre link. This has the capacity of 120 Gbps per fibre (12×10 Gbps channels). To fully utilise this capacity, a few digitised element or tile beam signals could be transmitted on each link. The cost is composed of transmit (at antenna) and receive (at station) units, connectors and the fibre. A simplistic cost breakdown is a cost of €120 for the electronics and connectors and €1.0 m⁻¹ for the fibre, which approximates to $C_{\text{var1}} = \text{€}1 \text{ Gbps}^{-1}$ and $C_{\text{var2}} = \text{€}0.01 \text{ Gbps}^{-1} \text{ m}^{-1}$ respectively.

The parameter $\overline{L_{e-st}}$ is the average link length between the element or tile and the station processing. A simplified calculation (average radius to a circle centre) applies to an irregular layout of uniform element distribution, such that $\overline{L_{e-st}} \approx D_{st}/3$.

The data rate out of the digitiser R_{dig} is given by

$$R_{\text{dig}} = N_{\text{pol}} N_{\text{bit-dig}} R_{\text{sample}} OH \quad (8)$$

where OH is the overhead, assumed to be 1.25 for digital encoding.

D.6 Station beamformer (including coarse channel filterbank)

Station beamforming is required for the SKA to reduce the number of inputs to the correlator. Digital beamforming can be done in the time domain, or in the frequency domain on the channelised signal. The computational cost of the frequency and time domain beamforming approaches is discussed in Barott et al. (2011) and Khlebnikov et al. (2010), where computation costs are expressed as a function of the number of beams, input antennas and frequency channels, and other costs to implement a time delay (where necessary) and the FFT. These latter costs are architecture specific, as is the cost scaling with the number of channels. Jones et al. (2011) discuss beamforming architectures in more detail.

The station beamformer cost is approximated using Equation 11 below, and is calculated as cost per input per output beam. This cost is extrapolated from Faulkner et al. (2011); 11 264 inputs and 160 output beams (averaged over the band) is assumed to make the extrapolation. The bottom-up SKADS station beamformer cost already takes into account the processing discount from the two-stage beamforming. The reference class LOFAR cost in Table 4 of Bij de Vaate et al. (2011) is for only 50 MHz bandwidth, however it is also for 2007 technology. We assume that newer technology will allow for the beamforming of the full 380 MHz bandwidth for the same cost.

D.6.1 Computational cost of frequency and time domain beamforming

From Barott et al. (2011) and Khlebnikov et al. (2010), for a given architecture and number of channels, the frequency and time domain station beamformer processing load can be respectively simplified to

$$P_{\text{BF}[\nu]} \propto N_{\text{inputs}}(K_{\text{CFB}} + K_{\text{BF}[\nu]}N_{\text{b-st}}) \quad (9)$$

and

$$P_{\text{BF}[t]} \propto N_{\text{b-st}}(K_{\text{BF}[t]}N_{\text{inputs}} + K_{\text{CFB}}), \quad (10)$$

where N_{inputs} is the number of elements or tiles being beamformed, $N_{\text{b-st}}$ is the number of station beams formed, the constant K_{CFB} is the coarse filterbank cost per frequency channel and $K_{\text{BF}[\nu]}$ and $K_{\text{BF}[t]}$ are the beamforming costs per channel (frequency domain) or antenna (time domain).

If the CFB cost does not dominate (i.e. $N_{\text{b-st}} \gg K_{\text{CFB}}/K_{\text{BF}[\nu]}$ and $N_{\text{inputs}} \gg K_{\text{CFB}}/K_{\text{BF}[t]}$), the cost scaling is the same for both frequency and time domain beamforming. The processing cost of the station beamformer is thus approximated by

$$P_{\text{BF}} \propto N_{\text{inputs}}N_{\text{b-st}}. \quad (11)$$

In this analysis, N_{inputs} is either $N_{\text{e/st}}$ or $N_{\text{tile/st}}$ and $N_{\text{b-st}}$ is $\overline{N_{\text{b-st}}}$.

This approximation is used to derive the unit costs from the cost data sources. In deriving the station beamformer cost from the reference class LOFAR estimate, a factor of 16 fewer inputs (equal to the number of elements per tile) is used relative to the bottom-up SKADS station beamformer cost estimate, which is calculated from the aggregate of the first-stage and station processing costs. This results in a factor of 26 difference in station beam unit cost (Table 12). The same scaling approximation is applied to 80% of the station bunker cost (see Appendix D.7), hence the factor of 43 difference in the variable unit cost for that sub-system.

D.6.2 Hierarchical beamforming

Hierarchical digital beamforming reduces the data transport and processing load on the system. A simple example of this is shown here. Faulkner et al. (2010) presents a two-stage digital beamforming approach and this is reflected in Table 3 of Faulkner et al. (2011), where the first stage consists of a tile of 256 antenna elements as inputs ($N_{\text{inputs-tile}} = 256$). There are 44 tiles in a station ($N_{\text{tile/st}} = 44$), so one beam from each of the 44 tiles (all pointing in the same direction) are input into the second-stage (station) beamformer ($N_{\text{inputs-stn}} = 44$). The total station processing load to form $N_{\text{b-st}}$ station beams (from Equation 11) is approximately:

$$P_{\text{BF}} \propto N_{\text{tile/st}}N_{\text{inputs-tile}}N_{\text{b-tile}} + N_{\text{inputs-stn}}N_{\text{b-st}}. \quad (12)$$

Given $N_{\text{e/st}} = N_{\text{tile/st}}N_{\text{inputs-tile}}$ and $N_{\text{inputs-stn}} = N_{\text{tile/st}}$, this becomes

$$P_{\text{BF}} \propto N_{\text{e/st}}N_{\text{b-tile}} + N_{\text{tile/st}}N_{\text{b-st}}. \quad (13)$$

For this example, $P_{\text{BF}} \propto 11\,264N_{\text{b-tile}} + 44N_{\text{b-st}}$. In comparison, for a single stage of beamforming, where $N_{\text{inputs}} = 11\,264$, $P_{\text{BF}} \propto 11\,264N_{\text{b-st}}$. Hence when $N_{\text{b-st}} > 1$, the two-stage beamforming reduces processing costs. However, caution should be used to ensure that the assumptions for Equation 11 still hold.

D.6.3 Trading $N_{\text{e/st}}$ for N_{st}

From Equation 11, the total processing cost for N_{st} single-stage station beamformers is approximately

$$P_{\text{BF-total}} \propto N_{\text{st}}N_{\text{e/st}}\overline{N_{\text{b-st}}}. \quad (14)$$

Given $N_{\text{st}} \propto 1/(N_{e/\text{st}} FF_{\text{st}} d_{\text{avg}}^2)$ for constant $A_{e\text{-arr}}$ (Equation 57) and $\overline{N_{\text{b-st}}} \propto N_{e/\text{st}} d_{\text{avg}}^2$ (Equation 27),

$$P_{\text{BF-total}} \propto \frac{N_{e/\text{st}}}{FF_{\text{st}}}, \quad (15)$$

where FF_{st} is the frequency-dependent station filling factor (Equation 55). If d_{avg} and the antenna element gain G_e do not change, then the function FF_{st} remains constant and

$$P_{\text{BF-total}} \propto N_{e/\text{st}}. \quad (16)$$

As long as the assumptions for the approximation (Equation 11) still hold, the scaling relationship can also be applied to hierarchical beamforming.

As shown in Appendix E.2, the ratio of the average number of beams between single and dual-band implementations $\overline{N_{\text{b-st}}}$ (dual : single) is independent of N_{st} for constant $A_{e\text{-arr}}$. Because $P_{\text{BF-total}} \propto \overline{N_{\text{b-st}}}$, the beamformer processing cost ratio between the single and dual-band implementations is independent of station diameter, although the absolute (euro) cost difference is less for the smaller stations.

D.7 Station infrastructure (bunker)

Within a station array, it is assumed that the antenna elements are closely packed, hence cables (power and fibre) would be laid as part of the station construction, rather than individual trenches being dug. Thus these costs scale with area. However, this areal infrastructure cost is difficult to estimate with much accuracy until after the site selection. There are also costs for a controlled environment housing at each station for the processing hardware. This cost would increase linearly with the amount of processing, although there will be a fixed cost for the housing. These costs are extrapolated from Faulkner et al. (2011) to obtain a cost per input signal per output beam and a fixed cost. We estimate the zeroth-order breakdown of costs between the variable and fixed costs to be 80% and 20% respectively.

D.8 Station-CPF link transmission

The output data from the station beamformer is transmitted over fibre to the central processing facility. This analysis only considers the transmission costs; the per metre trenching and cabling cost is ignored because the layout (configuration) of the SKA₁-low stations do not change significantly between representative systems. The layouts shown in Bolton et al. (2011) have a compact core and spiral arms. The spiral arms may require trenching for the data links, but for the compact core this can be absorbed into the areal infrastructure cost. For the HLSD, 97% of the network infrastructure costs are in the trench network (McCool, 2011a). This means that although a higher data rate may require more strands of fibre, the cost of the fibre cable is not significant, being less than 3%.

For the transmission costs, there are technology steps, where more expensive transmission equipment is required for longer distance. An estimate of dense wavelength division multiplexing (DWDM) transmission system costs per channel are derived from the SKA Design Studies costing work in SKACost (Bolton et al., 2009b). Although there is some variation with distance and the discrete cost steps of DWDM transmission, for this first order costing it is sufficient to estimate an average cost of €1 k per 10 Gbps channel for all links, or €100 per Gbps.

The total data rate out of a station beamformer is given by

$$R_{\text{st}} = \overline{N_{\text{b-st}}} N_{\text{pol}} N_{\text{bit-FCFB}} \Delta\nu \times OS \times OH \times \text{Nyq.}, \quad (17)$$

where $\overline{N_{\text{b-st}}}$ is the average number of station beams formed over the band. The number of bits out of the coarse channel filter-bank $N_{\text{bit-FCFB}} = 4$, oversampling $OS = 1.1$, digital encoding overhead $OH = 1.25$ and the data is Nyquist sampled: $\text{Nyq.} = 2$.

Table 14: Cost multiplier estimates for the dual-band array, where each multiplier is a fraction of the single-band unit cost shown in Table 12.

Block name	Low-band	High-band	Comments
Active antenna element ^a	C_{fix} : 0.83	C_{fix} : 0.57	See Appendix D.1.
Optional: RF tile beamformer	C_{var} : 1	C_{var} : 1	
Element/tile–digitiser RF link	C_{fixRF} : 1 C_{fixDig} : 1	C_{fixRF} : 0.3 C_{fixDig} : 0.3	Closer spacing means smaller tiles and stations.
Digitiser ^a	C_{fix} : 0.4	C_{fix} : 1	Sampling speed is set by ν_{max} of each band (0.4 GS/s for the low-band). Assumes that cost is linearly proportional to sampling speed.
Digitiser–bunker link	C_{var1} : 1 C_{var2} : 1	C_{var1} : 1 C_{var2} : 1	C_{var1} : Per unit of data. C_{var2} : Per unit of data per unit length.
Station beamformer ^a	C_{var} : 0.29	C_{var} : 0.71	Assumes cost is linearly proportional to processed bandwidth.
Station infrastructure ^a	C_{fix} : 1 C_{var1} : 1 C_{var2} : 0.29	C_{fix} : 1 C_{var1} : 1 C_{var2} : 0.71	Processing infrastructure is the same fraction as the station beamformer.
Station–CPF link transmission	C_{var} : 1	C_{var} : 1	Per unit of data.

^a These values are for a dual-band split frequency of 180 MHz; they will vary for other split frequencies and overlapping bands.

D.9 Dual-band station costs

The dual-band implementation is costed as a separate a low-band (70–180 MHz) and high-band (180–450 MHz) array. For each station block (sub-system), its cost will either remain the same, or be some fraction of the single-band cost, depending on how each block is modelled. This ‘cost multiplier’ is then applied to the costs in Table 12. Table 14 shows the cost multipliers used for each block in the low and high-band arrays. The cost multipliers chosen are reasonable approximations; this is an area that requires expert attention to verify these numbers.

E Constant FoV as a function of frequency

E.1 Single-band implementation

If a constant FoV as a function of frequency is a requirement, then determining the average number of beams required over the receptor bandwidth can simplify calculations (Alexander et al., 2009). The number of beams as a function of frequency can be given by

$$N_{\text{b-st}}(\nu) = N_{\text{b-st}}(\nu_0) \left(\frac{\nu}{\nu_0} \right)^2, \quad (18)$$

where $N_{\text{b-st}}(\nu_0)$ is the number of dual-polarisation beams required at frequency ν_0 , calculated as

$$N_{\text{b-st}}(\nu_0) = \Omega_{\text{req}}/\Omega_{\text{st}}(\nu_0). \quad (19)$$

Integrating Equation 18 over the processed bandwidth $\Delta\nu = \nu_{\max} - \nu_{\min}$ gives the number of beams of unit bandwidth:

$$\begin{aligned} N_{\text{b-st-Hz}} &= \int_{\nu_{\min}}^{\nu_{\max}} N_{\text{b-st}}(\nu_0) \left(\frac{\nu}{\nu_0} \right)^2 d\nu \\ &= \frac{N_{\text{b-st}}(\nu_0)}{\nu_0^2} \left[\frac{\nu^3}{3} \right]_{\nu_{\min}}^{\nu_{\max}} \\ &= \frac{N_{\text{b-st}}(\nu_0)(\nu_{\max}^3 - \nu_{\min}^3)}{3\nu_0^2}. \end{aligned} \quad (20)$$

The average number of dual-polarisation beams over the band is

$$\overline{N_{\text{b-st}}} = \frac{N_{\text{b-st-Hz}}}{\nu_{\max} - \nu_{\min}}. \quad (21)$$

Also, given $\Omega_{\text{st}} \propto D_{\text{st}}^{-2}$ and $N_{\text{b-st}} \propto \Omega_{\text{st}}^{-1}$, substitution into Equation 21 shows that

$$\overline{N_{\text{b-st}}} \propto D_{\text{st}}^2. \quad (22)$$

An actual implementation requires that a discrete number of beams be formed at each frequency channel. This introduces some error, because enough beams need to be formed for every frequency channel such that the FoV requirement is always met; i.e. $N_{\text{b-st}}(\nu)\Omega_{\text{st}}(\nu) \geq \Omega_{\text{req}}$. An actual calculation requires a summation to replace the integral, where the ceiling $\lceil N_{\text{b-st}}(\nu) \rceil$ is taken for each frequency channel (strictly speaking, $N_{\text{b-st}}(\nu)$ should to be calculated at the maximum frequency of each channel, not the centre frequency). Although the error is larger at the lower frequencies where Ω_{st} is larger, even at 70 MHz the error is $<10\%$ for $\Omega_{\text{req}} = 20 \text{ deg}^2$ (higher error for smaller FoV).

E.2 Dual-band implementation

The dual-band implementation is more complex. Equation 21 can be applied separately to each band in the dual-band array, resulting in the average number of beams in each of the low ($\overline{N_{\text{b-st[L]}}}$) and high ($\overline{N_{\text{b-st[H]}}}$) bands. The average number of beams over the full band is given by

$$\overline{N_{\text{b-st[D]}}} = \frac{(\nu_{\text{split}} - \nu_{\min})\overline{N_{\text{b-st[L]}}} + (\nu_{\max} - \nu_{\text{split}})\overline{N_{\text{b-st[H]}}}}{\nu_{\max} - \nu_{\min}}, \quad (23)$$

where ν_{split} is the frequency split between the bands and ν_{\min} and ν_{\max} are the minimum and maximum frequencies of the dual-band implementation (i.e. 70 and 450 MHz). From Equation 21,

$$\overline{N_{\text{b-st[L]}}} = \frac{N_{\text{b-st[L]}}(\nu_0)(\nu_{\text{split}}^3 - \nu_{\min}^3)}{3\nu_0^2(\nu_{\text{split}} - \nu_{\min})}, \quad (24)$$

and an equivalent substitution can be made for $\overline{N_{\text{b-st[H]}}}$.

The ratio of the average number of beams across the band between the dual and single-band implementations, given by $\overline{N_{\text{b-st}}(\text{dual} : \text{single})} = \overline{N_{\text{b-st[D]}}} / \overline{N_{\text{b-st[S]}}}$, is a useful metric to compare the data rate from the station and also the processing costs in the central processing facility. Substitution gives

$$\overline{N_{\text{b-st}}(\text{dual} : \text{single})} = \frac{N_{\text{b-st[L]}}(\nu_0)(\nu_{\text{split}}^3 - \nu_{\min}^3) + N_{\text{b-st[H]}}(\nu_0)(\nu_{\max}^3 - \nu_{\text{split}}^3)}{N_{\text{b-st[S]}}(\nu_0)(\nu_{\max}^3 - \nu_{\min}^3)}, \quad (25)$$

or

$$\overline{N_{\text{b-st}}(\text{dual} : \text{single})} = \frac{D_{\text{st[L]}}^2(\nu_{\text{split}}^3 - \nu_{\min}^3) + D_{\text{st[H]}}^2(\nu_{\max}^3 - \nu_{\text{split}}^3)}{D_{\text{st[S]}}^2(\nu_{\max}^3 - \nu_{\min}^3)}, \quad (26)$$

where the L, H and S sub-scripts indicate low, high and single-band arrays respectively. Thus for a constant FoV across the processed bandwidth $\Delta\nu$, the ratio depends on both the station diameter of each band and the frequency split between the low and high-band arrays.

E.3 Trading $N_{e/st}$ for N_{st}

As shown in Appendix G.3, the station diameter is both a function of the number of elements in the station and the average inter-element spacing. To make a distinction between these effects, Equations 22 and 26 requires the substitution of $D_{st} \propto \sqrt{N_{e/st}} d_{avg}$ (Equation 59), such that

$$\overline{N_{b-st}} \propto N_{e/st} d_{avg}^2 \quad (27)$$

and

$$\overline{N_{b-st}}(\text{dual} : \text{single}) = \frac{N_{e/st[L]} d_{avg[L]}^2 (\nu_{split}^3 - \nu_{min}^3) + N_{e/st[H]} d_{avg[H]}^2 (\nu_{max}^3 - \nu_{split}^3)}{N_{e/st[S]} d_{avg[S]}^2 (\nu_{max}^3 - \nu_{min}^3)}. \quad (28)$$

For the representative implementations considered in this analysis, $N_{e/st[L]} = N_{e/st[H]} = N_{e/st[S]}$, thus $N_{e/st}$ is constant as a function of frequency, resulting in

$$\overline{N_{b-st}}(\text{dual} : \text{single}) = \frac{d_{avg[L]}^2 (\nu_{split}^3 - \nu_{min}^3) + d_{avg[H]}^2 (\nu_{max}^3 - \nu_{split}^3)}{d_{avg[S]}^2 (\nu_{max}^3 - \nu_{min}^3)}. \quad (29)$$

So if D_{st} is traded for N_{st} (for fixed A_{e-arr}), this ratio still holds as long as the same trade is made for all bands. For example, if D_{st} is halved, then $N_{e/st}$ decreases by a factor of 4. But given $N_{e/st[L]} = N_{e/st[H]} = N_{e/st[S]}$, $\overline{N_{b-st}}(\text{dual} : \text{single})$ does not change.

F Parametric models and costs for other SKA sub-systems

The presentation of the models and costs in this section are, in general, similar to Appendix D. However, only zeroth-order cost estimates are given, with the purpose of illustrating system-level costs (Section 5). Table 15 summarises the quantity and the cost scaling of the blocks which are not SKA₁-low sub-systems, while the detailed block descriptions provide further justification and references for the cost scaling. Table 16 lists the fixed and variable unit costs of each block.

F.1 Site-related costs

Although site-related costs are not publicly available, a comparison of single and dual-band implementations can be made by only considering the costs that vary between implementations, while excluding costs which remain fixed. For example, if an activity such as site preparation is being undertaken, the fixed costs of that activity could include contractor mobilisation and demobilisation, whereas the variable costs are one or more pro rata (such as per hour or per m²) costs of undertaking the activity.

Some site-related costs are independent of whether the implementation is single or dual-band. The first-order array infrastructure costs discussed in the HLSD, such as road networks and power and fibre reticulation, will generally be independent of the number of stations or their exact location and are not considered here. In the core region, the spatial density of stations will be high enough that any infrastructure work can be incorporated into the site preparation costs. For the inner and mid region stations, located beyond the core, the stations are placed in groups (clusters) on spiral arms (Bolton et al., 2011). The array infrastructure requirements to connect cluster will be similar between the single and dual-band implementations, regardless of the number of stations at each cluster. For the central processing facility buildings, there may be some cost scaling with the amount of processing.

F.1.1 Antenna element deployment

Faulkner et al. (2011) costs deployment of the antenna elements at less than €50 per element. This excludes the deployment and connection of the rest of the infrastructure, such as tile or station processing nodes. To show the sensitivity of the single versus dual-band comparison to changes in this cost, two deployment costs are considered: €50 and €100 per element.

Table 15: Summary of blocks and scaling for other sub-systems relevant to SKA₁-low.

Block name	Quantity in SKA ₁	Parametric equation	Block coverage
Antenna element deployment	$N_{\text{st}}N_{\text{e/st}}$	C_{fix}	deployment
Site preparation	$N_{\text{st}}N_{\text{e/st}}$	$d_{\text{avg}}^2 C_{\text{var}}$	site preparation
Correlator	1	$\frac{d_{\text{avg}}^2}{N_{\text{b-st}}N_{\text{st}}^\alpha} C_{\text{var}}; 1 < \alpha < 2$	see Appendix F.2.2
Correlator–computing data transport	1	$R_{\text{corr-out}} C_{\text{var}}$	fibre transmission
Imaging processor	1	$R_{\text{corr-out}} C_{\text{var}}$	
Non-imaging processor	1	see Appendix F.2.5	

Table 16: Unit costs for other sub-systems relevant to SKA₁-low (€2007).

Block name	Cost estimate A	Cost estimate B	Block unit
Antenna element deployment	C_{fix} : 50	C_{fix} : 100	per element
Site preparation	C_{var} : 10 m^{-2}	C_{var} : 100 m^{-2}	per element
Correlator	C_{var} : 40 k per input beam	C_{var} : same as A	per correlator
Correlator–computing data transport	C_{var} : 200 Gbps^{-1}	C_{var} : same as A	
Imaging processor	20 M for single-band implementation	same as A	N/A
Non-imaging processor	30 M for single-band implementation	same as A	N/A

F.1.2 Site preparation cost

There is no published data on site preparation costs, and it is likely to be highly dependent on what activities the site preparation involves. For example, is it a simple land clearing activity, or are earthworks and trenching required? To show the sensitivity of the single versus dual-band comparison to changes in this cost, two areal site preparation costs are considered: € 10 m^{-2} and € 100 m^{-2} .

F.2 Central processing facility sub-systems

F.2.1 Correlator frequency resolution and integration time requirements

Two parameters which are relevant to the correlator and image processor design are the correlator frequency resolution (channel width) $\Delta\nu_{\text{ch}}$ and integration time Δt ; these need to be small enough to respectively keep the radial and circumferential smearing below some acceptable threshold (Thompson et al., 2001). The frequency resolution and integration time required is inversely proportional to antenna or station beamwidth (Turner et al., 2011). If the maximum baseline (distance between antenna pairs) and station beam taper \mathcal{K}_{st} are constant, then

$$\Delta\nu_{\text{ch}} \propto D_{\text{st}} \quad (30)$$

and

$$\Delta t \propto D_{\text{st}}. \quad (31)$$

However, SKA₁-low has a more stringent requirement on frequency resolution which makes it independent of station size. The HLSD (Table 4) specifies a scientifically derived requirement of $\Delta\nu_{\text{ch}} = 1 \text{ kHz}$ for AAs, while Turner et al. (2011) calculates $\Delta\nu_{\text{ch}} = 590 \text{ kHz}$ to meet the 2% smearing requirement with a 180 m diameter station. Given the much more stringent specification in the HLSD, any change in D_{st} for

SKA-low will not affect $\Delta\nu_{\text{ch}}$.

F.2.2 Fine channelisation and correlation

The ‘FX’ correlator cost scalings can be understood by analysing the data streams flowing through the fine filterbank (channelisation) and cross-correlation sub-systems, described in Appendix C. The station beamformer outputs coarsely channelised station beams, where each channel has width $\Delta\nu_{\text{ch-CFB}}$. A single data stream from a station will contain one coarse channel from one station beam. Each data stream is input into a fine filterbank (FFB) and split into channels of smaller frequency resolution. The total processing cost of the FFBs is thus

$$P_{\text{FFB}} = N_{\text{ch/CFB}} \overline{N_{\text{b-st}}} N_{\text{st}} K_{\text{FFB}}, \quad (32)$$

where $N_{\text{ch/CFB}}$ is the number of channels per coarse filterbank ($N_{\text{ch/CFB}} = \Delta\nu/\Delta\nu_{\text{ch-CFB}}$) and K_{FFB} is the FFB processing cost for a single data stream.

The value of K_{FFB} is not easily determinable, because the filterbank processing architecture is designed so that, for each filterbank, the data flow, mathematical operations and memory usage are optimised for some output frequency resolution (e.g. Bunton, 2010; Barott et al., 2011). However, K_{FFB} is constant in the present analysis, because the FFB output frequency resolution (equal to $\Delta\nu_{\text{ch}}$) is fixed by the scientific requirements described above. Additionally, $\Delta\nu_{\text{ch-CFB}}$ is held fixed in the present analysis; Bij de Vaate et al. (2011) specifies $\Delta\nu_{\text{ch-CFB}} = 0.25$ MHz. Therefore a re-evaluation of Equation 32 gives

$$P_{\text{FFB}} \propto \Delta\nu \overline{N_{\text{b-st}}} N_{\text{st}}. \quad (33)$$

Once the data streams are split into fine channels, equivalent data streams (i.e. m^{th} fine channel of the n^{th} beam) from each antenna pair ($\sim N_{\text{st}}^2/2$ pairs) are cross-correlated, at a correlation rate equal to the sample rate $\Delta\nu_{\text{ch}}$ (Bunton, 2000). Because there are $N_{\text{ch}} = \Delta\nu/\Delta\nu_{\text{ch}}$ fine channels to be correlated, and $\Delta\nu_{\text{ch}}$ is constant, the correlation processing cost is approximately

$$P_{\text{X}} \propto \Delta\nu \overline{N_{\text{b-st}}} N_{\text{st}}^2. \quad (34)$$

Additional to the ‘F’ and ‘X’ computation hardware, there are also processing costs in the form of memory buffers and the inter-connects (corner turn) between the filterbanks and correlation devices (Turner et al., 2011). These costs are design dependent, and one or more of these costs may dominate the total correlator processing hardware cost. But it is reasonable to expect that the total cost will scale as

$$P_{\text{corr}} \propto \Delta\nu \overline{N_{\text{b-st}}} N_{\text{st}}^\alpha, \quad (35)$$

where $1 < \alpha < 2$ depending on the design and technologies used. If N_{st} is held constant,

$$P_{\text{corr}} \propto \Delta\nu \overline{N_{\text{b-st}}}. \quad (36)$$

Dual-band implementation

The correlator processing for the dual-band implementation simply requires the substitution of $\overline{N_{\text{b-st[D]}}}$ (Appendix E.2) into Equation 36. The correlator processing ratio between the dual and single-band implementations is therefore

$$P_{\text{corr}}(\text{dual} : \text{single}) = \overline{N_{\text{b-st[D]}}}(\text{dual} : \text{single}). \quad (37)$$

Trading $N_{e/st}$ for N_{st}

For constant A_{e-arr} , Equations 27 and 57 can be substituted into Equation 35. Assuming d_{avg} and the antenna element gain G_e remain constant,

$$P_{corr} \propto \Delta\nu N_{e/st}^{1-\alpha}, \quad (38)$$

where $1 < \alpha < 2$.

Because N_{st} changes equally for both the single and dual-band implementations, Equation 37 still holds true. Although the cost of the correlator processing increases with N_{st} , the relative cost is independent of the N_{st} vs. $N_{e/st}$ trade-off.

Fine channelisation and correlation costs

There are a range of correlator cost estimates (<€1M to nearly €100M) for SKA₁ in Turner (2011), representing different architectures, technologies and options for flexibility. The correlation of SKA₁-low stations, rather than the dishes, represent most of the cost. The cost estimates generally only encompass the processing units and data inter-connects; doubling the cost accounts for all the accessory hardware required to support these processing units. Costs such as non-recurring engineering, which are generally not included in the estimates, can be considered a fixed cost. A zeroth-order estimate of the cost of the parts of the SKA₁-low correlator which scale as the number of input beams is €20M; this equates to a GPU-class correlator. This estimate is specified for 480 station beams ($\Delta\nu = 380$ MHz), which is approximately €40k per station beam.

F.2.3 Correlator–computing data transport

Each datum produced from the correlator (Equation 34) is integrated for time Δt . Thus the data rate out of the correlator is:

$$R_{corr-out} \propto \frac{N_{ch} \overline{N_{b-st}} N_{st}^2}{\Delta t}. \quad (39)$$

For a fixed processed FoV Ω_{proc} , the data rate out of the correlator $R_{corr-out}$ is independent of station diameter when the frequency resolution and integration time are set by the maximum smearing requirements (Equations 30 and 31). In that case,

$$R_{corr-out} \propto \frac{\Delta\nu \overline{N_{b-st}} N_{st}^2}{D_{st}^2} \quad (40)$$

$$\propto \Delta\nu \Omega_{proc} N_{st}^2, \quad (41)$$

given $\Omega_{proc} \propto \overline{N_{b-st}} \Omega_{st} \propto \overline{N_{b-st}} D_{st}^{-2}$. This result is independent of station diameter.

However, the maximum smearing requirements do not set the frequency resolution for SKA₁-low. The more stringent requirement on frequency resolution discussed earlier means that $\Delta\nu_{ch}$, hence N_{ch} , does not vary with station diameter. Thus a re-evaluation of Equation 39 gives

$$R_{corr-out} \propto \frac{\Delta\nu \overline{N_{b-st}} N_{st}^2}{D_{st}}. \quad (42)$$

This is consistent with the more detailed analysis in McCool (2011b).

Dual-band implementation

For the dual-band implementation, $R_{corr-out}$ is calculated separately for the low and high band station diameters and summed to achieve a data rate for the full bandwidth. Thus

$$R_{corr-out} \propto \left(\frac{(\nu_{split} - \nu_{min}) \overline{N_{b-st[L]}} N_{st[L]}^2}{D_{st[L]}} + \frac{(\nu_{max} - \nu_{split}) \overline{N_{b-st[H]}} N_{st[H]}^2}{D_{st[H]}} \right). \quad (43)$$

Given $N_{\text{st}[L]} = N_{\text{st}[H]} = N_{\text{st}[S]}$ and $\overline{N_{\text{b-st}}} \propto D_{\text{st}}^2$ (Equation 22), the ratio $R_{\text{corr-out}}(\text{dual} : \text{single})$ can be simplified to

$$R_{\text{corr-out}}(\text{dual} : \text{single}) = \frac{D_{\text{st}[L]}(\nu_{\text{split}}^3 - \nu_{\text{min}}^3) + D_{\text{st}[H]}(\nu_{\text{max}}^3 - \nu_{\text{split}}^3)}{D_{\text{st}[S]}(\nu_{\text{max}}^3 - \nu_{\text{min}}^3)}. \quad (44)$$

Trading $N_{\text{e/st}}$ for N_{st}

For constant $A_{\text{e-arr}}$, Equations 27, 57 and 59 can be substituted into Equation 42. Assuming d_{avg} and the antenna element gain G_{e} remain constant,

$$R_{\text{corr-out}} \propto \frac{\Delta\nu}{N_{\text{e/st}}^{3/2}}. \quad (45)$$

To account for the trade between $N_{\text{e/st}}$ and N_{st} for fixed $A_{\text{e-arr}}$, as well as the different inter-element spacing between the low and high-band arrays, $D_{\text{st}} \propto \sqrt{N_{\text{e/st}}}d_{\text{avg}}$ (Equation 59) can be substituted into Equation 44. Because $N_{\text{e/st}[S]} = N_{\text{e/st}[L]} = N_{\text{e/st}[H]}$,

$$R_{\text{corr-out}}(\text{dual} : \text{single}) = \frac{d_{\text{avg}[L]}(\nu_{\text{split}}^3 - \nu_{\text{min}}^3) + d_{\text{avg}[H]}(\nu_{\text{max}}^3 - \nu_{\text{split}}^3)}{d_{\text{avg}[S]}(\nu_{\text{max}}^3 - \nu_{\text{min}}^3)}. \quad (46)$$

Although the correlator output data rate increases with N_{st} (Equations 42 and 43), the relative data rate between the single and dual-band implementations is independent of the N_{st} vs. $N_{\text{e/st}}$ trade.

Correlator–computing data transport cost

For SKA₁-low, the HLSD lists an average data rate of 332×10^9 bytes s^{-1} (2.66 Tbps) from the correlator to the computer; a factor of 1.25 encoding overhead brings this to 3.32 Tbps. Taking an approach similar to the station-CPF link (Appendix D.8), only the correlator–computing data transmission is costed; the trenching and cabling cost is ignored. Assuming that the computing is off-site at a nearby city or other suitable location, a cost-effective option is to multiplex the signals onto fibre using DWDM technology (e.g. Figure 26 of Bolton et al., 2009).

The DWDM transmission can be split into a data transmit–receive cost and a signal amplification cost. McCool (2010) costs the transmitter–receiver pair at €2 k per 10 Gbps channel and the optical amplifier and dispersion compensator at €10 k per 16-channel unit. The optical signal amplification is required every 80 km. If three amplification units are required, this results in a conservative estimate of €4 k per 10 Gbps channel, or €400 per Gbps for the data transmission. This is higher than the average cost of the station–CPF transmission, because of the greater distances. The correlator–computing transmission cost for the HLSD is then approximately €1.3 M.

F.2.4 Imaging

The SKA post-correlator processing requirements and algorithms, and their effect on computational cost, is an area of active research (e.g. Alexander, 2011). The ‘imaging’ sub-system encompasses the processing of visibilities from the correlator into imaged data products, as outlined in Alexander et al. (2009). Considered here are the ‘gridding’ operations on the visibility data which are the main computational cost (Cornwell, 2004; Alexander et al., 2009). Many of the imaging operations act on the data from the correlator, thus buffering of these data is required (Faulkner et al., 2010). Assuming that the imaging cost is dominated by the data buffer, rather than the operations cost of the imaging algorithms, then the data rate out of the correlator (Appendix F.2.3) can be used as an indicator of cost (Alexander et al., 2009).

If the processing cost is considered, then there is a contribution from the data volume, but also a cost for correcting for non-coplanar baselines in wide-field images. For continuum imaging, which requires high

dynamic range in the presence of confusing sources, Perley & Clark (2003) and Cornwell (2004) establish scaling relationships for an array of single-pixel feed dishes. Cornwell (2005) extends this analysis to multi-beam systems such as aperture arrays and dishes equipped with phased array feeds. The processing cost and its scaling as a function of dish or station diameter varies: the data rate out of the correlator is one factor; the other is the cost per visibility to correct for non-coplanar baselines. That cost depends on whether the correction can be done by separately imaging each independently pointed station beam, imaging the entire processed FoV at once, or by using some other algorithm. Modelling the cost of this processing and its scaling relationship with station diameter is beyond the scope of this work.

Imaging processor cost

The hardware implementation for SKA computing is currently ill-defined, but a simple estimate can be derived from the SKA budget. Garrett et al. (2010) budget €350 M for SKA₁-low capital investment, which includes a “significant element of contingency”. We use €20 M as a zeroth-order estimate of the processing hardware and related infrastructure for the imaging aspect of the computing. Software is the other major computing cost, but estimating any cost difference between single and dual-band is beyond the scope of this work.

F.2.5 Non-imaging processing

The main sub-systems of the non-imaging processing are a central beamformer, and pulsar searching and timing on the beams formed, as described in Turner et al. (2011). Each beam is a phased or ‘tied’ array beam, formed using some or all the stations in the array as inputs to the beamformer. (In contrast, station beams are formed from the antenna elements or tiles in the station).

The pulsar survey costs are assumed to be dominant, compared to the pulsar timing costs (Turner, 2011). Also, although the central beamformer may be a combined with the correlator sub-system (e.g. Turner et al., 2011), the processing for the pulsar survey is likely to be a significantly larger cost. The search for pulsars is conducted on a ‘per beam’ basis and can be computationally expensive, especially if searching for binary pulsars using acceleration searches. For example, Smits et al. (2009) calculate the number of computational operations required for the acceleration search with SKA Phase 2, for a fiducial set of search parameters; the number of operations for the acceleration search are two orders of magnitude greater than for the array beamforming. However, determining the algorithm for optimal processing loads and data rates for the SKA requires further investigation (Turner et al., 2011).

Regardless of the algorithm, the general processing trend can be analysed because the search is conducted on each beam. The number of array beams $N_{\text{b-arr}}$ required to survey the sky depends on the FoV of each beam. That in turn depends on the frequency of observation, and the diameter of the array from which the beams are formed: $N_{\text{b-arr}} \propto (\nu D_{\text{arr}})^2$. Although using more stations increases sensitivity, it also increases D_{arr} . To limit the computational requirements, Smits et al. (2011) suggest that only stations in the 1 km diameter core be used to form the processed FoV.

The single-band implementation (Figure 5) has a 1 km diameter core. However, for the high band of our representative dual-band implementation, the smaller inter-element spacing means that the core is only 0.5 km in diameter (Figure 6). This results in the required FoV being met with factor of four fewer core array beams. The cost of beamforming is approximately linearly proportional to the number of beams (Appendix D.6.1) and the subsequent processing to search for pulsars is conducted on the per beam basis, hence the processing cost for the dual-band implementation is 25% of the single-band implementation.

To realise the factor of 4 cost reduction, the 0.5 km diameter high-band core must be physically separate to the low-band core, as shown in Figure 6. Also, the processing capacity (hence cost) of the non-imaging processor is assumed to be specified by the AA pulsar survey, rather than the dish pulsar survey. But if the requirements for the dish pulsar survey set the processing capacity, a factor of 4 increase in AA pulsar survey performance is still achievable, despite no cost reduction being realised. This is because

the smaller diameter of the high-band core results in the FoV of each core array beam increasing by a factor of 4, meaning fewer beams are searched to survey the same sized area of sky.

Turner et al. (2011) assume that the 35 SKA₁-low stations (180 m diameter) in the central 5 km of the array are used for pulsar searches. In that case, more compact stations will not necessarily decrease this 5 km diameter, hence the dual-band array provides no extra benefit. However, using all the stations within the 5 km is not cost-effective. As Table 3 of Colegate & Clarke (2011) shows, outside the densely packed core of the SKA₁-low array, the cost-effectiveness of high time resolution searches is significantly reduced; the extra sensitivity gained from including more stations is insufficient to offset the many more array beams which must be formed to meet the required FoV.

Another aspect to non-imaging processing is searches for ‘fast transients’, which are highly energetic, single-pulse events. Like pulsars, these searches are generally conducted on a per beam basis, where for SKA₁, the beams would be either core array beams or station beams, depending on the search strategy (see Colegate & Clarke, 2011, and references therein). Thus the fast transients processing cost for the high-band array is 25% of the single-band implementation. If searches are done with the low-band array, the cost is equal to the single-band implementation.

Non-imaging processor cost

Turner (2011) provides a cost of €28 m for a pulsar search concept description by Knittel & Horneffer (2011). This cost is for processing hardware including server cases. Adding in racks and power distribution (which scale approximately linearly with processing), we round the cost up to €30 m. The concept description does not specify whether processing hardware searches the 1.25 deg² FoV or some subset of that. However, given the search is done on a per beam basis, this is not important because the relative cost applies regardless.

F.3 Power demand

The power demand estimate is sourced from the bottom-up SKADS power budget in Faulkner et al. (2011). The power budget is for the all-digital station architecture, but extrapolation to the RF tile beamforming architecture is done by including a power cost for the RF beamformer. The scaling relationships for power demand are shown in Table 17 and the unit costs in Table 18.

G Station performance considerations

G.1 Sensitivity requirements and inter-element spacing

Telescope sensitivity is a key requirement on the system. The required sensitivity is usually derived from the required minimum detectable flux density and the telescope time available for each pointing (patch of sky being observed). An exception is some time-domain astronomy where further integration of a single pointing does not increase sensitivity. Sensitivity is generally given as the metric $A/T = A_{e\text{-arr}}/T_{\text{sys}}$, where $A_{e\text{-arr}}$ is the effective area of the telescope array and T_{sys} is the system temperature. For the electronically steered aperture arrays, significant variations in A/T are caused by:

- inter-element spacing
- scan angle
- strong sources in the sidelobes.

Additionally, the effect of these parameters on sensitivity is frequency dependent. The effect of inter-element spacing is the most relevant to this analysis, and the basic trends are considered here. While the other parameters are also important, a complete analysis is beyond the scope of this document.

The inter-element spacing defines the frequency at which the antenna elements transition from ‘dense’ to ‘sparse’. There is no single definition for when an array is dense or sparse. The broad definition

Table 17: Summary of blocks and scaling for power demand in SKA₁-low station sub-systems (RF first-stage beamforming is optional).

Block name	Quantity in SKA ₁	Power scaling	Block coverage
Active antenna element	$N_{\text{st}}N_{e/\text{st}}$	C_{fix}	LNA and antenna gain
Analogue (RF) tile beamformer ^a	$N_{\text{st}}N_{\text{tile}/\text{st}}$	$N_{\text{b-tile}}C_{\text{var}}$	beamformer
Digitiser	RF: $N_{\text{st}}N_{\text{tile}/\text{st}}N_{\text{b-tile}}$ Dig: $N_{\text{st}}N_{e/\text{st}}$	$C_{\text{fix}} + R_{\text{sample}}C_{\text{var}}$	C_{fix} : analogue signal conditioning, clock distribution C_{var} : analogue to digital converter
Digitiser–bunker link ^b	Dig: $N_{\text{st}}N_{e/\text{st}}$	$C_{\text{var}}R_{\text{dig}}$	copper communication from digitiser and fibre transmission electronics
Station beamformer ^c	N_{st}	RF: $\overline{N_{\text{b-st}}}N_{\text{tile}/\text{st}}C_{\text{var}}$ Dig: $\overline{N_{\text{b-st}}}N_{e/\text{st}}C_{\text{var}}$	digital processing, inter-connections and control
Station–CPF link transmission	N_{st}	$R_{\text{st}}C_{\text{var}}$	fibre transmission

^a Optional block. If analogue tile beamforming is included, subsequent quantities and costs are denoted ‘RF’. If not, the system is all-digital beamforming, denoted by ‘Dig’.

^b Optional block. Assumes no digital beamforming at the tile. Alternative architectures are discussed in Section 7.3.

^c Approximate cost scaling, see Appendix D.6.1.

Table 18: Unit costs for the power demand of SKA₁-low station sub-systems.

Block name	Power demand estimate (mW)	Block unit ^a
Active antenna element	C_{fix} : 180	per element
RF tile beamformer	C_{var} : 400 per output beam	per tile
Digitiser	C_{fix} : 180 C_{var} : 200 per GS/s	per signal
Digitiser–bunker link transmission	C_{var} : 12.4 per Gbps	per link
Station beamformer ^b	C_{var} : 18.6 per input per output beam	per station
Station–CPF link transmission	C_{var} : Not available	per link

^a All elements, beams, inputs and signals are dual polarisation.

^b Dual-band station beamformer power demand is 29% and 71% of this value, for the low and high-bands respectively.

used in this work is that an array is dense when the aperture is fully sampled, such that effective area is approximately constant with frequency: $A_{e\text{-arr}}(\nu) = \text{constant}$. When the array is sparse, the effective area of each isolated element contributes to the array effective area, hence $A_{e\text{-arr}} \propto \lambda^2$. There is also a transition region between dense and sparse, which occurs at an inter-element spacing of $0.5 - 1.5\lambda$ for dipole-like antennas (Braun & van Cappellen, 2006), or at a spacing typically greater than 2λ for more directive antennas (Rogers, 2008).

To give an indication of how the inter-element spacing affects the representative systems, Figure 17 plots A/T as a function of frequency, using the first-order analysis of the problem in Nijboer et al. (2009) and the HLSD. The array effective area is given by

$$A_{e\text{-arr}} = \begin{cases} N_{\text{st}} \frac{\pi}{4} D_{\text{st}}^2 & \nu < \nu_{\text{transition}} \text{ (dense)} \\ N_{\text{st}} N_{e/\text{st}} \frac{\lambda^2}{3} & \nu > \nu_{\text{transition}} \text{ (sparse)}, \end{cases} \quad (47)$$

where $\nu_{\text{transition}}$ is the frequency of the dense–sparse transition. The system temperature is approximated by the sum of the receiver and sky noise temperatures:

$$T_{\text{sys}} = 150 + 60\lambda^{2.55}. \quad (48)$$

The ‘always sparse’ curve in Figure 17 reflects the isolated antenna element case, where $\nu > \nu_{\text{transition}}$ is always true. The frequency at which this curve peaks depends somewhat on the receiver and sky noise models. At the higher frequencies, the arrays are sparse for all four spacing values and A/T is independent of the inter-element spacing. At the lower frequencies, the inter-element spacing defines the discontinuity. This is the transition frequency; the point at which the aperture becomes fully sampled and A/T begins to drop below the always sparse curve.

Figure 17 applies to the single-band implementation and the low (70–180 MHz) band of the dual-band implementation. The sensitivity for the high (180–450 MHz) band is plotted in Figure 18. In this figure, the discontinuities exist for the 0.5 m and 0.75 m inter-element spacing. The 1 m spacing transition frequency is lower than 180 MHz, so the A/T curve is the same as the always sparse curve. The representative single-band A/T is also equal to the always sparse curve, due to its 1.5 m inter-element spacing. Although the canonical dual-band array is designed for comparable performance to the single-band array, the 0.75 m spacing means the dual-band array has less sensitivity between 180 and 230 MHz.

In reality, the layout of the tile elements within a station will affect the form of the discontinuity and the slope of the curve at frequencies below this discontinuity. Intra-station layouts such as golden ratio spiral (GRS)⁵, fractal patterns and irregular arrays will have a distribution of inter-element spacing, i.e. a minimum (d_{min}), maximum (d_{max}) and average (d_{avg}) spacing. The station will be dense once the frequency is low enough that those elements with spacing of d_{max} become dense. The station will be sparse once the frequency is high enough that those elements with spacing of d_{min} become sparse. Between these frequencies, this distribution of inter-element spacing causes the station to be ‘semi-sparse’, and neither case in Equation 47 is applicable. Such layouts can broaden the discontinuity at the dense–sparse transition and reduce the slope of the A/T curve, as can be seen in Figures 22 to 27 of Bij de Vaate et al. (2011).

Although this simple analysis gives some indication of how A/T changes with inter-element spacing, there is scope for more detailed investigation. The station effective area changes as a function of zenith angle θ and azimuth angle ϕ , due to a changing beam pattern. The beam pattern itself, pointed at a particular direction (θ, ϕ), is dependent on the intra-station layout pattern (this also defines the station beam FoV). For example, van Cappellen et al. (2006) compares regular and irregular layouts of uniform aperture distribution for sparse AA stations. Strong astronomical sources in the sidelobes of these station beams will also greatly influence T_{sys} (hence A/T), as shown in Wijnholds & van Cappellen (2011). Also, spatial tapering would increase the A/T at lower frequencies. But the extent of this increase, and the related frequency-dependent effect on beam pattern (hence Ω_{st}) requires further investigation.

The station effective area calculations also depend on the gain or directivity of the antenna element. For example, log-periodic, conical spiral and Vivaldi elements are discussed in Bij de Vaate et al. (2011). These have higher directivity (at $\theta = 0$) than the proposed element in the HLSD. However, the directivity as a function of scan angle depends on the antenna design. Thus the station directivity (hence $A_{\text{e-st}}$) must be considered down to the maximum scan angle (zenith angle) θ_{max} , which Bij de Vaate et al. (2011) specifies as $\theta_{\text{max}} = 45^\circ$. Appendix G.4 details further work to refine station sensitivity estimates.

G.2 Filling factor and station calibration

The ability to calibrate the SKA₁-low telescope also has system-wide implications. To achieve the desired performance, the instrumental response of the telescope needs to be accurately characterised via calibration (e.g. Wijnholds et al., 2010) and calibrating the station beams is one aspect of this. Wijnholds et al.

⁵GRS is a form of spatial taper, with the density of elements reducing with increased radius from the centre.

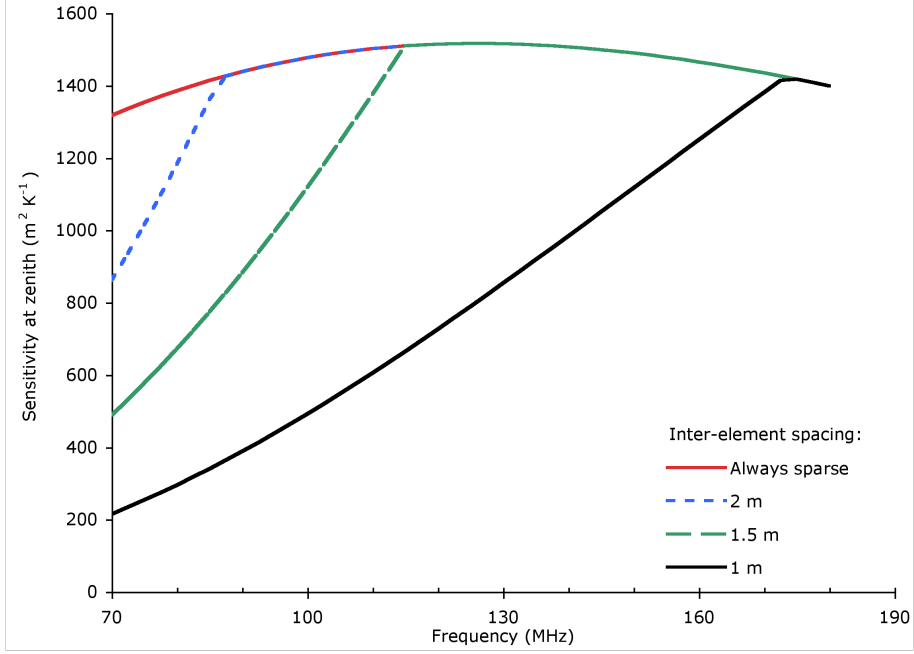


Figure 17: Approximate SKA₁-low sensitivity (A/T) at zenith as a function of frequency (70–180 MHz) and inter-element spacing, using Equations 47 and 48.

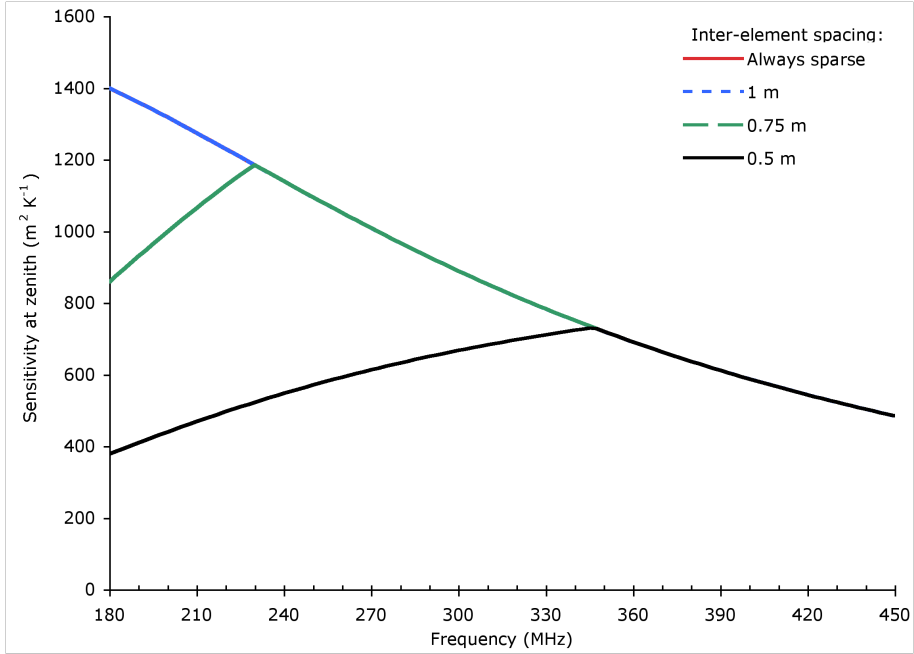


Figure 18: Approximate SKA₁-low sensitivity (A/T) at zenith as a function of frequency (180–450 MHz) and inter-element spacing, using Equations 47 and 48.

(2011b) discusses station calibration and determines that 3–5 calibration sources need to be detectable in the station beam, assuming that the station size meets the requirements outlined in Wijnholds et al. (2011a). A metric which is related to the number of detectable sources is the station filling factor FF_{st} , given by

$$FF_{st} = \frac{A_{e-st}}{A_{g-st}}, \quad (49)$$

where A_{e-st} is the station effective area, and A_{g-st} is the geometrical (physical) area occupied by the station. For a station with a uniform taper (aperture distribution), a fractional bandwidth of 20% and an antenna and receiver noise of 50 K, Wijnholds et al. (2011b) require a filling factor of 0.2–0.4 at 400 MHz.

The competing effects of array sparseness to maintain sensitivity at low frequencies and array density for station calibration at high frequencies is problematic. Wijnholds & Bregman (2011) propose that a dual-band implementation should be used, unless a solution can be found by either optimising the intra-station layout of the single band array to meet both requirements, or using multiple beams at the higher frequencies to detect the required calibration sources. The dual-band array has more flexibility to adjust the high-band design to meet the filling factor requirement.

This problem is reflected in the single-band implementation considered in this analysis, where $FF_{\text{st}} = 0.08$ at 400 MHz for a zenith pointing. For the representative dual-band implementation, $FF_{\text{st}} = 0.33$ at the same frequency and pointing. Although in this case, the filling factor is clearly too low for the single-band implementation, the required and calculated filling factors will vary, depending on the intra-station layout and element gain of the single-band design. Determining whether single-band solution can meet the filling factor requirements is a current work in progress within the SKA aperture array community.

G.3 Trading $N_{\text{e/st}}$ for N_{st} and the relationship with station diameter

For constant array effective area $A_{\text{e-arr}}$, there is a trade-off between aperture array station diameter D_{st} and the number of stations N_{st} , where $N_{\text{st}} \propto 1/D_{\text{st}}^2$. This is analogous to previous investigations trading dish diameter for the number of dishes (e.g. Chippendale et al., 2007; Schilizzi et al., 2007). However, this does not completely describe the independent variables in the trade-off. A parabolic dish (with single-pixel feed) can be thought of as a densely sampled aperture, with the mechanical structure performing the beamforming. If the aperture array is dense, such that the aperture is fully sampled (see Appendix G.1), then $N_{\text{st}} \propto 1/D_{\text{st}}^2$. But when the antenna elements are sufficiently spaced such that the AA is sparse over some or all frequencies, then D_{st} is a function of two independent parameters, $N_{\text{e/st}}$ and the average inter-element spacing d_{avg} , as shown below.

Array effective area is given in Equation 47, but it can be more generally described by

$$A_{\text{e-arr}}(\nu) = N_{\text{st}}A_{\text{e-st}}(\nu), \quad (50)$$

where $A_{\text{e-st}}$ is the station effective area at some frequency ν . Assuming an irregular intra-station element layout with an approximately uniform element distribution,

$$A_{\text{e-st}}(\nu) \approx N_{\text{e/st}}A_{\text{e-e}}(\nu), \quad (51)$$

where $A_{\text{e-e}}(\nu)$ is the antenna element effective area. For an isolated antenna element,

$$A_{\text{e-e}}(\text{isolated}) = \frac{G_e \lambda^2}{4\pi}, \quad (52)$$

where G_e is the antenna gain. However, in the presence of neighbour elements, $A_{\text{e-e}}$ cannot be greater than the available physical area (Nijboer et al., 2009), thus

$$A_{\text{e-e}} \approx \min \left\{ \frac{G_e \lambda^2}{4\pi}, \text{available geometric area} \right\}, \quad (53)$$

where, for a uniform intra-station element distribution, the available geometric area is approximated by d_{avg}^2 . Restating Equation 53 in terms of the frequency-dependent station filling factor (Equation 49) gives

$$A_{\text{e-e}} = d_{\text{avg}}^2 FF_{\text{st}}, \quad (54)$$

where

$$FF_{\text{st}} \approx \min \left\{ \frac{G_e \lambda^2}{4\pi d_{\text{avg}}^2}, 1 \right\}. \quad (55)$$

As expected, $FF_{\text{st}} \leq 1$; a filling factor of 1 signifies that the array is dense.

In its full form, Equation 50 is thus

$$A_{e\text{-arr}}(\nu) \approx N_{\text{st}} N_{e/\text{st}} d_{\text{avg}}^2 FF_{\text{st}}(\nu). \quad (56)$$

When the function $A_{e\text{-arr}}$ is held constant,

$$N_{\text{st}} \propto \frac{1}{N_{e/\text{st}} FF_{\text{st}} d_{\text{avg}}^2}. \quad (57)$$

If d_{avg} and the function FF_{st} also remain constant (i.e. G_e does not vary in FF_{st}), then

$$N_{\text{st}} \propto \frac{1}{N_{e/\text{st}}}. \quad (58)$$

This is not applicable for intra-station layouts with non-uniformly distributed antenna elements (see Appendix G.1), because the approximation for $A_{e\text{-st}}$ (Equation 51) does not hold.

The relationship with station diameter can also be determined, assuming that the array is dense at the lowest frequency. Equation 53 shows that $A_{e\text{-e}} \lesssim d_{\text{avg}}^2$, therefore the maximum station effective area is $A_{e\text{-st}}(\text{max}) \approx N_{e/\text{st}} d_{\text{avg}}^2$. From geometry, $A_{e\text{-st}}(\text{max}) \propto D_{\text{st}}^2$, hence

$$D_{\text{st}} \propto \sqrt{N_{e/\text{st}} d_{\text{avg}}}. \quad (59)$$

This relationship is important, because it shows that station diameter is not an independent parameter, but is influenced by both the number of elements in the station and the average spacing between the elements.

The veracity of Equation 57 can be confirmed by considering the extreme cases. If the array is completely dense, such that $FF_{\text{st}} = 1$, then

$$N_{\text{st}} \propto 1/D_{\text{st}}^2. \quad (60)$$

If the array is completely sparse, then

$$FF_{\text{st}} = \frac{G_e \lambda^2}{4\pi d_{\text{avg}}^2} \quad (61)$$

and

$$N_{\text{st}} \propto \frac{1}{N_{e/\text{st}} A_{e\text{-e}}(\text{isolated})}. \quad (62)$$

G.4 Further work to refine station performance metrics

Matching the top-level science requirements to the telescope performance requires an understanding of the telescope's A/T and processed FoV performance. The A/T performance of a higher-frequency dish-based aperture synthesis telescope is well-understood (e.g. Crane & Napier, 1989). The A/T performance of an aperture synthesis telescope composed of aperture array stations, in the lower frequency, sky noise dominated regime, is more complex (e.g. Wijnholds & van Cappellen, 2011).

Considering the factors affecting sensitivity discussed in Appendix G.1, the requirements and performance metrics can be specified as $A/T(\theta, \phi, \nu)$ and $\Omega_{\text{req}}(\theta, \phi, \nu)$, or at least a minimum A/T and Ω_{req} as a function of frequency over some range of (θ, ϕ) . Some simple rules-of-thumb are used in this analysis, but more accurate estimates could be obtained through array layout simulation software, such as Xarray⁶ and OSKAR (Dulwich et al., 2009).

For each layout, simulation of a small set of interdependent input parameters and performance metrics would be useful inputs for the parametric analysis. They are:

⁶<http://sites.google.com/site/xarraytool/>

Table 19: SKA₁-low station details for the half-diameter station example.

	Single-band	Dual-band	
		Low band	High band
Diameter	90 m	90 m	45 m
Number of elements per station	2 800	2 800	2 800
Number of stations	200	200	200
Average spacing between elements	1.5 m	0.75 m	1.5 m

- input parameters
 - antenna element pattern
 - intra-station layout and inter-element spacing
 - number of elements per station
 - number of elements per tile (if used)
- performance metrics
 - effective area as a function of frequency and direction
 - station beam FoV as a function of frequency and direction.

A layout will also have advantages and disadvantages which cannot be captured in the parametric analysis (e.g. station beam pattern, sidelobes and calibration); these must be considered separately.

Improved accuracy will also be obtained if the simulations take into account effects such as

- mutual coupling between elements
- the non-ideal gain of the antenna element, as a function of ν , θ and ϕ (this parametric analysis assumes ideal gain)
- LNA response
- the effect on gain due to the analogue beamformer, as a function of ν , θ and ϕ .

H Smaller station diameter example

We present a simple comparative example showing the effect of smaller stations, where the diameter of every single-band, low-band or high-band station is halved. The system details for the single and dual-band implementations of this half-diameter example are listed in Table 19.

H.1 Station hardware costs

Costing the smaller station diameters requires consideration of the location of the station processing node. As in the dual-band implementation, we assume that each smaller station continues to have its own station beamformer processing node—the bunker. The only change to the cost model (Appendix D) is to halve the unit cost of the tile–digitiser RF link to €40 per link, due to the smaller station diameter. For the all-digital architecture, the digitiser–bunker link cost equation already has a distance-dependent term, so remains the same. Also, the dual-band cost multipliers (Appendix D.9) do not change.

Figure 19 plots the hardware cost of all the SKA₁-low stations in the half-diameter example alongside that of the full-sized stations previously shown in Figure 7. Because the number of elements per station differ by a factor of 4, the cost of all stations is a more useful comparison than the cost per station. The total number of elements in the array remain constant, hence the total cost of the active antenna elements, RF links (for the all-digital architecture) and digitisers do not vary. Compared to the full-sized stations, the smaller average distance to the bunker reduces the total cost of the RF links in the RF tile beamforming architecture and the digitiser–bunker links in the all-digital architecture.

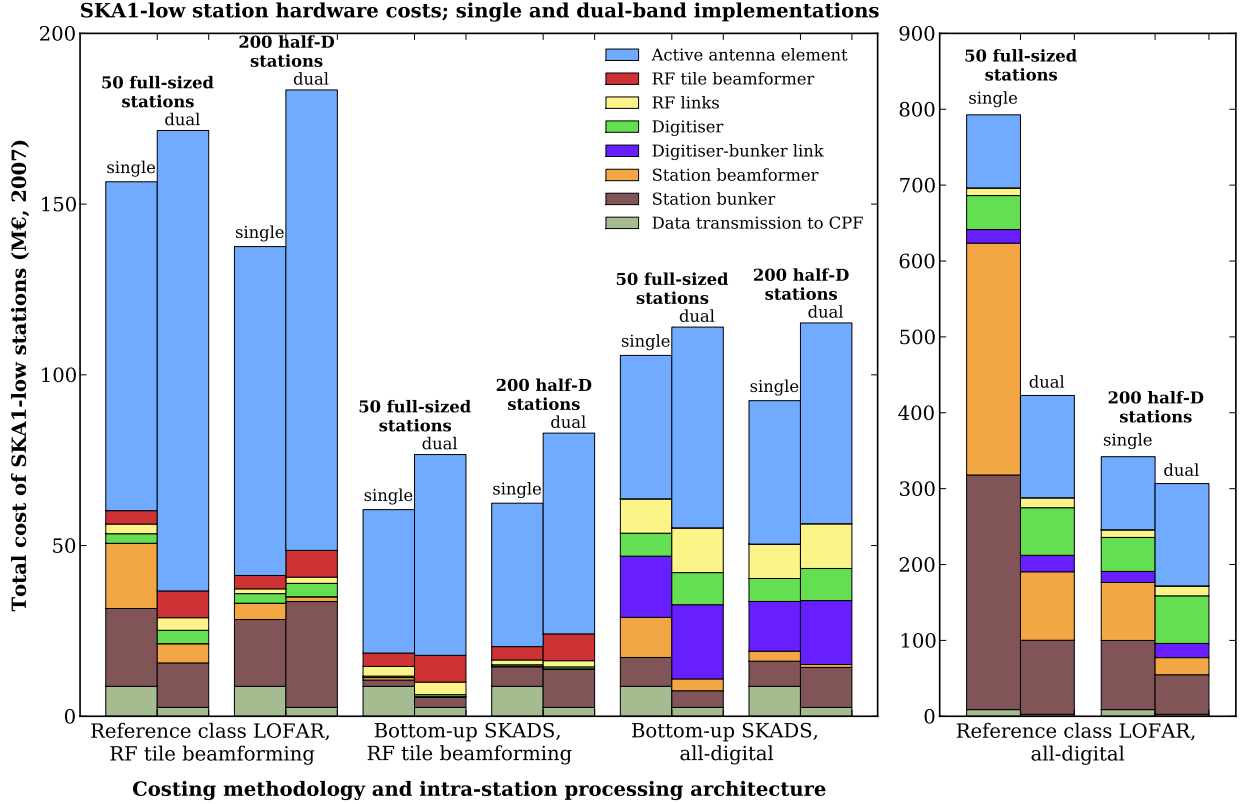


Figure 19: SKA₁-low station hardware cost, for 50 full-sized stations (per band) and 200 stations of half the diameter, hence a quarter of the number of elements per station. Other details as per Figure 7.

The average number of station beams is varied to maintain the required FoV. For this reason, the total processing cost of N_{st} beamformers (Equation 16, p 40) can be approximated by

$$P_{BF-total} \propto N_{e/st}, \quad (63)$$

which is a factor of 4 reduction for the half-diameter stations. But despite the decrease in intra-station signal transport and beamformer processing costs, the station bunker puts upwards cost pressure on the total cost. Although a part of the station bunker cost varies with station beamformer processing, the fixed-cost portion of each bunker begins to become significant with the smaller stations. Because there are more bunkers (one for each station), the total fixed cost portion of the bunker is higher. This trend is further exacerbated in the dual-band implementation, where twice as many bunkers are used (one for each low-band and high-band station).

In the present analysis, the fixed cost portion of the bunker is set at 20% of the source data cost estimates (bottom-up SKADS and reference class LOFAR); the other 80% is assumed to scale linearly with the amount of station processing. Although the fixed cost is a zeroth-order estimate, its purpose is to recognise that there may be inefficiencies in providing environmental conditioning (cooling), RFI shielding and power to many smaller controlled environments (the bunkers), as well as higher construction, testing and deployment costs. Potential solutions such as shared processing nodes are discussed in Appendix H.3.

H.2 System implications of trading $N_{e/st}$ for N_{st}

As in the single and dual-band comparison (Section 5), there are other costs that vary with the N_{st} vs. $N_{e/st}$ trade-off. The only costs in Section 5 which vary are the correlator and imaging processor costs. The constant A_{e-arr} means that the total area occupied by the array and the total number of antenna elements in the array do not change, thus the site preparation and antenna element deployment costs do not change. Of course, there will still be twice as many antenna elements in the dual-band implementation

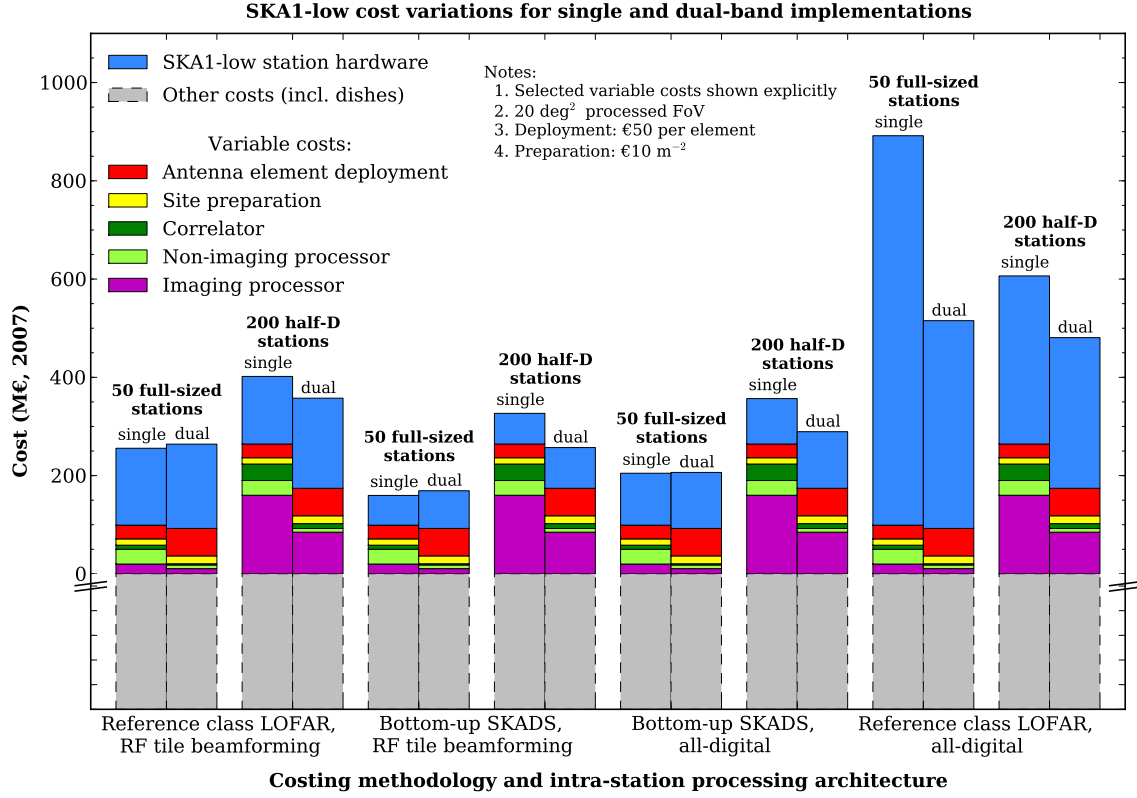


Figure 20: Comparison of significant variable costs (excluding power) for 50 full-sized stations (per band) and 200 stations of half the diameter. The correlator processing cost is assumed to scale as $1/N_{e/st}$. Other details as per Figure 8.

and it will occupy an extra 25% area, as shown in Table 7. The non-imaging processor cost does not change, because it depends on the diameter of the core, which remains the same.

The correlator and imaging processor costs do increase as the number of elements per station are traded for more stations, as derived in Appendix F.2. These increases apply equally to both the single and dual-band implementations. The correlator processing (Equation 38) is

$$P_{\text{corr}} \propto N_{e/st}^{1-\alpha}, \quad (64)$$

where $1 < \alpha < 2$ depending on the correlator design and technologies used. The correlator output data rate, and hence imaging processor cost (Equation 45) is

$$R_{\text{corr-out}} \propto \frac{1}{N_{e/st}^{3/2}}. \quad (65)$$

For the half-diameter station example, where there are a quarter of the number of elements per station, the correlator cost increases by up to 400%. Although the number of correlations increases by N_{st}^2 (i.e. a factor of 16), the number of beams required to produce the 20 deg² processed FoV is reduced by a factor of 4 for the half-diameter stations, resulting in only a factor of 4 increase in correlation cost. For the post-correlation imaging processor, the cost increases by 800%.

Figure 20 plots the variable costs, for the zeroth-order cost estimates used in Section 5. A value of $\alpha = 2$ is used for the correlator processing cost. The correlator and imaging processor costs are significant for the half-diameter example, more so for the single-band implementation. Although the cost for the reference class LOFAR, all-digital beamforming scenario remains significantly larger than the others, the cost of single-band implementation of that scenario has reduced considerably.

The principal cost differences arise from whether the processing is distributed amongst the station beamformers or centralised at the correlator and image processor, however the magnitude of the cost differences

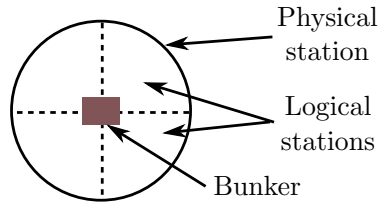


Figure 21: Schematic of logical stations within a physical station, and the shared processing node (bunker).

depend on the implementation. The power demand, which scales with the amount of processing, also follows the same trend. The power demand of the station is not plotted, because it should be considered in context with the power demand of the correlator and imaging processor, which is beyond the scope of the present analysis.

H.3 Station diameter and shared processing nodes

To control the bunker cost, which is higher due to the increased number of stations, shared station nodes may be the preferable option for some architectures. Conceptually, this leads to two different sized stations: a ‘logical’ and ‘physical’ station, to borrow from software engineering terminology (e.g. Kruchten, 1995). The logical (functional) station is the beamformed station, where the beams are input to the correlator. The physical (infrastructure) station has one node (bunker) shared between a number of the beamformed stations. In the centrally condensed part of the array, where there is a ‘sea’ of antenna elements, the logical stations could be re-configurable in diameter, to suit the scientific application (Alexander, 2011).

As shown in Figure 21, an obvious alternative in the half-diameter station example is to have 4 logical stations per physical station, which would mean the physical station size is similar to the full-diameter stations. This would be viable if the cost reduction of a single larger bunker outweighs the higher intra-station link costs. The link costs are higher due to the larger average distance to the bunker; inefficiencies and losses could be introduced in the longer RF and power cables, or alternatively, more expensive cables or digital transmission equipment may be required. A higher ratio of logical to physical stations may be cost-effective, especially for the high band of the dual-band array, which is already smaller in diameter.

There are some real-world examples of aperture array telescopes which have differing logical and physical stations. The Murchison Widefield Array (MWA) is a telescope which will have 128 aperture array tiles, each with an RF beamformer, distributed out to a distance of 1.5 km from the array centre⁷. A receiver node digitises and applies a coarse filterbank to the single tile beam from each RF beamformer and transmits the digital data to the correlator (Lonsdale et al., 2009). The receiver node serves 8 tiles, rather than each beamformer having its own node. In this context, the tiles, as inputs to the correlator, are the logical stations and the 8 tiles connected to the receiver node forms the physical station. The LOFAR stations also have different logical and physical stations. The ‘core’ stations at the inner region of the telescope are each composed of a set of low band antennas (LBA) and two sets high band antennas (HBA). These antennas are served by a single processing node (Gunst & Bentum, 2010).

The required geographical layout of stations, which determines (u, v) coverage, is another trade-off consideration. To maintain comparable infrastructure costs, the half-diameter station example assumes that the 4 smaller stations are located adjacent to each other, as will already be the case in the centrally condensed part of the array. But for stations placed outside of the centrally condensed part of the array, ‘clustering’ or grouping of antennas is proposed as a method to reduce the infrastructure costs (Bolton et al., 2011). Beyond the 5 km ‘inner’ region of SKA₁, the HLSD describes clusters of receptors, containing 5 dishes and a single SKA₁-low station. Each physical station could be divided into 4 adjacently located smaller logical stations. However, if the purpose of reducing station diameter (thereby increasing the number of stations) is to improve (u, v) coverage through more diverse placement of stations, then

⁷<http://www.mwatelescope.org/instrument/specs.html>

such a strategy will not be particularly useful. Estimating the extra infrastructure cost to separate the stations with larger distances is beyond the scope of this analysis.

I Reduced fixed beam–bandwidth product

If the aperture array system has a fixed processing capacity, then the processed FoV and processed bandwidth are tradable quantities. There are a few contemporary examples of this approach to aperture array system design:

- The trade-offs in the SKADS aperture array designs are based on the capacity to transmit data from the station to the central processing facility being a primary limitation (Bolton et al., 2009b).
- The LOFAR station processing is reconfigurable such that processed bandwidth can be traded for station beams, thus maintaining a set data rate from the station (de Vos et al., 2009).
- The MWA design has 220 MHz of sampled bandwidth available, but at any one time it only transports 30.72 MHz of this bandwidth to the central processing hardware (Lonsdale et al., 2009).
- The Long Wavelength Array (LWA) design constrains the bandwidth for multiple station beams, due to limitations in transporting data from the stations to the correlator (Ellingson et al., 2009).

The amount of FoV that can be processed over some bandwidth can be constrained by fixing the beam–bandwidth product, $\overline{N_{b-st}}\Delta\nu$, where $\overline{N_{b-st}}$ is the average number of beams formed over the bandwidth $\Delta\nu$. Assuming that the data consists of many channelised beams (Appendix C), the processing capacity of the station beamformer, station–CPF data transmission and the central processing sub-systems can then be determined by $\overline{N_{b-st}}\Delta\nu$.

I.1 Strawman details

An alternative analysis by Faulkner⁸ of the SKA₁ Design Reference Mission (DRM₁) version 2.0 (SSWG, 2011) considers the beam–bandwidth product required for individual DRM₁ chapters. We do not examine the details of such an analysis, but simply consider a strawman example where the largest beam–bandwidth product is defined by requirement to observe 20 deg² processed FoV over the 70–180 MHz band. However, we note that a frequency split at 200 MHz (hence a 70–200 MHz low band) for the dual-band implementation would provide a better fit to the science relevant to SKA₁-low in the current DRM₁ (Chapters 2–5); three of those science chapters specify either a maximum or minimum frequency of 200 MHz.

For this strawman, 20 deg² FoV (70–180 MHz) equates to $\overline{N_{b-st}} = 44$ over the band; this applies to both the single and dual-band implementations, because the station diameters are equal between 70 and 180 MHz. The beam–bandwidth product is thus 4.8 GHz. In contrast, to achieve 20 deg² FoV (70–450 MHz) for the single and dual-band representative implementations, the beam–bandwidth capacity is 80 GHz and 24 GHz respectively.

The same 4.8 GHz of beam–bandwidth product can be applied to the dual-band array, although the strawman requires further design decisions to be assumed. We maintain the original assumption of separate low and high-band cores (p 6), hence the same 4.8 GHz beam–bandwidth requirement applies to each station in each core. The stations beyond the core are co-located (p 13), but we now assume that the station node hardware (beamformer, bunker and station–CPF data transmission) is shared between each pair of low and high-band stations; this is conceptually similar to the LOFAR station design (Gunst & Bentum, 2010). A different design of the dual-band strawman could have a single core populated with both low and high-band stations, with shared processing. However, this would result in a larger core, which will have consequences on the science applications, such as low surface brightness density and non-imaging processing observations.

⁸AA-low system & station architecture for SKA₁, 18 January 2012

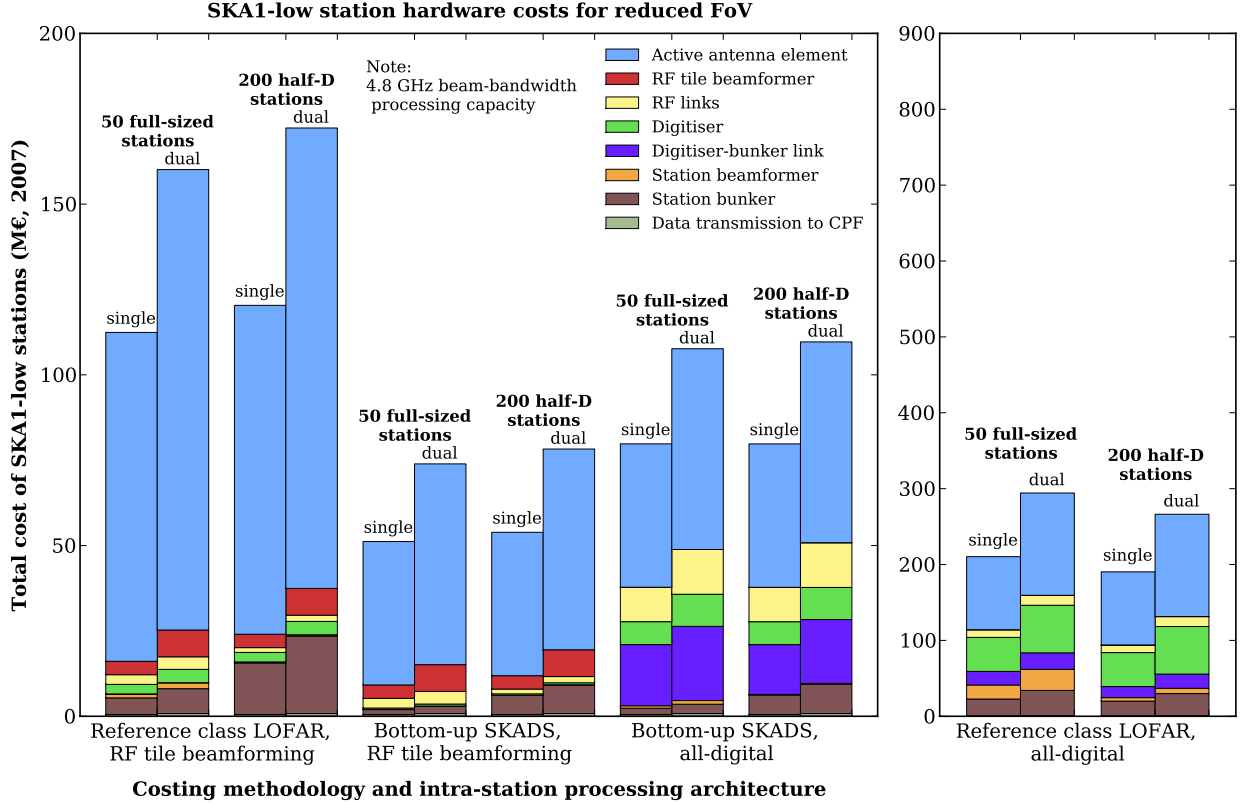


Figure 22: SKA₁-low station hardware cost for a beam-bandwidth product limited to 4.8 GHz, which is equivalent to a processed FoV of 20 deg² over a 70–180 MHz band. Other details as per Figure 19.

Because the station beamforming computational capacity and the maximum rate of station-CPF data transmission is defined by the beam-bandwidth product, observations with other processed FoV and bandwidth combinations are possible, although the observations cannot be concurrent. For example, an observation over the 180–450 MHz frequency range with the single-band array results in a processed FoV of $\Omega_{\text{proc}} = 1.3 \text{ deg}^2$. The same observation with the dual-band results in a processed FoV four times larger, due to the smaller diameter of the high-band station.

I.2 Station hardware costs

Figure 22 shows the station hardware costs for the fixed 4.8 GHz beam-bandwidth product. For all scenarios, the single-band implementation is cheaper than the dual-band, at approximately 70% of the dual-band cost. The station beamformer and station-CPF data transmission costs are now insignificant. This is because the beam-bandwidth capacity of the station node hardware in Figure 22 is reduced by a factor of approximately 17 and 5, compared to the representative single and dual-band implementations respectively. The station bunker cost does not reduce to the same extent as the station beamformer, due to the fixed cost portion of the bunker (see Appendix H.1). Meanwhile, the cost of the station hardware sub-systems located in the signal path prior to the station beamformer remain the same; they are independent of changes to the beam-bandwidth product. The net result is a reduction in station hardware cost for each scenario, compared to when processed FoV of 20 deg² over 70–450 MHz is required.

The previous results, calculated for the representative implementations, show that the dual-band implementation puts downward pressure on the station beamformer and station-CPF transmission costs, which counteracts, to varying extent, the increase in the cost of other station hardware sub-systems in the dual-band implementation. But for this strawman, which is limited by the beam-bandwidth product, the downward pressure is insignificant. Thus in all the scenarios, the cost of the dual-band station hardware is higher. The increase in cost not only depends on the cost data source and intra-station architecture,

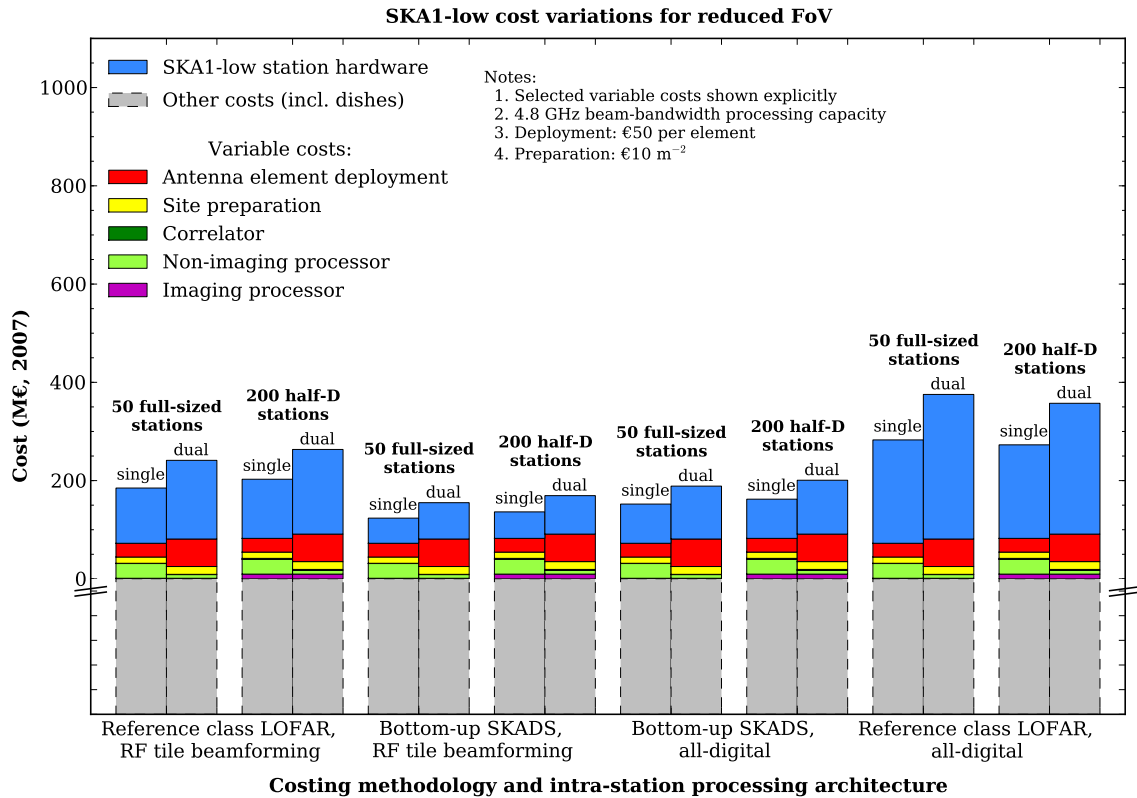


Figure 23: Comparison of significant variable costs (excluding power) for a beam-bandwidth product limited to 4.8 GHz. Other details as per Figure 20.

but given the dominance of the active antenna element costs, the cost multipliers (Appendix D.9) used to determine the active antenna element costs for the dual-band implementation will have a strong influence.

I.3 System implications

A fixed beam-bandwidth product also has implications for the downstream processing. The processing capacity of the correlator and imaging processor sub-systems scales linearly with the beam-bandwidth product (see Appendix F.2). The cost of these sub-systems is thus $4.8/80 = 6.0\%$ of the single-band costs listed in Table 16 (p 44). Because the processing capacity of these sub-systems is now defined by the same beam-bandwidth product for each implementation, the cost does not change between the single and dual-band implementation. However, the cost scaling effects due N_{st} vs. $N_{e/st}$ trade (Appendix H.2) still apply: more stations of smaller diameter increase the correlator and imaging processor costs.

Figure 23 shows the significant variable costs for SKA₁-low. For all scenarios in Figure 23, the single-band implementation is cheaper than the dual-band, at approximately 80% of the dual-band cost. The station hardware, correlator and imaging processor costs are smaller than when a processed FoV of 20 deg² over 70–450 MHz is required (Figure 23); the latter two are no longer significant costs. The antenna element deployment and site preparation costs do not change, because the number and location of the antenna elements is independent of changes to the beam-bandwidth product. The non-imaging processor also remains unchanged, because the strawman presented in this section still has a separate high-band core, with half the diameter of the single-band core.

References

- Alexander, P. 2011, AA Processing Requirements for SKA1, AAVP 2011, Dwingeloo, the Netherlands, 12-16 December
- Alexander, P., Bregman, J. A., & Faulkner, A. J. 2009, in *Widefield Science and Technology for the SKA: SKADS Conference*, ed. S. A. Torchinsky, A. van Ardenne, A. van den Brink-Havinga, A. J. van Es, & A. J. Faulkner, Château de Limelette, Belgium
- Alexander, P., & Hall, P. 2010, Design issues and implementation challenges, AAVP 2010, Cambridge, UK, 8-10 December
- Barott, W. C., Milgrome, O., Wright, M., MacMahon, D., Kilsdonk, T., Backus, P., & Dexter, M. 2011, *Radio Science*, 46, RS1016
- Bij de Vaate, J.-G., et al. 2011, AA Concept Descriptions, AA CoDR document WP2-010.020.010-TD-001 Rev E, SPDO
- Bolton, R., Millenaar, R., & Harris, G. D. 2011, SKA configurations design, System Delta CoDR document WP3-050.020.000-R-002 Rev A, SPDO
- Bolton, R., Scaife, A., Grigorescu, G., Millenaar, R., & Lobanov, A. 2009a, in *Widefield Science and Technology for the SKA: SKADS Conference*, ed. S. A. Torchinsky, A. van Ardenne, A. van den Brink-Havinga, A. J. van Es, & A. J. Faulkner, Château de Limelette, Belgium
- Bolton, R. C., Alexander, P., Ford, D. C., Colegate, T. M., & Hall, P. J. 2009b, in *Widefield Science and Technology for the SKA: SKADS Conference*, ed. S. A. Torchinsky, A. van Ardenne, A. van den Brink-Havinga, A. J. van Es, & A. J. Faulkner, Château de Limelette, Belgium
- Bolton, R. C., et al. 2009, SKADS benchmark scenario design and costing 2 (The SKA Phase 2 AA scenario), SKA Memo 111
- Braun, R., & van Cappellen, W. 2006, Aperture Arrays for the SKA: Dense or Sparse?, SKA Memo 87
- Bunton, J. 2000, An Improved FX Correlator, ALMA Memo 342
- . 2003, Multi-resolution FX Correlator, ALMA Memo 447
- Bunton, J. D. 2010, Strawman SKA Correlator, SKA Memo 126
- Chippendale, A. P., Colegate, T. M., & O’Sullivan, J. D. 2007, SKAcost: a tool for SKA cost and performance estimation, SKA Memo 92
- Colegate, T. M., & Clarke, N. 2011, *Publications of the Astron. Soc. of Australia*, 28, 299
- Cornwell, T. J. 2004, *Experimental Astronomy*, 17, 329
- . 2005, SKA computing costs for a generic telescope model, SKA Memo 64
- Crane, P. C., & Napier, P. J. 1989, in *Astronomical Society of the Pacific Conference Series*, Vol. 6, *Synthesis Imaging in Radio Astronomy*, ed. R. A. Perley, F. R. Schwab, & A. H. Bridle, 139–165
- de Vos, M., Gunst, A. W., & Nijboer, R. 2009, *IEEE Proceedings*, 97, 1431
- Dewdney, P., Lonsdale, C., Roovers, R., & Williams, R. 2011a, SKA Aperture Arrays Concept Design Review Panel Report, AA CoDR document, SPDO
- Dewdney, P. E. 2010, SKA Science–Technology Trade-Off Process, System CoDR document WP2-005.010.030-MP-004 Rev 1.2, SPDO
- Dewdney, P. E., Bij de Vaate, J.-G., Cloete, K., Gunst, A. W., Hall, D., McCool, R., Roddis, N., & Turner, W. 2010, SKA Phase 1: Preliminary System Description, SKA Memo 130
- Dewdney, P. E., Hall, D., McCool, R., Roddis, N., Turner, W., Gunst, A., University of Cambridge, & CSIRO. 2011b, SKA1: High level system description, System Delta CoDR document WP2-005.030.010-TD-002 Rev A, SPDO
- Dulwich, F., Mort, B. J., Salvini, S., Zarb Adami, K., & Jones, M. E. 2009, in *Widefield Science and Technology for the SKA: SKADS Conference*, ed. S. A. Torchinsky, A. van Ardenne, A. van den Brink-Havinga, A. J. van Es, & A. J. Faulkner, Château de Limelette, Belgium
- Ellingson, S. W., Clarke, T. E., Cohen, A., Craig, J., Kassim, N. E., Pihlstrom, Y., Rickard, L. J., &

- Taylor, G. B. 2009, *IEEE Proceedings*, 97, 1421
- Faulkner, A. J., Bij de Vaate, J. G., & van Ardenne, A. 2011, AA deployment and operation, AA CoDR document WP2-010.020.010-TR-001 Rev F, SPDO
- Faulkner, A. J., et al. 2010, Aperture Arrays for the SKA: the SKADS White Paper, SKA Memo 122
- Ford, D., Bolton, R., Colegate, T., Alexander, P., & Hall, P. 2010, The SKA Costing and Design Tool, SKA Memo 120
- GAO. 2009, GAO Cost Estimating and Assessment Guide, GAO-09-3SP, Government Accountability Office
- Garrett, M. A., Cordes, J. M., Deboer, D. R., Jonas, J. L., Rawlings, S., & Schilizzi, R. T. 2010, A Concept Design for SKA Phase 1 (SKA1), SKA Memo 125
- Gunst, A. W. 2007, LOFAR Architectural Design Document of the Astronomical Applications, Tech. Rep. LOFAR-ASTRON-ADD-006 Rev 5, ASTRON
- Gunst, A. W., & Bentum, M. J. 2010, in *Phased Array Systems and Technology (ARRAY)*, 2010 IEEE International Symposium on, 632–639
- Hall, P. J. 2004, SKA Engineering Report, International SKA Conference 2004, Penticton, Canada, 18-22 July
- Hall, P. J. 2009, in *Widefield Science and Technology for the SKA: SKADS Conference*, ed. S. A. Torchinsky, A. van Ardenne, A. van den Brink-Havinga, A. J. van Es, & A. J. Faulkner, Château de Limelette, Belgium, 405–406
- Hall, P. J. 2011, in *Proceedings of the XXXth General Assembly of International Union of Radio Science (URSI)*, Istanbul
- Hall, P. J., Schilizzi, R. T., Dewdney, P. E., & Lazio, T. J. W. 2008, *The Radio Science Bulletin*, 326
- Horiuchi, S., Chippendale, A., & Hall, P. 2004, SKA system definition and costing: a first approach, SKA Memo 57
- Jones, M., Zarb Adami, K., Salvini, S., Faulkner, A., Khlebnikov, V., & Shenton, C. 2011, SKA station beamformer concept description, Signal processing CoDR document WP2-040.120.010-TD-001, SPDO
- Juswardy, B., Bij de Vaate, J. G., Schlagenhauer, F., Padhi, S., & Hall, P. J. 2011, Towards Robust Solar-powered SKA-low Front-end, The Path to SKA-low Workshop, Perth, Western Australia, 6-9 September
- Khlebnikov, V. A., Zarb Adami, K., Armstrong, R. P., & Jones, M. E. 2010, in *Phased Array Systems and Technology (ARRAY)*, 2010 IEEE International Symposium on, 911–916
- Knittel, G., & Horneffer, A. 2011, A scalable computer architecture for on-line pulsar search on the SKA, Signal processing CoDR document WP2-040.130.010-TD-002 Rev 1, SPDO
- Kraus, J. D. 1986, *Radio Astronomy*, 2nd edn. (Cygnus-Quasar Book)
- Kruchten, P. B. 1995, *IEEE Software*, 12, 42
- Lal, D. V., Lobanov, A. P., & Jiménez-Monferrer, S. 2009, Array configuration studies for the Square Kilometre Array—Implementation of figures of merit based on spatial dynamic range, SKA Memo 107
- Lonsdale, C. J., et al. 2009, *IEEE Proceedings*, 97, 1497
- Mailloux, R. J. 1995, *Phased array antenna handbook*, 2nd edn. (Artech House)
- McCool, R. 2010, Data Transmission Cost Scaling for Long Baselines in the SKA, SKA Memo 119
- . 2011a, Network infrastructure concept description, Signal Transport and Network CoDR document WP2-030.080.000-TD.001 Rev 1, SPDO
- . 2011b, STaN high level description, Signal Transport and Network CoDR document WP2-030.030.030-TD-001, SPDO
- McCool, R., Crosby, P., Hall, D., Colegate, T., Bolton, R., & Ford, D. 2010, SKA costing strategy (draft), System Delta CoDR document MGT-040.070.000-MP-001 Rev C, SPDO
- NASA. 2007, *NASA Systems Engineering Handbook*, Tech. Rep. NASA/SP-2007-6105 Rev 1, NASA

- . 2008, 2008 NASA Cost Estimating Handbook, Tech. rep., NASA
- Nijboer, R. J., Pandey-Pommier, M., & de Bruyn, A. G. 2009, LOFAR imaging capabilities and system sensitivity, SKA Memo 113
- Perini, F. 2011, Antenna network for AA-lo: Concept description, Signal Transport and Network CoDR document WP2-030.050.010-TD-002 Rev 1, SPDO
- Perley, R., & Clark, B. 2003, Scaling Relations for Interferometric Post-Processing, EVLA Memo 63
- Rogers, A. E. E. 2008, SNR of dense and sparse arrays, Deuterium Array Memo 70
- Rohlfs, K., & Wilson, T. L. 2004, Tools of Radio Astronomy, 4th edn. (Springer)
- Schilizzi, R. T., et al. 2007, Preliminary Specifications for the Square Kilometre Array, SKA Memo 100
- Schilizzi, R. T., et al. 2011, Project execution plan: pre-construction phase for the Square Kilometre Array (SKA), Tech. Rep. MGT-001.005.005-MP-001 Rev K, SPDO
- Smits, R., Kramer, M., Stappers, B., Lorimer, D. R., Cordes, J., & Faulkner, A. 2009, Astronomy and Astrophysics, 493, 1161
- Smits, R., Stappers, B., Kramer, M., & Karastergiou, A. 2011, Pulsar survey with SKA Phase 1, Signal processing CoDR document WP2-040.030.010-TD-003 Rev 1, SPDO
- SSWG. 2011, The Square Kilometre Array Design Reference Mission: SKA Phase 1 (draft), Tech. Rep. SCI-020.010.020-DRM-002 Rev 2.0, SPDO
- Stevenson, T. J. 2011, System engineering management plan, System Delta CoDR document WP2-005.010.030-MP-001 Rev F, SPDO
- Thompson, A. R., Moran, J. M., & Swenson Jr, G. W. 2001, Interferometry and Synthesis in Radio Astronomy, 2nd edn. (New York: Wiley)
- Turner, W. 2011, SKA signal processing costs, Signal processing CoDR document WP2-040.030.020-TD-001 Rev 1, SPDO
- Turner, W., Faulkner, A. J., Stappers, B. W., Ransom, S. M., Webster, R. L., Eatough, R. P., & Kramer, M. 2011, High-level SKA signal processing description, Signal processing CoDR document WP2-040.030.010-TD-001 Rev 1, SPDO
- van Ardenne, A., Bregman, J. D., van Cappellen, W. A., Kant, G. W., & Bij de Vaate, J. G. 2009, IEEE Proceedings, 97, 1531
- van Cappellen, W. A., Wijnholds, S. J., & Bregman, J. D. 2006, in Radar Conference, 2006. EuRAD 2006. 3rd European, 76 –79
- van Es, A., van Ardenne, A., Faulkner, A., Gunst, A., & bij de Vaate, J.-G. 2011, Aperture Array Risk Register, AA CoDR document WP2-010.020.010-RE-001 Rev C, SPDO
- Wijnholds, S., van der Tol, S., Nijboer, R., & van der Veen, A. 2010, IEEE Signal Processing Magazine, 27, 30
- Wijnholds, S. J., & Bregman, J. D. 2011, AA-lo station aspects illustrated by a fractal hexagonal structure, Tech. Rep. ASTRON-RP-468 Rev 1.1, ASTRON
- Wijnholds, S. J., Bregman, J. D., & van Ardenne, A. 2011a, Radio Science, 46
- Wijnholds, S. J., Nijboer, R., Grainge, K., & Bregman, J. D. 2011b, in Proceedings of the XXXth General Assembly of International Union of Radio Science (URSI), Istanbul
- Wijnholds, S. J., & van Cappellen, W. A. 2011, IEEE Transactions on Antennas and Propagation, 59, 1981